

# ŽELEZARSKI ZBORNIK

VSEBINA	Stran	CONTENTS	Page
Brudar Božidar — Iskra Kibernetika, Kranj		Brudar Božidar — Iskra Kibernetika, Kranj	
STRJEVANJE JEKLA V KOKILI	137	SOLIDIFICATION OF STEEL IN A MOULD	137
Kmetič Dimitrij, J. Žvokelj, V. Vodopivec, M. Jakupovič, B. Ralić — Metalurški inštitut Ljubljana		Kmetič Dimitrij, J. Žvokelj, V. Vodopivec, M. Jakupovič, B. Ralić — Metalurški inštitut Ljubljana	
F. Mlakar, V. Tucić — Železarna Store		F. Mlakar, V. Tucić — Železarna Store	
BELE KROMOVE LITINE LEGIRANE Z MOLIBDENOM ZA VALJE	151	WHITE CHROMIUM CAST IRONS FOR ROLLS, ALLOYED WITH MOLYBDENUM	151
Rodič Tomaz — Univerza Edvarda Kardelja v Ljubljani, FNT, VTOZD Montanistika		Rodič Tomaz — Univerza Edvarda Kardelja v Ljubljani, FNT, VTOZD Montanistika	
D. R. J. Owen — Dept. of Civil Engineering, University of Wales, Swansea, U. K.		D. R. J. Owen — Dept. of Civil Engineering, University of Wales, Swansea, U. K.	
OSNOVNI KONCEPT NUMERIČNE SIMULACIJE RADIALNEGA KOVANJA	167	BASIC CONCEPTS OF NUMERICAL SIMULATION OF A RADIAL FORGING PROCESS	167
Kosec Ladislav — Univerza Edvarda Kardelja v Ljubljani, FNT, VTOZD Montanistika		Kosec Ladislav — Univerza Edvarda Kardelja v Ljubljani, FNT, VTOZD Montanistika	
F. Kosec — Univerza Edvarda Kardelja v Ljubljani, Fakulteta za strojništvo		F. Kosec — Univerza Edvarda Kardelja v Ljubljani, Fakulteta za strojništvo	
NASTANEK IN RAST UTRUJENOSTNE RAZPOKE V KOROZIJSKEM MEDIJU	175	OCCURRENCE AND GROWTH OF FATIGUE CRACKS IN CORROSION ENVIRONMENT	175
Ule Boris, F. Vodopivec, J. Žvokelj, M. Grašič — Metalurški inštitut Ljubljana		Ule Boris, F. Vodopivec, J. Žvokelj, M. Grašič — Metalurški inštitut Ljubljana	
L. Kosec — Univerza Edvarda Kardelja v Ljubljani, FNT, VTOZD Montanistika		L. Kosec — Univerza Edvarda Kardelja v Ljubljani, FNT, VTOZD Montanistika	
ZAPOZNELI LOM JEKLA Z VISOKO TRDNOSTJO	183	DELAYED FRACTURE OF HIGH-STRENGTH STEEL	183
DOKTORSKA IN MAGISTRSKA DELA	193	PH. D. AND M. SC. THESES	193

LET 21 št. 4 — 1987

ŽEZB BQ 21 (4) 137—196 (1987)

## ŽELEZARSKI ZBORNIK

Izdajajo skupno Železarne Jesenice, Ravne, Štore in Metalurški inštitut Ljubljana

### UREDNIŠTVO

**Glavni in odgovorni urednik:** J. Arh

**Uredniški odbor:** A. Kveder, J. Rodič, A. Paulin, F. Grešovnik, F. Mlakar, K. Kuzman, J. Jamar

**Tehnični urednik:** J. Jamar

**Lektor:** R. Razinger

**Prevodi:** A. Paulin, N. Smajić (English), J. Arh (German), P. Berger (Russian)

**NASLOV UREDNIŠTVA:** Železarski zbornik, SŽ-Železarna Jesenice, 64270 Jesenice, Yugoslavia

**TISK:** TK Gorenjski tisk, Kranj

### IZDAJATELJSKI SVET

Prof. Dr. M. Gabrovšek (Predsednik), Železarna Jesenice

Dr. B. Brudar, Iskra, Kranj

Prof. Dr. V. Čižman, Univerza v Ljubljani

Prof. Dr. D. Drobniak, Univerza v Beogradu

Prof. Dr. B. Koroušić, Metalurški inštitut Ljubljana

Prof. Dr. L. Kosec, Univerza v Ljubljani

Prof. Dr. J. Krajcar, Metalurški inštitut Sisak

Prof. Dr. A. Križman, Univerza v Mariboru

Dr. K. Kuzman, Univerza v Ljubljani

Dr. A. Kveder, Metalurški inštitut v Ljubljani

Prof. Dr. A. Paulin, Univerza v Ljubljani

Prof. Dr. Z. Pašalić, Železarna Zenica

Prof. Dr. C. Pelhan, Univerza v Ljubljani

Prof. Dr. V. Prosenc, Univerza v Ljubljani

Prof. Dr. B. Sicherl, Univerza v Ljubljani

Dr. N. Smajić, Metalurški inštitut v Ljubljani

Prof. Dr. J. Sušnik, Zdravstveni dom Ravne

Dr. L. Vehovar, Metalurški inštitut Ljubljana

Prof. Dr. F. Vodopivec, Metalurški inštitut Ljubljana

Published jointly by the Jesenice, Ravne and Štore Steelworks, and The Institute of Metallurgy Ljubljana

### EDITORIAL STAFF

**Editor:** J. Arh

**Associate Editors:** A. Kveder, J. Rodič, A. Paulin, F. Grešovnik, F. Mlakar, K. Kuzman, J. Jamar

**Production editor:** J. Jamar

**Lector:** R. Razinger

**Translations:** A. Paulin, N. Smajić (English), J. Arh (German), P. Berger (Russian)

**EDITORIAL ADDRESS:** Železarski zbornik, SŽ-Železarna Jesenice, 64270 Jesenice, Yugoslavia

**PRINT:** TK Gorenjski tisk, Kranj

### EDITORIAL ADVISORY BOARD

Prof. Dr. M. Gabrovšek, (Chairman), Železarna Jesenice

Dr. B. Brudar, Iskra, Kranj

Prof. Dr. V. Čižman, Univerza v Ljubljani

Prof. Dr. D. Drobniak, Univerza v Beogradu

Prof. Dr. B. Koroušić, Metalurški inštitut Ljubljana

Prof. Dr. L. Kosec, Univerza v Ljubljani

Prof. Dr. J. Krajcar, Metalurški inštitut Sisak

Prof. Dr. A. Križman, Univerza v Mariboru

Dr. K. Kuzman, Univerza v Ljubljani

Dr. A. Kveder, Metalurški inštitut v Ljubljani

Prof. Dr. A. Paulin, Univerza v Ljubljani

Prof. Dr. Z. Pašalić, Železarna Zenica

Prof. Dr. C. Pelhan, Univerza v Ljubljani

Prof. Dr. V. Prosenc, Univerza v Ljubljani

Prof. Dr. B. Sicherl, Univerza v Ljubljani

Dr. N. Smajić, Metalurški inštitut v Ljubljani

Prof. Dr. J. Sušnik, Zdravstveni dom Ravne

Dr. L. Vehovar, Metalurški inštitut Ljubljana

Prof. Dr. F. Vodopivec, Metalurški inštitut Ljubljana

# ŽELEZARSKI ZBORNIK

IZDAJajo ŽELEZARNE JESENICE, RAVNE, ŠTORE IN METALURŠKI INŠTITUT

LET 21

LJUBLJANA

DECEMBER 1987

Vsebina	Stran	Contents	Page
B. Brudar <b>Strjevanje jekla v kokili</b> UDK: 669.18:669.112.223:620.192.43 ASM/SLA: N21, M28h, E25n, D9p, 9-69	137	B. Brudar <b>Solidification of Steel in a Mould</b> UDK: 669.18:669.112.223:620.192.43 ASM/SLA: N21, M28h, E25n, D9p, 9-69	137
D. Kmetič, F. Mlakar, V. Tucić, J. Žvokelj, F. Vodopivec, M. Jakupovič, B. Ralič <b>Bele kromove litine legirane z molibdenom za valje</b> UDK: 669.15'26-194:669.14.018.255 ASM/SLA: M28, N8b, TSk, 5, Cr, W23k	151	D. Kmetič, F. Mlakar, V. Tucić, J. Žvokelj, F. Vodopivec, M. Jakupovič, B. Ralič <b>White Chromium Cast Irons for Rolls, Alloyed with Molybdenum</b> UDK: 669.15'26-194:669.14.018.255 ASM/SLA: M28, N8b, TSk, 5, Cr, W23k	151
T. Rodič, D. R. J. Owen <b>Osnovni koncept numerične simulacije radialnega kovanja</b> UDK: 621.73.045:519.6 ASM/SLA: F22, Q24, I-66, U4g, U4k	167	T. Rodič, D. R. J. Owen <b>Basic Concepts of Numerical Simulation of a Radial Forging Process</b> UDK: 621.73.045:519.6 ASM/SLA: F22, Q24, I-66, U4g, U4k	167
L. Kosec, F. Kosel <b>Nastanek in rast utrujenostne razpoke v koroziskem mediju</b> UDK: 620.193.01 ASM/SLA: R1h, R1e, R2j, Q26p	175	L. Kosec, F. Kosel <b>Occurrence and Growth of Fatigue Cracks in Corrosion Environment</b> UDK: 620.193.01 ASM/SLA: R1h, R1e, R2j, Q26p	175
B. Ule, F. Vodopivec, J. Žvokelj, M. Grašič, L. Kosec <b>Zapozneli lom jekla z visoko trdnostjo</b> UDK: 669.14.018.2:539.56:620.192.3 ASM/SLA: Q26s, SGBa, ST, 2-60, EGn, 3-66	183	B. Ule, F. Vodopivec, J. Žvokelj, M. Grašič, L. Kosec <b>Delayed Fracture of High-strength Steel</b> UDK: 669.14.018.2:539.56:620.192.3 ASM/SLA: Q26s, SGBa, ST, 2-60, EGn, 3-66	183
Doktorska in magistrska dela	193	PH. D. and M. SC. Theses	193

OBSESSION



# ŽELEZARSKI ZBORNIK

IZDAJAJO ŽELEZARNE JESENICE, RAVNE, ŠTORE IN METALURŠKI INSTITUT

LET 21

LJUBLJANA

DECEMBER 1987

## Strjevanje jekla v kokili

## Solidification of Steel in a Mould

B. Brudar \*

UDK: 669.18:669.112.223:620.192.43  
ASM/SLA: N21, M28h, E25n, D9p, 9-69

### UVOD

Proces strjevanja jekla v kokili je opisan že v najrazličnejši strokovni literaturi<sup>1-10</sup> s področja metalurgije in matematične fizike.

Pritem pa ne gre zgolj za samo opisovanje pojavov, ki nastopajo pri strjevanju. Tu mislimo predvsem na izceje<sup>11</sup>, notranje napetosti<sup>12, 13</sup> in lunker. Vedno več je poskusov, da te pojave razložimo in jih opišemo z enačbami matematične fizike.

Pri računalniški simulaciji strjevanja jekla v kokili, pri kateri smo raziskovali vpliv eksotermnih plošč na obliko primarnega lunkerja, smo namreč dobili zanimive rezultate, ki so nam dali ideje za nadaljnje raziskovalno delo.

Tako se nam je z rekonstrukcijo kokile OK 650 posrečilo, da smo bistveno vplivali na porazdelitev izceje v prerezu strjenega bloka. Uspelo nam je zmanjšati sekundarni lunker in prišli smo do novih spoznanj o samem procesu strjevanja — da je namreč mogoče vplivati tudi na strukturo strjenega bloka.

V nadaljevanju je natančneje opisan sam poskus in dobljeni rezultati.

Gre za novo gledanje na pojav strjevanja, ki je mora nekoliko neobičajno. Prvi poskusi pa so dali odlične rezultate in odpirajo se nove možnosti v prizadevanjih za izboljšanje kvalitete strjenih blokov tudi drugačnih oblik.

### VPLIV EKSOTERMNIH PLOŠČ NA VELIKOST PRIMARNEGA LUNKERJA

Izolacijske eksotermne plošče, ki jih montiramo v zgornji del kokile, služijo za to, da ohranimo zgornji del taline čim dalj v tekočem stanju. Pri strjevanju se pa volumen zmanjša približno za 4 %. Želimo, da bi bilo to zniževanje gladine taline čim bolj počasno in na čim večjem prerezu. Tako bi dosegli najmanjšo globino primarnega lunkerja.

Na tržišču se pojavljajo vedno nove kvalitete izolacijskih plošč z vedno boljšimi izolacijskimi sposobnostmi, pa tudi z novo ceno. S pomočjo poenostavljenega modela smo že leli oceniti, kako vplivajo te lastnosti na globino primarnega lunkerja.

### INTRODUCTION

The process of solidification of steel in a mould is described elsewhere in various textbooks and in professional literature<sup>1-10</sup> from the metallurgical science and the mathematical physics. Usually it is not limited only to phenomenological descriptions of the effects observed with solidification. Here we mean especially the appearance of segregations<sup>11</sup>, the internal stresses<sup>12, 13</sup> and the shrinkage holes. There are more and more efforts to explain these effects and to describe them by the equations of the mathematical physics.

With the computer simulation of solidification of steel in a mould where special exothermic plates were used to reduce the primary shrinkage hole, very interesting results were obtained that gave us new ideas for the further research work.

By the reconstruction of the mould OK 650 we succeeded in influencing the distribution of various segregations in the middle of the cross-section of the ingot and in reducing the secondary shrinkage hole. So we came to a new knowledge — how the structure of the solidified ingot could be modified. In the due text the experiment itself is described thoroughly together with the most important results. The idea about our vision of the process of solidification is perhaps a little unusual. But our first experiments gave us excellent results and new possibilities in improving the quality of solid ingots of different forms were opened.

### INFLUENCE OF EXOTHERMIC PLATES UPON THE PRIMARY SHRINKAGE HOLE

The isolating exothermic plates that are usually mounted at the top of the mould are supposed to enable the upper part of the liquid steel to stay liquid as long as possible. By the process of solidification the liquid shrinks for about 4 %. It is desired to lower the level of the liquid steel as slow as possible and to keep it in the largest possible cross-section. In this way the smallest depth of the primary shrinkage hole is obtained.

On the market there are permanently new qualities of isolating plates available with better isolating properties and naturally with new prices.

\* ISKRA Kibernetika, Kranj

V ta namen smo izdelali matematični model, s katerim smo simulirali proces strjevanja, in pri tem izhajali iz naslednjih predpostavk:

- kokila ima obliko pokončnega valja z enakomerno debelo steno,
- kokila stoji na debeli livni plošči iz podobnega materiala,
- velikost kokile, debelino stene in plošče lahko poljubno spremojamo, prav tako tudi fizikalne lastnosti, kot sta specifična toplota in toplotna prevodnost strjenega bloka in kokile,
- talina se pri vlivanju v kokilo dviga enakomerno z določeno hitrostjo,
- gladina jeklene taline je idealno izolirana: toplotna prevodnost praška za posipanje je enaka 0,
- temperatura taline je enaka temperaturi tališča, strjevati se začne, ko je kokila nalita do vrha,
- latentna toplota ni vključena v specifično toploto, strjevaje v celoti poteče pri temperaturi tališča,
- topotni stik med talino in kokilo naj bo ves čas idealen: strjeni blok je ves čas v tesnem stiku s kokilo,
- na zunani steni kokile predpostavljamo ohlajanje s konvekcijo s konstantnim konvekcijskim koeficientom,
- v zgornjem delu kokile imamo izolacijske plošče z znanimi lastnostmi, ki segajo od vrha kokile do določene globine.

Za takšen poenostavljen primer smo izdelali računalniški program, s katerim smo lahko izračunali temperaturni profil v prerezu kokile in bloka in pri tem spremljali ugrezjanje gladine in napredovanje meje med tekočo in trdno fazo.

Variirali smo lastnosti materiala, iz katerega so izdelane eksotermne plošče, dimenzijske plošče in hitrost ulivanja. Poročilo o tej raziskavi je shranjeno v strokovni knjižnici Železarne Jesenice.

Računalniški program smo uspešno uporabili tudi pri študiju strjevanja valjavniških valjev<sup>14</sup>, ki so bili uliti v železarni Štore, in se prepričali, kolikšna je upravičenost omenjenih predpostavk.

Prišli smo še do naslednjih spoznanj:

- če bi ulivali brez eksotermnih plošč, bi dobili zelo globok primarni lunker, ki bi segal skoraj do polovice višine bloka,
- pri vsakem ulivanju z eksotermnimi ploščami pa opazimo pojav »mostu« iz strjenega jekla, ki nastane nekje na 3/4 višine bloka.

V trenutku, ko nastane most, se pač en del taline nahaja pod njim, drugi del taline pa nad mostom. Delež taline nad mostom je tem večji, čim boljše izolacijske sposobnosti imajo eksotermne plošče in čim hitreje se dviga talina v kokili.

Most nastane v vsakem primeru.

Pojavlja pa se drugo vprašanje: Kaj se zgodi z mostom in kako se talina pod njim struje, če upoštevamo, da se pri nadaljnjem strjevanju volumen ujetne taline zmanjša za 4 %.

Odgovore na to vprašanje je mogoče najti v različnih člankih, ki govorijo o rahli sredini v bloku, o notranjih razpokah, luknjicah, različnih vrstah poroznosti<sup>15</sup>, sekundarnem lunkerju in podobno.

Mnogi avtorji trdijo, da pri tem pride do ugrezanja strjenega dela mostu.

Po naših izračunih in po natančnejšem ogledu Baumannovega odpisa prerezanega bloka iz avtomatnega jekla Č3990<sup>16</sup> smo ugotovili, da je verjetno res šlo za ugrezjanje strjenega mostu oziroma za vdiranje nečistoč, ki se nabirajo v glavi, v notranjost bloka.

Using the simplified mathematical model we wished to estimate how all these different properties influence the depth of the primary shrinkage hole.

For this purpose the mathematical model is made to simulate the process of solidification based on the following assumptions:

- the mould has the form of a cylinder with a uniform thick wall,
- the mould is put upon a thick casting plate made of the same material,
- the dimensions of the mould, the thickness of the wall and of the casting plate can be varied together with the physical properties of the material like specific heat, the thermal conductivity of the solid ingot and of the mould,
- the level of the liquid steel is isolated perfectly: the thermal conductivity of the isolating powder on the top is equal zero,
- the temperature of the liquid steel is equal to the melting point, the solidification starts to proceed in the moment when the mould gets completely filled,
- the latent heat of the liquid steel is not included into the specific heat and the solidification is proceeded at the melting point,
- the thermal contact between the liquid and the mould is ideal all the time, even the solid ingot stays attached to the wall of the mould, there is no air gap,
- at the outer surface of the mould the convective heat transfer with a definite coefficient of convection is assumed,
- inside in the upper part of the mould the exothermic isolating plates are mounted extending from the top of the mould to a certain depth into the liquid steel.

For such a simplified case the computer program is made for calculation of the temperature profile in the cross-section of the mould and in the ingot. It is possible to follow the lowering of the liquid metal and to study the improving of the boundary between the solid and the liquid phase.

The properties of the isolating plates were varied together with the dimensions and with the casting speed.

The detailed report of this research work could be obtained at Strokovna knjižnica Železarne Jesenice.

The computer program was also successfully applied to the study of solidification of the steel cylinder<sup>14</sup> for the rolling mill, cast in Železarna Štore, and the validity of the suppositions mentioned above could be verified.

The following conclusions were found:

- casting without exothermic plates would cause very deep primary shrinkage hole extending nearly to the half height of the ingot,
- with any case where exothermic plates were used, the formation of a "bridge" of the solid steel could be observed at about 3/4 of the ingot height.

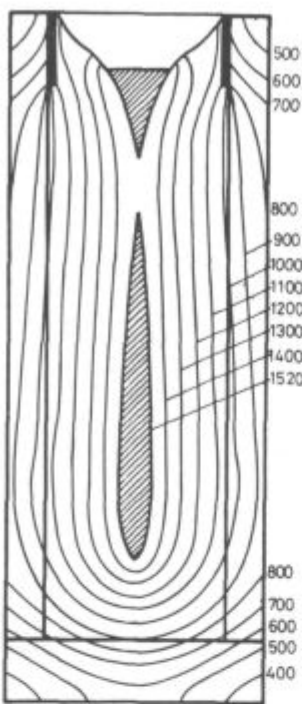
In the moment of the formation of the bridge one part of the liquid steel remains above the bridge, the second part gets caught under the bridge. The amount of the liquid metal under the bridge is somehow proportional to the isolating properties of the isolating plates and to the speed of raising of the liquid metal in the mould.

The bridge is formed in any case.

Now a new question arises.

What happens to the bridge and how is the solidification improving when the reduction of the volume (4 %) of the caught liquid metal is taken into account.

The answer to this question could be found in the articles describing the formation of the "soft middle" in the ingot, the internal cracks, the holes and various types of



**Slika 1:**  
Izoterme v prerezu bloka v kokili. Toplotna prevodnost eksotermnih plošč  $1.563 \text{ W m}^{-1} \text{ K}^{-1}$ , hitrost dviganja taline 200 mm/min, stanje po 106 minutah.

**Fig. 1:**  
Isotherms in the cross-section of the ingot and the mould. Thermal conductivity of the exothermic plates  $1.5 \text{ W m}^{-1} \text{ K}^{-1}$ , the speed of raising of the liquid steel 200 mm/min, the situation after 106 minutes.

Izračunani potek meje med trdno in tekočo fazo v simulaciji strjevanja bloka pa nas je napeljal še na novo idejo.

**Slika 1** prikazuje izoterme v trenutku, ko je pri omenjeni simulaciji nastal most.

Ali se morda meja med trdno in tekočo fazo ne ujemata s črtami, ki na odtisih po Baumannu običajno poimenjuje izceje MnS v obliki črke A?

Izredna podobnost v poteku linij izceje MnS v obliki črke A in izračunanih izoterm nas je silila v iskanje dokaza za tako predpostavko.

Po nekaterih razlagah<sup>17, 18</sup> naj bi bila za to kriva koničnost kokile. V svojih izračunih pa smo predpostavljeni, da kokila ni konična.

Kasneje smo našli poročilo, ki opisuje enake oblike izceje pri kokili, ki je celo širša v zgornjem delu<sup>19, 20</sup>. To je bil dokaz, da so razlage, ki se pojavljajo tudi v metallurških učbenikih, včasih zelo pomanjkljive.

Če so izceje v obliki črke A zares slike trenutne meje med tekočo in trdno fazo v prerezu bloka, ki naj bi nastale ob strjevanju, bi bilo mogoče na to porazdelitev vplivati, če bi lahko vplivali na hitrost strjevanja.

Z omenjenim računalniškim programom smo naredili simulacijo, pri kateri smo pogoje ohlajanja spremnili.

Tako smo si »izmisli« dodatno plast iz šamotne opeke, ki naj bi bila pritrjena na zunanjji strani v zgornji polovici kokile. Izračunali smo, kako bi se spremenil potek strjevanja v takem primeru. Ugotovili smo, da bi to prav nič ne vplivalo na hitrosti strjevanja in da bi bile razlike v temperaturni porazdelitvi v trenutku, ko bi nastal most, zanemarljivo majhne. Seveda nismo naredili nobenega praktičnega poskusa, saj ni bilo potrebno.

Druga ideja je bila, da bi kokilo »postavili« na vodo hlajeno bakreno livno ploščo. Tudi ta simulacija je pokazala, da s tem ne bi prav nič vplivali na tvorbo mostu.

V vsakem primeru je bila stena kokile predebela, da bi bilo mogoče kakorkoli vplivati na potek strjevanja v notranjosti oziroma na potek meje med trdno in tekočo fazo v trenutku, ko nastane omenjeni most.

porosity<sup>15</sup>, secondary shrinkage holes and similar things. Many authors are suggesting the lowering of the solidified bridge.

According to our calculations and after a thorough examination of the sulphur prints in the cross-section of the ingot<sup>16</sup>, it was found out that in fact the lowering of the bridge and the penetration of impurities from the top into the middle of the ingot could be assumed.

The calculated course of the boundary between the liquid and the solid phase in the simulation of solidification of a steel ingot led us to a new idea.

**Fig. 1** is representing the isotherms in the moment of the formation of the bridge according to our simulation.

Is it possible to assume that the boundary between the solid and the liquid phase were equal to the lines that correspond to the segregations of MnS in the sulphur prints in the form of the letter A?

The outstanding similarity in the course of the lines corresponding to segregations of MnS in the form of the letter A with the calculated isotherms forced us to look for the confirmation of our assumptions.

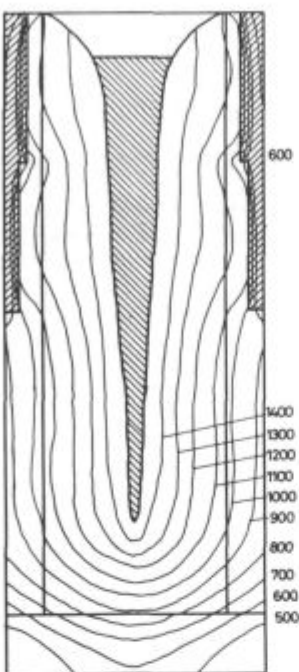
According to some interpretations<sup>17, 18</sup> about the process of solidification this effect could be explained simply by the conicity of the mould.

In our calculations, however, it was assumed that the mould was not conical. Later we found the articles where the same form of segregations were reported<sup>19, 20</sup> even in the moulds that were wider at the top. It was the proof that explanations appearing in metallurgical textbooks are sometimes too superficial.

If the so called A-segregates are really corresponding to the boundaries between the liquid and the solid phase in the cross-section of the ingot that should be formed at solidification it would be possible to influence them if we could influence the speed of solidification.

With the computer program different simulations were made with different cooling conditions.

An additional layer of recovery that would be "fixed" at the outer side of the upper half of the mould was simulated. It was calculated how the solidification would be changed in such case. It was found out that it would



Slika 2:

Izoterme pri simuliranem primeru brez mosta. Toplotna prevodnost zunanje obloge  $1.5 \text{ W m}^{-1} \text{ K}^{-1}$ , hitrost dviganja taline  $200 \text{ mm/min}$ , stanje po 109 minutah

Fig. 2:

Isotherms in the cross-section of the simulated case. The thermal conductivity of the isolating layer outside  $1.5 \text{ W m}^{-1} \text{ K}^{-1}$ , the speed of raising of the liquid steel  $200 \text{ mm/min}$ , the situation after 109 minutes.

Ostala nam je torej samo še ena možnost:  
v zgornjem delu »stranjšati« steno kokile in jo še dodatno izolirati z zunanje strani.

V omenjenem programu za simulacijo strjevanja smo postopoma »tanjsali« steno kokile in »dodajali« izolator toliko časa, da smo prišli do zaželenega rezultata.

Rezultat pa je bil takle: (slika 2).

Jeklena talina se je strjevala tako, da se most sploh ni pojavil. Meje med tekočo in trdno fazo so dobile obliko črke U. V sredini je sicer prišlo do primarnega lunkerja, o sekundarnem lunkerju, ugrezjanju mostu oziroma o vdiranju nečistoč iz glave v notranjost pa ni bilo sledu.

Seveda je bilo vse to izračunano na matematičnem modelu.

Model sam je temeljil na razmeroma hudih poenostavitevah<sup>21</sup> glede stika med kokilo in talino, vendar pa nam je dal ideje za nadaljnje raziskovalno delo. Na osnovi rezultatov omenjene simulacije smo naredili praktični poskus s tako imenovano rekonstruirano kokilo.

### REKONSTRUIRANA KOKILA

Odločili smo se za stanjšanje stene kokile tako, kot prikazuje slika 3. Zgornjo polovico smo konično posneli z zunanje strani in preostalo debelino nadomestili z izolatorjem. Potrebna je bila posebna konstrukcija, ki je omogočala stripanje in polnjenje zgornjega dela z izolacijskim sredstvom. Na ta način smo hoteli zmanjšati topotno kapaciteto zgornjega dela kokile v primerjavi s spodnjim delom in dodatno zmanjšati hitrost strjevanja v glavi bloku. Zaradi primerjave rezultatov smo ulili en blok v klasično kokilo.

Odločili smo se za format OK 650 ( $650 \times 650 \times 2000$ ) in za jeklo, kvalitete Č 3990. Pri tem jeklu je namreč mogoče opazovati izredno intenzivne izceje MnS in je zato tudi primerjava med različnimi bloki lažja.

Napravili smo 4 poskuse:

1. jeklo ulito v klasično kokilo (A)

2. jeklo ulito v kokilo  $d=40 \text{ mm}$  izolacija: livarski pesek (B)

not influence the solidification at all and that the temperature differences in the moment of the formation of the bridge would be negligibly small.

The second idea was to "put" the mould upon a water-cooled casting plate made of copper. Also the results of this simulation showed that this would not influence the formation of the bridge at all.

In all cases the wall thickness seemed to be too large to be able to influence the process of solidification inside, especially the course of the boundary between the solid and the liquid phase in the moment of the formation of the bridge.

There was only one possibility still left.

To lessen the thickness of the wall in the upper part of the mould and to isolate it additionally from the outside. In the program for the simulation of solidification the thickness of the wall was gradually "thinned" and an isolator was "added" till the final result was obtained.

The final result was the following (Fig. 2).

The liquid steel became solid in such a way that the bridge was not formed at all. The boundaries between the solid and the liquid phase got the form of the letter U. In the middle the primary shrinkage hole could be calculated, but there was no secondary shrinkage hole, no lowering the bridge or penetrating impurities from the top into inside.

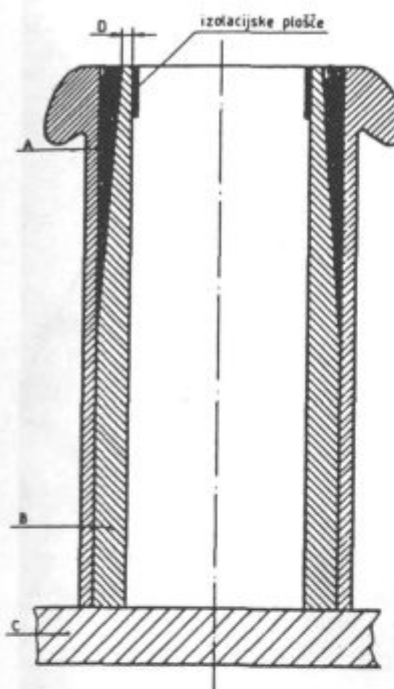
Naturally all this was calculated according to mathematical model.

The model itself based on rather severe simplifications concerning the thermal contact<sup>21</sup> between the mould and the liquid steel but it gave us anyway the ideas for the further research work. On basis of these simulations we performed the experiment with the so-called reconstructed mould.

### RECONSTRUCTED MOULD

We decided to thin the mould wall according to Fig. 3.

The upper part was taken off conically and the remaining thickness was replaced by the thermal isolator.



**Slika 3:**  
Prerez  
rekonstruirane  
kokile:  
A izolator  
B kokila  
C livna plošča

**Fig. 3:**  
The cross-section  
of the  
reconstructed  
mould:  
A isolator  
B mould  
C casting plate

3. jeklo ulito v kokilo  $d = 40$  mm izolacija: perlit (C)
  4. jeklo ulito v kokilo  $d = 20$  mm izolacija: perlit (D).
- (V primeru 4 je bil perlit posebej sušen.)

Na slikah 4, 5, 6 in 7 so prikazani odtisi po Baumanu za vse 4 primere obenem z ustreznim slike jedkane površine prereza.

#### POJASNILO K POSAMEZNIM SLIKAM

Slika 4 je zelo podobna sliki iz leta 1973<sup>16</sup>. Prav lepo se vidijo izceje v obliki črke A in v sredini izceje MnS v obliku črke V. Na fotografiji jedkane površine se zelo lepo vidijo vzdolžne razpoke, ki potekajo praktično po vsej dolžini bloka.

Blok B na sliki 5 je bil pa ulit v rekonstruirano kokiло. Očitno je število razpok v področju sekundarnega lunkerja bistveno manjše, potek izceje v obliku črke A pa ni bistveno drugačen, kot pri bloku A. Ta ugotovitev nas je v prvem trenutku nekoliko razočarala, saj smo pričakovali znatnejše razlike v poteku teh izcej. Pojav smo si razložili s tem, da so izolacijske sposobnosti livarskega peska verjetno razmeroma majhne.

Pri bloku C smo namesto livarskega peska uporabili perlit (U2), ki se uporablja za izolacijo fasad na zgradbah. Pokazalo se je, da smo vendarle na pravi poti.

S slike 6 se jasno vidi, da je izcej v obliku črke V v sredini prereza manj in praktično tudi ni več razpok v sredini prereza v področju sekundarnega lunkerja. Glava je nekoliko bolj čista, robne izceje v obliku črke A potekajo nekoliko bolj pokončno, kot pri bloku A, nečistoči v obliku črke V v sredini prereza so manj izrazite.

Opazili pa smo nekaj, kar nam prej ni zbudilo pozornosti.

Osrđnji del v glavi, v katerem sicer vidimo mnogo izcej V, (primerjaj blok A!), je tu najširši, če med seboj primerjamo prereze blokov A, B in C. To področje je omejeno nekako z dvema paralelnima navpičnima črtama.

A special construction was necessary to enable the stripping of the ingot and the filling of the isolating material.

The thermal capacity of the upper part of the mould in comparison with the bottom part was reduced and we hoped that the speed of solidification in the top would be additionally reduced too. To make the comparison among different experiments easier one ingot was cast into the ordinary mould.

For our practical experiment the mould OK 650 ( $65 \times 650 \times 2000$ ) and the quality of the free-cutting steel C 3990 were chosen. With this type of steel very intense segregates of MnS could be detected so that the comparison among different ingots is easier.

The following experiments were performed:

- steel cast into an ordinary mould (A)
- steel cast into the reconstructed mould with  $D = 40$  mm and with the casting sand used as the isolating material (B)
- steel cast into the reconstructed mould with  $D = 40$  mm and with the pearlite used for the thermal isolation (C)
- steel cast into the reconstructed mould with  $D = 20$  mm and with the pearlite used for the thermal isolation (D)

In the last case the pearlite was specially dried.

The Figs. 4, 5, 6 and 7 show the sulphur prints for all the four cases together with the corresponding photos of the etched surfaces of the cross-sections.

#### COMMENTS TO THE FIGURES

Fig. 4 is very similar to the figure from the year 1973<sup>16</sup>. The segregations in the front of the latter A are clearly seen and the V-segregations of MnS in the middle of the cross-section are evident. From the photos of the etched surface the longitudinal cracks are shown, being practically distributed all along the length of the ingot.

The ingot B from Fig. 5 was cast into the reconstructed mould. It is evident that the number of cracks in the region of the secondary shrinkage hole is significantly smaller and the course of the segregates in the form of the letter A is not much different from that one of the ingot A.

This effect disappointed us at the first moment since considerable differences in the course of these segregates were expected. This could be explained by the fact that the isolating properties of the casting sand were not good enough.

With the casting of the ingot C instead of casting sand the pearlite (U2) was used. This is the same material that is so often used for the thermal isolation of facades of houses. It was shown at once that we were nevertheless on the right way.

From Fig. 6 it can be easily seen that there are not so many V-segregates just in the middle of the cross-section and that there are not so many cracks in the region of the secondary shrinkage hole. The top of the ingot is a little cleaner, the A-segregates are a little more steep than they are in the case of the block A. The impurities in the form of the letter V are less expressed.

But we observed something what was not evident at the first moment. The middle top region (Fig. 6), where there are normally many V-segregates, is the largest if the ingots A, B and C are compared. This region is somehow limited by two vertical parallel lines of segregates. We wished to increase the isolating properties of the upper part of the mould. So the thickness of the wall



Slika 4:

Ingot A — odoris po Baumannu  
sulphur print

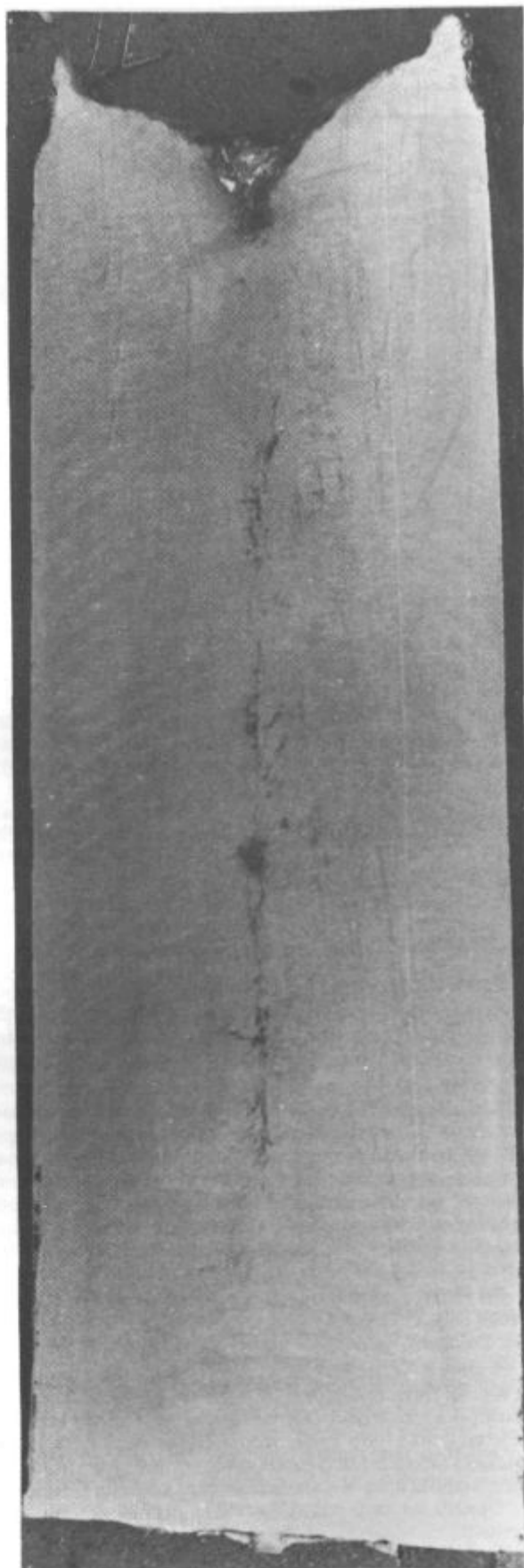
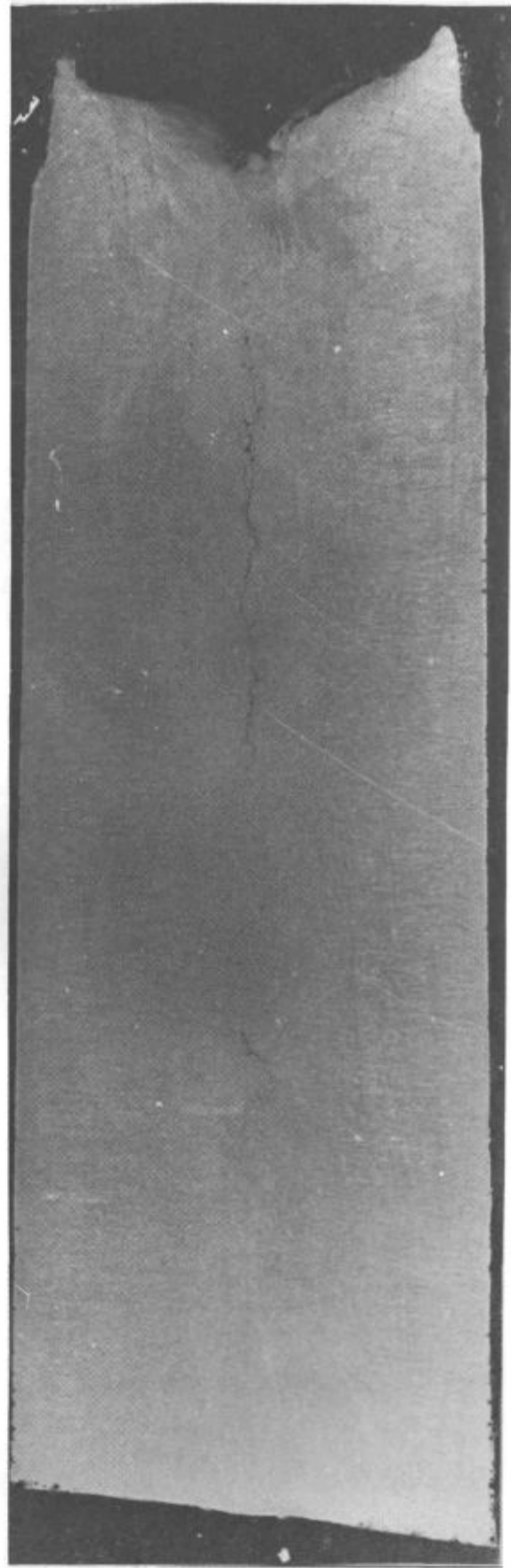
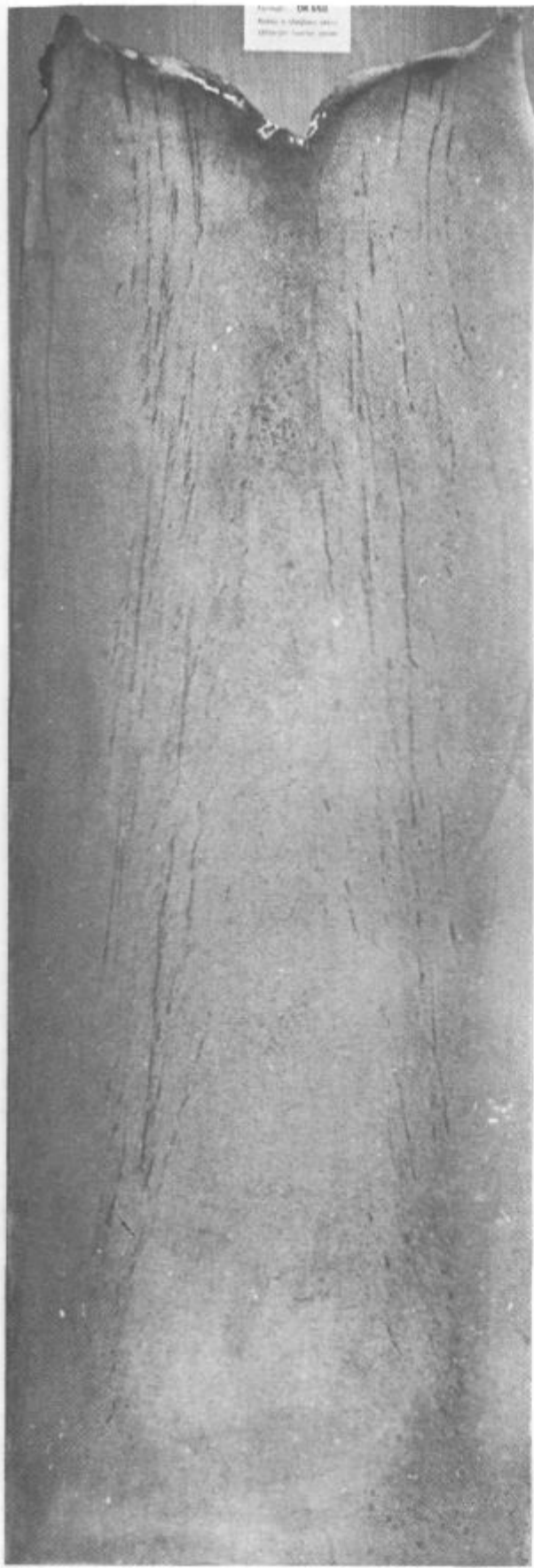


Fig. 4:

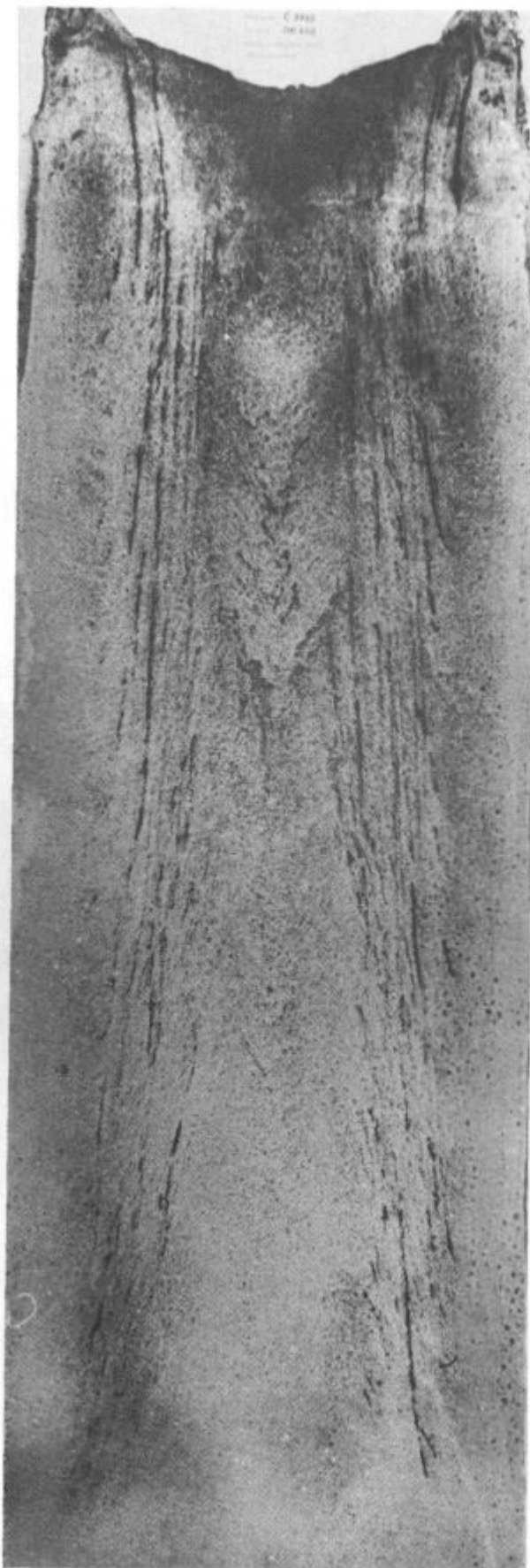
Ingot A — jedkana površina prereza  
the etched surface of the cross-section



**Fig. 5:**  
Ingot B — jedkana površina prereza  
the etched surface of the cross-section



**Slika 5:**  
Ingot B — odtis po Baumannu  
sulphur print



Slika 6:

Ingot C — odtis po Baumannu  
sulphur print

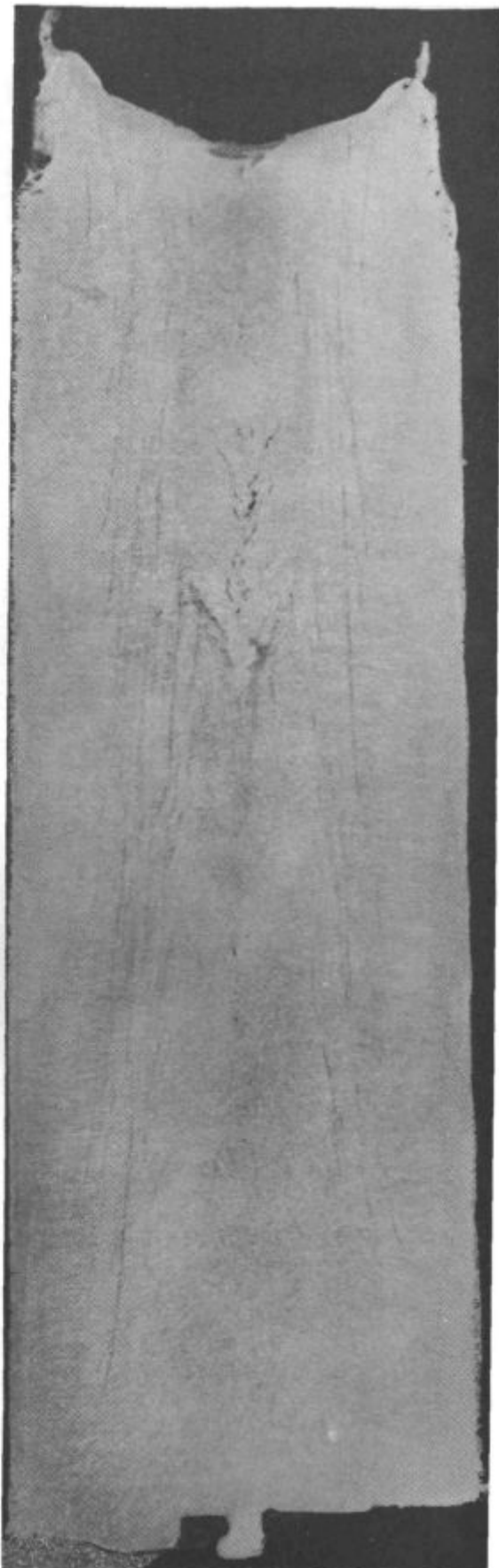


Fig. 6:

Ingot C — jedkana površina prereza  
the etched surface of the cross-section



Slika 7:

Ingot D — odtis po Baumannu  
sulphur print



Fig. 7:

Ingot D — jedkana površina prerezna  
the etched surface of the cross-section

Hoteli smo še bolj povečati izolacijske sposobnosti v zgornji polovici kokile, zato smo dodatno stanjšali steno kokile in spet uporabili perlit. V tem primeru smo namenoma šli v skrajnost glede debeline stene kokile. Po pričakovanju se je ta stena zelo močno ogrela, ponekod celo nad tališče perlita, zaradi česar smo morali perlit med samim strjevanjem dodajati. (Končno nam ga je celo nekoliko zmanjkalo). Stena kokile pa se je v zgornjem stanjanem delu toliko ogrela, da se je nekoliko usločila (napihnila se je) in smo jo morali končno razrezati, da smo dobili blok iz kokile.

Rezultat na sliki 7 pa je tisto, kar smo pričakovali.

V tem primeru je področje homogene strukture med obema paralelnimi potekajočima izcejama še širše, kot v primeru C. Če gledamo od roba proti sredini prereza, potem končne izceje, ki so še jasno izražene, nimajo več oblike črke A, ampak opazujemo namesto konice pri A dvoje paralelnih navpičnih črt. Izceje bi laže opisali z dvema polovicama na glavo postavljene črke Y, ki sta nekoliko razmagnjeni.

Razlika med slikama 4 in 7 je očitna.

Nekoliko pa nas je vseeno razočaral »V« v sredini prereza, saj ga v tem primeru nismo pričakovali. Pozneje smo našli razlago tudi za ta pojav.

## NAŠA HIPOTEZA STRJEVANJA JEKLA V KOKILI

Na osnovi rezultatov predhodnih računalniških obdelav in proučevanja slik 4—7 smo postavili naslednjo hipotezo o poteku strjevanja:

Problem prehoda toplotne med talino in kokilo opisuje več avtorjev. Nekateri govorijo o tanki plasti strjevega jekla, ki se tvori ob stiku taline s hladno kokilo. Ker se strjena »srajčka« skrči, odstopi od kokile. To pa povzroči, da se toplotni tok iz taline zmanjša in zato se »srajčka« ponovno pretali itd. To naj bi se periodično ponavljalo toliko časa, dokler se ne bi »srajčka« toliko zdebela, da se ne bi več pretalila in bi že vzdržala hidrostatični tlak.

Težko verjamemo, da bi prišlo do take periodične tvorbe »srajčke«, ki se enkrat dotika kokile, drugič pa spet ne.

Gre za neke vrste neidealnega kontakta. Po našem narašča koeficient prenosa toplotne od zgoraj navzdol zaradi večjega ferostatičnega tlaka. Iz taline torej odteka toplota v stene kokile, tako da se stene intenzivneje ogrevajo spodaj kot pa zgoraj. Talina se pri tem meša zaradi temperaturnih razlik. To pomeni, da se, po našem mnenju, vsa toplota, ki je shranjena v talini zaradi pregretja, odteče v stene kokile in jih neenakomerno ogreje (spodaj bolj, zgoraj manj), tako da temperatura stene kokile približno linearno narašča od zgoraj navzdol.

Pričakujemo, da ni bistvenih razlik v debelini »srajčke« zgoraj in spodaj v trenutku, ko ingot odstopi od stene kokile v celoti. Zgoraj se sicer zelo hitro naredi, vendar je tanka, saj je tudi ferostatični tlak manjši. Spodaj pa mora biti debelejša, saj blok kasneje odstopi od stene.

Ko blok po vsej višini odstopi od stene kokile, pa zaradi nadaljnega odtekanja toplotne narašča debelina strjene »srajčke«. To pa poteka v vsakem primeru hitreje v zgornjem delu kot pa v spodnjem.

Če namreč pomislimo, kolikšna je temperatura onstran zračne reže v steni kokile v zgornjem delu, je takoj jasno, da mora potekati strjevanje zgoraj hitreje. Spodnji deli kokile so se le precej bolj ogreli v tistem času, ko je bilo odtekanje toplotne v steno kokile zaradi nastajajoče »srajčke« intenzivnejše. Zato trdimo, da v nada-

was additionally reduced and the pearlite was used for the thermal insulation again. In this case we deliberately decided for an extreme situation concerning the thickness of the wall. As expected the wall became very hot and the temperature raised somewhere even above the melting point of the pearlite so that pearlite had to be added continuously during the process of solidification. (Before the end of the experiment practically all the isolating material available was used).

Due to rather high temperatures the wall of the mould became deformed in the upper thinner region so that the ingot had to be cut out of it.

The results shown in Fig. 7 are something what was expected before.

The region of the homogenous structure between both parallel flowing segregates is still larger than it is in the case C. Looking towards the center the final still recognizable A-segregates are no more of the form of the letter A. Instead of the top of A, two parallel vertical lines could be observed. The segregations could be better described by two separated halves of the inverted letter Y.

The differences between the Figs. 4 and 7 are evident. However the "V" in the middle of the cross-section in such an extreme case was not expected any more. An explanation also for this effect was found later.

## OUR HYPOTHESIS OF SOLIDIFICATION OF STEEL IN A MOULD

On the basis of the results of the computer simulations made before and from the careful examination of Figs. 4 to 7 the following hypothesis seems to be valid for the process of solidification.

The problem of the heat transfer between the mould and the liquid metal was described by several authors. Some of them suggest the formation of a very thin layer of solid steel (shell) formed at the contact of the liquid steel with the cold mould. Because the solid shell shrinks, an air gap is formed and it prevents the further heat flux from the inside of the liquid pool. The shell melts again and this process is supposed to be continued so long until the shell gets so thick that it does not melt any more and until it can endure the ferrostatic pressure of the liquid steel inside.

It can be hardly believed in the periodic formation of the shell that once sticks to the mould and then melts again. We mean that there must be some kind of non-ideal thermal contact. According to our vision we have to do with an increasing coefficient of the heat transfer when looking from the top to the bottom of the mould due to increasing ferrostatic pressure. From the liquid metal the heat flux flows into the mould so that the walls become more intensively heated at the bottom than at the top. We suppose that the liquid is mixing all the time due to temperature differences. It means that according to our idea all the superheat that is stored in the liquid metal, flows to the walls of the mould and warms them non-uniformly (more at the bottom and less at the top) so that the temperature of the mould wall increases approximately linearly from the top to the bottom.

We expect that there are not great differences between the thickness of the shell formed at the bottom and at the top in the moment of the formation of the air gap all along the length of the ingot. At the top a thin shell is formed very quickly together with the air gap because of very small ferrostatic pressure. At the bottom

Ijevanju strjevanja debelina stene narašča linearno od spodaj navzgor.

Tudi izceje v obliki črke A so v področjih bliže steni kokile praktično ravne črte, ki so enako strme v vseh štirih primerih.

To si razlagamo tako, ker mislimo, da v začetku strjevanja različna debelina stene v posameznih področjih kokile še ne pride do izraza. Kasneje pa se slika spremeni.

Zmanjšana topotna kapaciteta in povečana izolacija v primerih blokov B, C in D lahko znatno vplivata šele proti koncu strjevanja. Pri rekonstruirani kokili dobi torej talina proti koncu strjevanja obliko prisekanega stožca, ki se nadaljuje v valj. Sirina tega valja se veča od slike 4 proti sliki 7. Kljub temu, da pri sliki 7 nismo pričakovali mostu, pa je vseeno mogoče videti, da se je del izceje v obliki črke A v sredini ugreznil v obliku črke V, čeprav ne posebno globoko (manj, kot je pa to razvidno s slike 4). Tudi za to smo našli razlagi, ki je opisana v nadaljevanju.

## KAKO SI ZAMIŠLJAMO NASTANEK IZCEJ MnS

Ob fronti dendritov, ki rastejo pravokotno na mejo med tekočim in trdnim, se bogati talina z vsebnostjo MnS, tako da ni mogoče več »tolerirati« tolikšne koncentracije. Čisti kristali potiskajo pred seboj talino, ki postane prenasacišena. Zato naenkrat pride do izločanja MnS v obliki izceje, kar pa verjetno sprosti nekaj topote. To pomeni, da se v nadaljevanju prodiranje dendritov proti sredini nekoliko zaustavi, saj odtekanje te reakcijske toplotne ne povzroči rasti strjene plasti. V tem času ima tisti del taline ob strjeni steni možnost, da se v njem ponovno izenači koncentracija MnS. Pri tem ima odločilno vlogo temperatura oziroma konvekcijski in difuzijski procesi.

Ko reakcijska toplota odteče, se vse skupaj ponovi.

Tako si razlagamo nastanek izceje MnS v obliku črke A — nastanejo paralelne črte, pri katerih se medsebojna razdalja manjša, če gremo od roba proti sredini prereza.

Omenjena oblika »taline« v obliku prisekanega stožca, ki se nadaljuje v valj, pa po našem mnenju dobi lastnosti težko se premikajoče »marmelade«, ki se pri nadalnjem odvajjanju toplotne pretvorji v plastično maso, podobno pudingu in se krči kot celota.

Predstavljamo si, da je ta plastična talina nekako »obešena« na stene, ki so se že prej strdile.

Ko se sama skrči, potegne za seboj navzdol tudi dele stene, ki so že prej nastali, pa še niso dovolj trdni. Nastanejo izceje v obliku črke V.

Na to idejo nas je navedlo dejstvo, ki smo ga lahko opazovali pri vseh odtisih po Baumannu na slikah 4 do 7, da so namreč praktično pri vseh blokih tudi 0.5 metra nad osnovno ploskvijo bloka kristali deformirani, zavrhani navzdol, podobno kot se to vidi v področju izceje V.

V primeru D, ko imamo nad prisekanim stožcem izrazito širok valj, pa se kljub temu nismo mogli izogniti izcejam v obliku črke V v sredini prereza.

Na jedkanem obrusu pa se vidi, da je v tistem področju glave, ki je po navadi kritičen, v primeru D izredno homogena struktura. Trdimo, da smo v zgornjem delu glave dosegli, da je material izredno homogen in čist in zanj ni mogoče več trditi, da je prišlo pri krčenju do vdiranja nečistoč iz glave v sredino prereza. Edino izcejo v obliku črke V v sredini pri bloku D pa lahko razložimo takole:

the thickness is larger but the air gap is formed much later.

After the air gap is formed completely, the further heat flux into the mould causes the increasing of the thickness of the solid shell. This process is improving more quickly in the upper part than in the lower part of the ingot.

If we just consider the temperature of the mould wall across the air gap in the upper part, it becomes quite evident that the solidification must proceed more quickly there. The bottom of the mould accepted much more heat, because the heat flux into the wall due to higher ferrostatic pressure with the formation of shell, was more intense. We say that after the air gap is formed in the further process of solidification the thickness of the shell increases linearly from the bottom to the top of the ingot.

Even the A-segregations in the region closer to the wall are practically straight lines with nearly the same steepness in all four cases. This could be explained by the fact that at the beginning of solidification the influence of the different thick walls in different heights with the reconstructed mould can not play its role yet.

In the cases of ingots B, C and D the influence of the smaller thermal capacity of the wall and the increasing thermal isolation of the mould become considerable only at the end of the solidification process.

With the reconstructed mould towards the end of solidification the liquid gets the form of a truncated cone that is continuing into a cylinder. The diameter of this cylinder is increasing if Figs. 4 to 7 are compared.

Although with the ingot D (Fig. 7) no bridge is expected, it is possible to see one part of an A-segregate in the middle of the cross-section is bent down in the form of the letter V, but not so deeply as it could be seen in Fig. 4. The explanation to this effect is also found and it is given later.

## HOW WE IMAGINE THE FORMATION OF THE SEGREGATIONS OF MnS

With the growth of the dendritic crystals rectangularly to the boundary between the liquid and the solid phase, the liquid gets richer on MnS so that once it is not possible to tolerate such concentration any more. Pure crystals are pushing the oversaturated liquid in front of them. At a certain moment the MnS starts to segregate and it causes most probably the generation of a small amount of heat. This would mean that in due course the growth of dendrites towards the center stops a little, because the reaction heat that flows into the mould does not cause further growth of crystals.

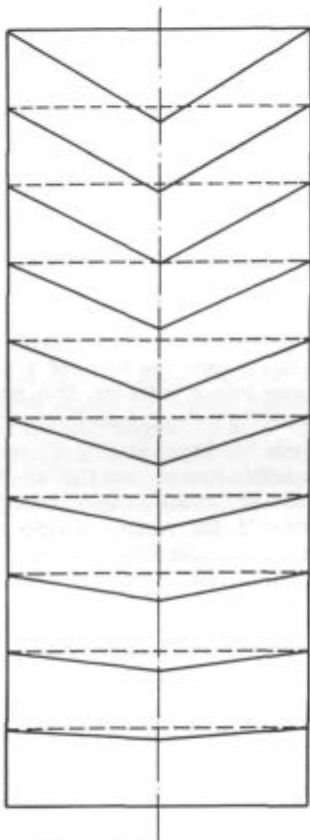
In this moment in the liquid region close to the solid shell the concentration of MnS equalizes again. Different diffusion and convective processes due to temperature differences are playing the most important role. When the flow of the reaction heat is finished, the whole story is repeated.

So we are explaining the formation of the A-segregates of MnS. The parallel lines can be observed and their mutual distance is decreasing when moving towards the center of the cross-section. The form of the liquid metal mentioned above in the form of a truncated cone continuing into a cylinder attains according to our assumptions the property of a very slowly moving "jam" that with the further cooling gets the properties of a

## IZCEJE V OBLIKI ČRKE V

Mislimo si, da ima talina obliko valja in da so stene tega valja trdne, narejene iz iste snovi. Ker se pri strjevanju zmanjšuje volumen, se pač lahko ugreza le sredina.

Predpostavljajmo, da valj razrežemo enakomerno na valjaste plasti po sliki 8. Volumen vsake od teh plasti se pri strjevanju zmanjša za 4 % in zgornja ploskev naj se ugrezne tako, da dobi obliko navzdol obrnjenega stožca. Na sliki 8 so s črtkano črto označene valjaste plasti taline, s polnimi črtami pa plasti, ki bi jih dobili po strjevanju. Takšno sliko bi dobili, če bi želeli, da ostane talina nekako »privezana« na stene valja.



Slika 8:  
Strjevanje taline valjaste oblike  
Fig. 8:  
Solidification of a cylindrical liquid.

### Drugi primer:

Mislimo si, da imamo namesto valjaste taline talino v obliki priskekanega stožca, ki pa naj ima, kot prej, trdno steno. Spet ga razrežemo na enako debele plasti in poskušajmo določiti, kako bi se morale ploskve med posameznimi plastmi deformirati, da bi talina ostala privezana na stene stožca. S slike 9 se vidi, da bi se morala potem ugnjetiti v sredini v zgornjem delu (9. plast na sliki 9) zgornja ploskev valjaste plasti bolj, kot se je ugnjetila spodnja ploskev te plasti ali talina se ne more strjevati tako, kot smo predpostavili, če naj bo »obešena« na stene stožca. Nujno potegne del strjene plasti na steni stožca navzdol, v sredino prereza bloka.

Ce gre za konično obliko taline, je mogoče celo izračunati, na kateri višini bi se to zgodilo, če bi šlo za krčenje v stožec.

plastic material similar to a jelly that shrinks as a whole in one piece.

We suppose that such a plastic "metal" is somehow hung on its boundary to the walls that have been solidified previously. When it shrinks, it pulls down also some parts of the wall, that are still plastic. So the V-segregations are formed.

This idea is supported by the fact that with all the sulphur prints from Figs. 4 to 7 in the structure found about 0.5 m above the basis of the ingot, the crystals are deformed similarly, as it can be seen in the region of the V-segregations above.

In the case of the ingot D where we have to do with a cylinder with a rather large diameter above the core the appearance of V-segregations could not be avoided. From the photo of the etched surface it could be seen that in the region that is normally critical, in the case of the ingot D the structure is extremely homogenous.

It could be stated that in the upper part of the ingot an extremely good and homogenous structure is achieved and it is no more possible to say that there are any impurities penetrating from the top into the middle of the ingot.

The only V-segregate in the middle of the ingot D can be explained in the following way.

## V-SEGREGATIONS

Let us suppose the liquid metal is of the form of a cylinder and the walls of this cylinder are solid, made of the same material. Due to shrinkage the volume gets smaller and the upper level moves down in the middle. Let us further suppose that the cylinder is cut uniformly to smaller equidistant layers according to Fig. 8. Due to solidification each layer shrinks for 4 % so that the upper flat circular surface moves down and it attains the form of an inverted cone. In Fig. 8 the subsequent cylindrical layers are indicated by dotted lines. The full lines indicate the form of these layers after the solidification. Such picture would be obtained if the liquid stays attached to the walls of the cylinder.

Another example:

If instead of a cylinder we have to do with a conical form of the liquid steel attached to solid walls of the same material. Let us again cut it into parallel layers of equal thickness and let us try to find out, how the flat basic surfaces of these layers would be deformed at solidification, if the liquid stays attached to the conical walls.

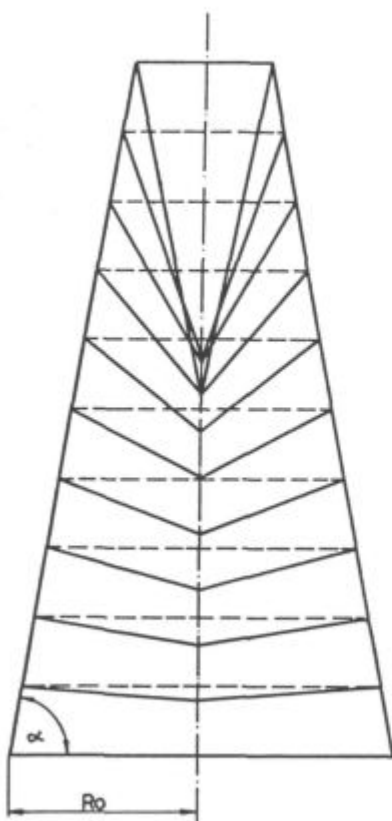
From Fig. 9 it can be seen that something new must happen if we want to fulfil previous condition.

According to Fig. 9 the upper surface of the 9th layer should move towards the center much deeper than the lower surface. With the other words:

The liquid metal can not be solidified in this way. It necessarily pulls a piece of the solid wall down into the middle of the cross-section of the ingot.

If the form of the liquid metal is conical, it is possible to evaluate also mathematically where it happens, if the basic surfaces of the subsequent layers get the form of an inverted cone.

Let the volume of the liquid steel of the form of a truncated cone with the radius  $R_0$  and with the angle  $\alpha$  (Fig. 9) be reduced for  $\eta$  in the process of solidification. The upper level is supposed to be lowered so that it stays attached to the conical wall. In the middle it attains the form of an inverted cone. The critical height, where



Slika 9:  
Strjevanje taline konične oblike  
**Fig. 9:**  
Solidification of a conical liquid.

Pri talini, ki ima obliko pokončnega prisekanega stožca, pri katerem je kot med stranskim robom osnega prereza in radijem  $\alpha$  in polmer osnovne ploskve  $R_o$ , naj se volumen pri strjevanju zmanjša za  $\eta$ . Gladina naj se ugrezne tako, da ostane na robu »privezana« na steno stožca, v sredini pa naj dobi obliko stožca, ki je z vrhom obrnjen navzdol. Kritična višina, pri kateri se v takem primeru prvič »strga« stena in ugrezne navzdol, se izračuna po formuli:

$$H = R_o \cdot \operatorname{tg} \alpha \cdot \left( 1 - \sqrt[3]{\frac{2\eta}{1-\eta}} \right)$$

Če se to ne bi zgodilo, bi se sicer morala zgornja ploskev 9. valjaste plasti po sliki 9 ugrezniti bolj kot spodnja. S slike 4 lahko ocenimo, da je približno  $\operatorname{tg} \alpha \approx 10$  in če je  $\eta = 0.04$ , lahko ocenujemo, da se bo pojavil prvi ugrez približno 1.5 metra nad osnovno ploskvijo ingota.

Natančnejši izračuni pa kažejo, da se pri pogojih strjevanja valjasta plast taline v sredini ugrezne celo nekoliko bolj, kot če bi šlo za ugrezanje v obliku stožca.

V primeru D opazujemo le eno večjo izcejo v obliki črke V v zgornjem delu prereza bloka, nekako tam, kjer se stožasti del konča in začenja valjasti del. To je razumljivo, saj smo s stanjšano steno kokile dosegli, da se stožec nadaljuje v dosti širok valj.

## ZAKLJUČEK

1. Na potek izcej in na strukturo v prerezu jeklenega bloka, ki je bil ulit v kokilo, lahko vplivamo s primerno regulacijo hitrosti strjevanja.

2. Z rekonstruirano kokilo smo nakazali, kako je mogoče odpraviti sekundarni lunker, rahlo sredino in povečano koncentracijo nečistoč v sredini bloka.

the boundary tears off and slips down, can be calculated from the following relationship:

$$H = R_o \cdot \operatorname{tg} \alpha \cdot \left( 1 - \sqrt[3]{\frac{2\eta}{1-\eta}} \right)$$

If it does not happen, the upper surface of the 9th layer according to Fig. 9 should be lowered deeper than the bottom surface of the same layer. From Fig. 4 it can be estimated that  $\operatorname{tg} \alpha \approx 10$  and if  $\eta = 0.04$  we can calculate the position of the first V-segregate. It would appear approximately 1.5 m above the basis of the ingot.

From more precise calculations it is evident that the lowering of the middle of the surface of a layer would be even deeper than it is the case with the inverted cone, if the real shrinkage is taken into account.

In the case of the ingot D only one V-segregate in the upper part of the ingot can be observed just in the place where the cone starts to continue into the cylinder. The thinner wall in the upper part of the mould thus enables the formation of a cylinder with a large diameter.

## CONCLUSION

1. The course of segregates and the structure in the cross-section of a steel ingot cast into a mould can be modified by a proper regulation of the speed of solidification.

2. With the reconstructed mould it is shown how the secondary shrinkage hole can be suppressed together with the "soft middle" and with the increased concentration of impurities in the middle of ingot.

3. Since with a proper form of the mould wall the homogeneity of the upper part of the ingot can be considerably increased it could be expected that difficulties

3. Ker znamo s primerno obliko kokile znatno povečati homogenost v zgornjem delu bloka, pričakujemo, da bi s tem odpravili težave, ki se pojavljajo pri valjanju nekaterih kvalitet zaradi nehomogenosti v sredini (dvo-plastnost in podobno).

4. To trditev bo treba še praktično preveriti. Nova oblika kokile bo seveda nekoliko drugačna. Opisani poskusi bodo služili za izhodišče za delo v proizvodnji.

5. Odpirajo se možnosti za razvoj računalniškega krmiljenja in avtomatizacijo ohlajanja tudi ulitih blokov drugačnih oblik, kar je še posebno pomembno v likarstvu.

appearing with the rolling of some qualities of steel slabs due to inhomogeneities in the middle could be avoided.

4. This statement must be also verified practically. The form of the reconstructed mould for practical purposes will be a little different. The results of the experiments discussed above will be starting point for the practical measures.

5. New possibilities in the development of the computer regulation and automation of process of cooling of the cast steel ingots of different forms seem to be opened. It would be very important especially for the technological development in foundries.

#### LITERATURA/REFERENCES

- P. N. Hansen: Numerical simulations of the solidification proces, 350—356, Solidification and Casting of Metals, Proceedings of International conference on Solidification, University Sheffield, 18—21 July 1977
- F. Weinberg, J. Lait, R. Pugh: Solidification of high carbon steel ingots, 334—339, Solidification and Casting of Metals, Proceedings of International conference on Solidification, University Sheffield, 18—21 July 1977
- F. Oeters, K. Rüttiger, H. J. Selenz: Wärmeübergang beim Blockguss, Giessen und Erstarren von Stahl, Band I., 144—195 Informationstagung, Luxembourg
- R. D. Pehlke, J. T. Berry, W. Erickson, C. H. Jacobs: Simulation of shaped casting solidification, 371—379, Solidification and Casting of Metals, Proceedings of International conference on Solidification, University Sheffield, 18—21 July 1977
- P. R. Beeley: Keynote Address Solidification and aspects of cast metal quality, 319—324, Solidification and Casting of Metals, Proceedings of International conference on Solidification, University Sheffield, 18—21 July 1977
- F. Oeters, K. Sardemann: Untersuchungen zum zeitlichen Verlauf der Erstarrung in der Randzone erstarrenden Eisens, Arch. Eisenhüttenwes. 45, (1974), 8, August, 517—524
- K. Schwerdtfeger: Anwendung der Methode des Wärmebilanzintegrals zur Berechnung der Erstarrungsgeschwindigkeit von Eisen-Kohlenstoff-Legierungen, Arch. Eisenhüttenwes. 44 (1973) 6, Juni, 411—418
- W. Schwarz, R. Jeschar: Thermohydraulisches Analogiemodell zur Simulation der Blockerstarrung, Arch. Eisenhüttenwes. 44 (1973), 6, Juni, 419—425
- Y. K. Chuang, K. Schwerdtfeger: Experimentelle und theoretische Untersuchung der Erstarrung einer Eisen-Kohlenstoff-Legierung mit 0.6 % C, Arch. Eisenhüttenwes. 44 (1973), 5, Mai, 341—347
- J. Szekely, N. J. Themelis: Rate Phenomena in Process Metallurgy John Wiley & Sons Inc., New York 1971
- T. Takahashi, K. Ichikawa, M. Kudou: Effect of fluid flow on macrosegregation in steel ingots 331—333, Solidification and Casting of Metals, Proceedings of International conference on Solidification, University Sheffield, 18—21 July 1977
- J. Froeber, F. Oeters: On the mechanical behaviour of steel during solidification, Arch. Eisenhüttenwes. 51 (1980) 2, Februar, 43—49
- R. Jha, T. Mukerjee: Shrinkage at peritectic temperature — its influence on cracking of steel ingots, Transactions of the Indian Institute of Metals, Vol. 29, 1, Feb. 1976, 30—35
- T. Kolenko, B. Brdar, F. Mlakar, V. Tucić, S. Paulin: Vpliv oblike in forme na strjevanje ulitih valjev, Poročilo VTOZD Montanistika, December 1983
- R. A. Entwistle, J. E. Gruzleski, P. M. Thomas: Development of porosity in aluminium-base alloys, 345—349, Solidification and Casting of Metals, Proceedings of International conference on Solidification, University Sheffield, 18—21 July 1977
- A. Razinger: Mehanizem porazdelitve svinca v jeklu in njegov vpliv na strukturne in fizikalne lastnosti v odvisnosti od prisotnih elementov, Magistrsko delo, Univerza v Ljubljani, FNT, Oddelek za montanistiko, odsek za metalurgijo, 1973
- A. J. Pokorny: De Ferri Metallographia III, 1967, Solidification of Steel, IRSID, Editor Berger — Levraut, Paris
- P. Oberhoffer: Das technische Eisen, S. 311, Julius Springer Verlag, Berlin 1936
- Ju. Ja. Skok, G. A. Lubenec, F. I. Nečeporenko, V. M. Dorefev, Z. L. Kozlova: Sniženje zonalnoj himičeskoj neodnorodnosti slitkov putem modificiranija stali, stal, 1986, 2, 19—22
- F. Beneš, L. Beračkova, M. Kepka, L. Novak: Nestejnородnosti v ingotech o velikih hmotnosech, Hutnické listy, 1986, č. 2, 87—92
- F. Esser, H. Brennecke: Rechnersimulation der Blockerstarrung in einer Kokille unter besonderer Berücksichtigung des Wärmekontakts Block/Kokille, Neue Hütte, 24, 1979, 12, 455—459

# Bele kromove litine za valje, legirane z molibdenom

## White Chromium Cast Irons for Rolls, Alloyed with Molybdenum

D. Kmetič\*, F. Mlakar\*\*, V. Tucić\*\*, J. Žvokelj\*,  
F. Vodopivec\*, M. Jakupovič\*, B. Ralić\*

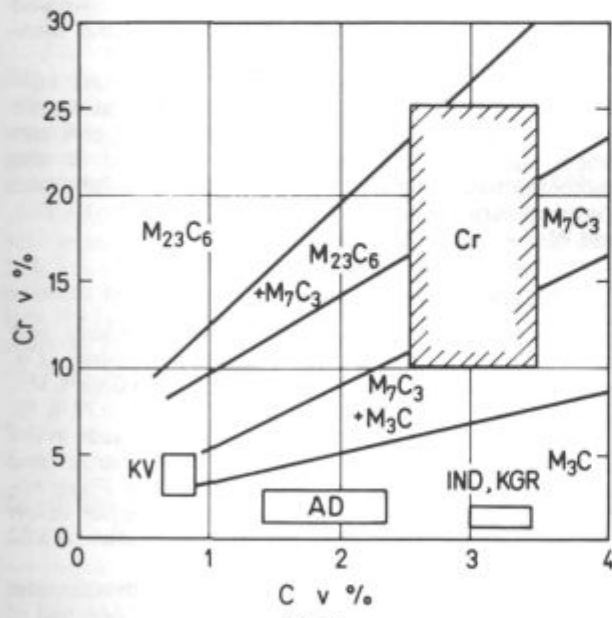
UDK: 669.15'26—194:669.14.018.255  
ASM/SLA: M28, N8b, TSk, 5, Cr, W23k

Kromove bele litine, legirane z molibdenom in še nekaterimi drugimi elementi, se zaradi dobre obrabne obstojnosti, trdote in zadovoljivih mehanskih lastnosti vedno več uporablajo za dvošlojne lite valje. Litine imajo tudi dobro korozionsko obstojnost.

Delo obravnava mikrostrukturne značilnosti zlitin v litem stanju in po topotni obdelavi. Narejena sta izotermska transformacijska diagrama za destabilizacijo avstenita in destabiliziran avstenit in kontinuirni transformacijski diagram za destabiliziran avstenit.

### UVOD

V valjarnah je poleg ustrezne kvalitete valjanih proizvodov zelo pomembna ekonomičnost proizvodnje. Določena jekla se vroče valjajo v nizkih temperaturnih



Sl. 1:

Kemična sestava belih kromovih litin in litin za druge vrste valjev v faznem diagramu (KV — kovani valji, AD — adamitni valji, IND — indefinitni valji, KGR — nodularni valji, Cr — bele kromove litine, 8)

Fig. 1

Chemical composition of white chromium cast irons, and cast irons for other types of rolls in the phase diagram (KV — forged rolls, AD — adamite rolls, IND — indefinite chill rolls, KGR — spheroidal-graphite rolls, Cr — white chromium cast irons, 8)

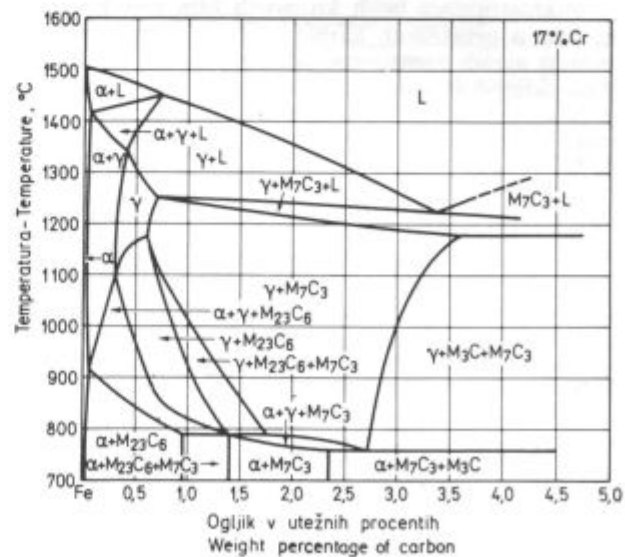
Chromium white cast irons alloyed with molybdenum and some other elements are more and more applied for compound cast rolls due to good wear resistance, hardness, and satisfactory mechanical properties. The cast irons have also good corrosion properties.

Paper treats the microstructural characteristics of cast irons as cast, and after the heat treatment. Isothermal transformation diagrams for the destabilization of austenite, and for the destabilized austenite were constructed next to the continuous transformation diagram for the destabilized austenite.

### INTRODUCTION

In rolling plants, the economy of manufacturing is very important next to the suitable quality of rolled products. Some steel is hot rolled in low-temperature regions with high partial reductions, and low permissible dimensional tolerances. Narrower and narrower tolerances are demanded also for the cold rolled strips. These are the reasons that rolls of white cast iron with high chromium content, and alloyed with Mo, Ni (Cu), V, Ti, and W are more and more used in hot and cold rolling plants. The rolls are cast by a compound centrifugal casting.

Data on chemical composition of rolls of white chromium cast irons are in references given in wide intervals. Data on manufacturing rolls, and on their heat treatment are scarce. The phase diagram in Fig. 1 pres-



Sl. 2:

Fazni diagram Fe-Cr-C za 17 % Cr

Fig. 2

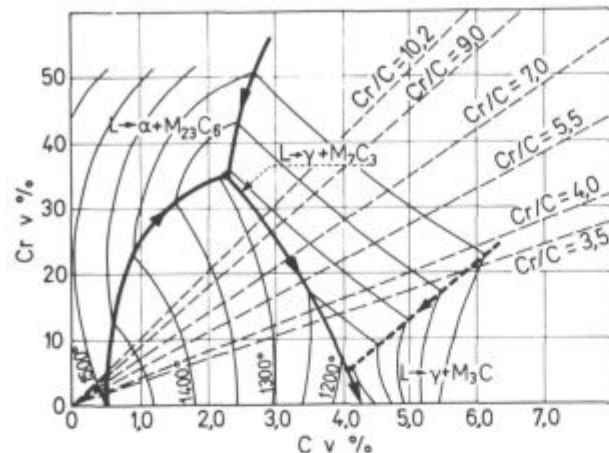
Fe-Cr-C phase diagram at 17 % Cr

\* SŽ — Metalurški inštitut Ljubljana

\*\* SŽ — Železarna Štore

\* Institute of Metallurgy, Ljubljana

\*\* Štore Ironworks



Sl. 3:  
Likvidus površine in lega zlitin glede na razmerje Cr/C v faznem diagramu Fe-Cr-C po R. S. Jacksonu (1)

Fig. 3

Liquidus surfaces and the position of alloys related to the Cr/C ratio in the Fe-Cr-C phase diagram, according to R. S. Jackson (1)

področjih z velikimi parcialnimi redukcijami, pri čemer se zahtevajo ozke dimenzijske tolerance. Vedno bolj ozke tolerance se zahtevajo tudi pri hladno valjanih trakovih. To so razlogi, da se v vročih in hladnih valjarnah vedno bolj uporabljajo valji iz bele litine z visoko vsebnostjo Cr, legirane še z Mo, Ni (Cu), V, Ti in W. Valji se izdelujejo po postopku dvoslojnega centrifugalnega litija.

Literaturni podatki o kemični sestavi valjev iz bele kromove litine so podani v širokih mejah. Podatki o izdelavi valjev in topotni obdelavi so zelo skopi. V faznem diagramu na sliki 1 je za primerjavo navedeno področje kemične sestave valjev iz bele kromove litine in drugih vrst valjev.

Zlitine Fe-Cr-C so že dolgo poznane in so v literaturi opisane številne raziskave. Fazni diagram Fe-Cr-C za 17 % Cr je prikazan na sliki 2 (3). Za razvoj teh zlitin so poleg začetnih raziskav F. Osmonda, ki je v mikrostrukturi omenjenih litin že leta 1892 opazil kompleksne karbide, najpomembnejše raziskave R. S. Jacksona, ki je v faznem diagramu Fe-Cr-C opredelil likvidus površine (sl. 3) in sistematične raziskave vpliva Mo na mikrostrukturne značilnosti, ki sta jih naredila F. Maratray in R. Usseglio-Nanot (1, 2, 4).

Mikrostruktura belih kromovih litin sestoji iz primarnih in evtektičnih karbidov in avstenitne maticice, oziroma njenih transformacijskih produktov (sekundarni karbidi, perlit, bainit, martenzit). Za mikrostrukturne značilnosti je zelo pomembno razmerje Cr/C in vsebnost legiranih elementov, predvsem Mo, Mn, Ni (Cu) in W.

## EKSPERIMENTALNO DELO

Na osnovi literaturnih podatkov, ki smo jih imeli na voljo, smo v železarni Štore izdelali preizkusne taline z različno vsebnostjo legirnih elementov, in sicer z 2,5 do 3,8 % C, 11,3 do 19,4 % Cr, 0,39 do 0,66 % Mo, 0,59 do 1,37 % Si, 0,68 do 0,93 % Mn, 0,56 do 0,78 % Ni, 0,023 do 0,11 % Ti in z 0,06 do 0,11 % V. Štiri zlitine smo legirali z 0,80 do 0,93 % W. Zlitine legirane z W so trše in se uporabljajo za valje za hladno valjanje trakov. Vsebnost P mora biti pod 0,08 % in S pod 0,05 %. Preizkusne zlitine imajo razmerje Cr/C od 3,62 do 7,76.

Vzorce, preizkusne valjčke, premera 100 in višine 150 mm, smo ulili tako, da je bila polovica valjčka ulita v kokilo in polovica v pesek. Tako smo dobili na enem vzorcu dve različni hitrosti strjevanja.

Pogoji litja bistveno vplivajo na izoblikovanje mikrostrukture in s tem na mehanske lastnosti litine. Zato

ents the regions of chemical compositions of rolls of white chromium cast iron, and of some other types of rolls (8).

Fe-Cr-C alloys are already for a long time known, and numerous investigations are cited in references. The Fe-Cr-C phase diagram for 17 % Cr is shown in Fig. 2 (3). For development of these alloys, the most essential are the investigations by R. S. Jackson who determined the liquidus surfaces in the Fe-Cr-C phase diagram (Fig. 3), and the systematic investigations on the influence of Mo on the microstructural characteristics done by F. Maratray, and R. Usseglio — Nanot, beside the initial investigations by F. Osmond who already in 1892 observed complex carbides in the microstructure of the mentioned cast irons (1, 2, 4).

Microstructure of white chromium cast irons consists of primary and eutectic carbides, and austenitic matrix, or of its transformation products (secondary carbides, pearlite, bainite, martensite). Essential for the microstructural characteristics are the Cr/C ratio and the content of alloying elements, mainly Mo, Mn, Ni (Cu), and W.

## EXPERIMENTAL WORK

Based on the data in references, being available, test melts with various contents of alloying elements, i.e. with 2.5 to 3.8 % C, 11.3 to 19.4 % Cr, 0.39 to 0.66 % Mo, 0.59 to 1.37 % Si, 0.68 to 0.93 % Mn, 0.56 to 0.78 % Ni, 0.023 to 0.11 % Ti, and 0.06 to 0.11 % V were made in the Štore Ironworks. Alloys with added W are harder and they are used for rolls for cold rolling of strips. Phosphorus content must be below 0.08 %, and sulphur below 0.05 %. The test melts had the Cr/C ratio between 3.62 and 7.76.

The samples as testing cylinders with diameter 100 mm and 150 mm high were cast so that one half of the cylinder was cast into mould, another one into sand. Thus two various solidification rates were obtained on the same specimen.

Casting conditions have essential influence on the formation of microstructure, and thus on the mechanical properties. Therefore melting points and solidification intervals were determined for some alloys.

Microstructural characteristics of as cast alloys, and after the heat treatment were determined by investigations with optical microscope, scanning electron microscope (SEM), and electron microanalyzer. To reveal the microstructural characteristics various etching agents (nital, Villela's, ferric chloride, alkaline picrate, Murakami's, and 4 % sodium hydroxide saturated with pota-

smo za nekatere zlitine določili temperature tališča in interval strjevanja.

Mikrostrukturne značilnosti zlitin vitem stanju in po topotni obdelavi smo opredelili s preiskavami z optičnim mikroskopom, v raster elektronskem mikroskopu (SEM) in v elektronskem mikroanalizatorju. Za odpravljanje mikrostrukturnih značilnosti smo uporabili različna jedkala (nital, Villela, feriklorid, alkalijski pikrat, Murakami in 4 % natrijev hidroksid, nasičen s kalijevim permanganatom). Sekundarne karbide in faze, nastale pri transformaciji avstenita, smo lahko dobro opredelili v SEM. V elektronskem mikroanalizatorju smo določili sestavo primarnih in evtektičnih karbidov in koncentracije nekaterih legirnih elementov v matici.

Za eno od zlitin z najstreznejšo kemično sestavo in mikrostrukturo smo naredili izotermska transformacijska diagrama za nedestabilizirano in destabilizirano avstenitno matico in kontinuirni transformacijski diagram za destabiliziran avstenit.

Od mehanskih lastnosti smo merili le trdoto zlitin in posameznih mikrostrukturnih faz. V literaturi smo sledili raziskave, ki obravnavajo upogibno trdnost in žilavost teh zlitin (13). Za valje je poznavanje teh parametrov zelo pomembno, vendar smo zaradi težavne priprave mehanskih preizkušancev te preiskave odložili na kasnejši čas.

## REZULTATI PREISKAV

### Tališča in interval strjevanja zlitin

Žilavost in obrabna obstojnost litine je tem boljša, čim bolj drobni so evtektični karbidi in čim enakomerne so porazdeljeni po matici. (19) Zato mora potekati strjevanje belih kromovih litin hitro. Pri previsokem pregrevu in počasnem strjevanju lahko nastanejo poleg grobih evtektičnih klarbidov še veliki primarni karbidi.

V talilnem mikroskopu smo določili tališča in interval taljenja nekaterih zlitin, izbranih tako, da smo pokrili ves interval razmerij Cr/C (tabela 1). Zaradi rekalcescence je razlika med talilnim in strjevalnim intervalom majhna. Zlitine so močno izcejane in se rezultati paralelk in vrednosti, izmerjene večkrat na istem vzoru, med seboj precej razlikujejo.

Tabela 1: Tališča in intervali taljenja

Zlitina	% C	% Cr	Cr/C	Nastanek kapljic °C	Začetek talj. °C	Staljeno °C	Interval talj. °C
1	2,49	19,31	7,76	1200	1245	1345	100
2	2,63	19,43	7,39	1170	1220	1350	130 (legirano z W)
3	2,72	14,90	5,48	1200	1250	1305	55
4	2,76	19,21	6,96	1210	1250	1325	75
5	3,20	17,95	5,61	1210	1250	1285	35
7	3,31	11,97	3,62	1190	1225	1300	75
8	3,48	16,23	4,66	1170	1215	1250	35 (legirano z W)

Zlitine imajo tališča med 1350 in 1250 °C. Čim bolje sestava zlitine približuje evtektični sestavi, ožji je interval strjevanja. Na sliki 2 se vidi, da ima zlina s 17 % Cr evtektično sestavo pri 3,4 % C. Na tališče in

ssium permanganate) were applied. Secondary carbides, and phases formed during the transformation of austenite were well determined by SEM. Electron micro-analyzer helped us to determine the composition of primary and eutectic carbides, and the concentrations of some alloying elements in the matrix.

For one of the alloys, with the most suitable chemical composition and the microstructure, the isothermal transformation diagrams for undestabilized and destabilized austenitic matrix, and the continuous transformation diagram for destabilized austenite were constructed.

Of mechanical properties only hardness of alloys and of single microstructural phases was measured. In references, investigations treating the bending strength, and the toughness of these alloys were found (13). Though the knowledge of these properties is very important for the behaviour of rolls, these investigations were postponed for later due to difficult preparation of testing specimens.

## RESULTS OF INVESTIGATIONS

### Melting Points and Solidification Interval of Alloys

Toughness and wear resistance of the alloy are the better the smaller are eutectic carbides, and the more uniformly they are distributed in the matrix (19). Therefore the solidification of white chromium cast irons must be fast. At a too high superheating and low solidification rate big primary carbides next to coarse eutectic carbides can be formed.

Melting points and solidification intervals of some alloys were determined by fusion microscope. The alloys were chosen in such a way that the whole interval of the Cr/C ratios was covered (Table 1). Due to recalescence the difference between the melting and the solidification interval is small. The alloys exhibit intensive segregating, thus the results of parallel tests, and the values measured more times on the same sample differ a great deal.

Table 1 Melting Points and Solidification Intervals

Alloy	% C	% Cr	Cr/C	Formation of drops		Begin. of melting °C	Melted °C	Melting interval °C
				°C	°C			
1	2,49	19,31	7,76	1200	1245	1200	1345	100
2	2,63	19,43	7,39	1170	1220	1170	1350	130 (allayed with W)
3	2,72	14,90	5,48	1200	1250	1200	1305	55
4	2,76	19,21	6,96	1210	1250	1210	1325	75
5	3,20	17,95	5,61	1210	1250	1210	1285	35
7	3,31	11,97	3,62	1190	1225	1190	1300	75
8	3,48	16,23	4,66	1170	1215	1170	1250	35 (allayed with W)

The alloys have the melting points between 1350 and 1250 °C. The closer is the alloy composition to the eutectic composition the narrower is the solidification interval. It is evident from the Fig. 2 that the alloy with 17 % Cr has eutectic composition at 3,4 % C. The melting points and the solidification intervals are mainly influenced by the carbon content, to a lesser extent by the Cr/C ratio,

interval strjevanja vpliva predvsem vsebnost ogljika, manj pa razmerje Cr/C in koncentracije ostalih legirnih elementov. Od vsebnosti ogljika, ki sicer znižuje temperaturo tališča, in razmerja Cr/C je odvisen delež karbidne faze v mikrostrukturi, kar tudi vpliva na tališče in interval strjevanja zlitin. Iz faznih diagramov Fe-Cr-C se vidi, da se z naraščajočo vsebnostjo Cr evtektična točka pomika v levo in k višjim temperaturam.

#### Mikrostruktura zlitin v litem stanju

Mikrostruktura zlitin je odvisna od kemične sestave, razmerja Cr/C in pogojev strjevanja. Vse zlitine smo legirali z Mo, zato imajo v mikrostrukturi poleg primarnih in evtektičnih karbidov  $M_7C_3$  tudi karbide  $Mo_2C$ .

Mikrostruktura evtektika je odvisna od deleža austenitne faze, ki nastaja med procesom strjevanja. Če nastane med strjevanjem veliko avstenita in je majhen delež preostale taline, ki se strdi kot evtektik, imajo evtektični karbidi tendenco, da segregirajo vzdolž kristalnih mej avstenitnih zrn. Take mikrostrukture, ki je značilna za zlitine z do 20 % karbidne faze, pri naših zlitinah, ki imajo od 25 do 35 % karbidne faze, nismo opazili.

V nekaterih zlitinah smo opazili v evtektiku bolj ali manj lamelarno izoblikovane karbide, ki rastejo iz sredine meddendritskih prostorov (sl. 4). Pri drugih zlitinah, pri katerih je avstenitne faze zelo malo in ta praktično ni omejevala strjevanja evtektika, imajo karbidi polpolnoma lamelarno obliko (sl. 5). Čeprav so veliki primarni karbidi heksagonalne oblike značilni za litine z nad 35 % karbidne faze, smo te opazili tudi pri nekaterih naših zlitinah, in to predvsem na sredini preizkusnih valjčkov, kjer so bili za njihov nastanek ustreznejši pogoji (sl. 6).

Deleže karbidne faze v mikrostrukturi smo za nekatere zlitine izračunali po enačbi (1):

$$\% K = 12,33 (\% C) + 0,55 (\% Cr) - 15,2$$

Izračunane vrednosti se dobro ujemajo z vrednostmi, ki smo jih dobili z meritvami po linearini intercepčijski metodi v optičnem mikroskopu (tabela 2). Vsebnosti Mo in W sta majhni in ne vplivata bistveno na delež karbidne faze.

Tabela 2: Delež karbidne faze (% K) v mikrostrukturi

Zlina	Cr/C	% C	% Cr	% K izračunan	% K izmerje
7	3,62	3,31	11,97	32,2	30
6	4,80	3,21	15,42	32,9	29
3	5,48	2,72	14,90	26,5	26
5	5,61	3,20	17,95	34,1	35
2	7,39	2,62	19,43	27,9	28
1	7,76	2,49	19,31	26,1	25

Mikrostruktura matice je odvisna od razmerja Cr/C, vsebnosti Mo in pogojev ohlajevanja. Matica ima v litem stanju avstenitno mikrostrukturo, oz. je med ohlajanjem potekla delna ali popolna transformacija avstenita v perlit. Pri litju v kokilo potekata strjevanje in ohlajanje hitreje, kot pri litju v pesek, in perlitna transformacija je zavrtala. Pri zlitinah brez Mo lahko pričakujemo popolnoma avstenitno matico pri razmerju Cr/C večjem od 7,2 (1,2). Z legiranjem z Mo se razmerje Cr/C, pri katerem dobimo popolnoma avstenitno matico, pomika proti nižjim vrednostim. To pomeni, da ima lahko litina pri isti vsebnosti Cr več C in zato v mikrostrukturi večji delež karbidne faze in avstenitno matico.

and the concentration of the other alloying elements. The carbon content which namely reduces the melting point, and the Cr/C ratio determine the amount of carbide phase in the microstructure which has also influence on the melting point and the solidification interval of alloys. The Fe-Cr-C phase diagrams show that the increasing Cr content shifts the eutectic point towards the left and to higher temperatures.

#### Microstructure of As Cast Alloys

Microstructure of alloys depends on the chemical composition, the Cr/C ratio, and the conditions of solidification. All the alloys were alloyed with Mo, thus the microstructure contains also  $Mo_2C$  carbides next to the primary and eutectic  $M_7C_3$  carbides.

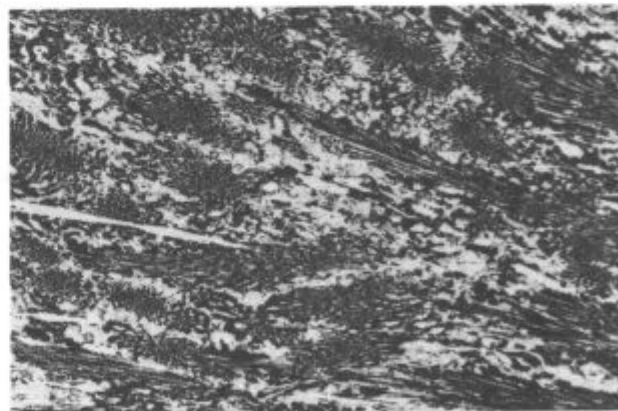
Microstructure of eutectic depends on the amount of austenitic phase which is formed during the solidification. If a high amount of austenite is formed during the solidification, and the portion of the remaining melt which solidifies eutectically is small, the eutectic carbides exhibit tendency to segregate along the boundaries of austenitic grains. Such a microstructure being characteristic for the alloys with up to 20 % of carbide phase was not observed in our alloys which contained 25 to 35 % of carbide phase.

In some alloys more or less lamellar carbides were observed which grow from the centre of interdendritic spaces (Fig. 4). In other alloys with a very low amount of austenitic phase which did not hinder the solidification of eutectic, the carbides exhibited fully lamellar shape (Fig. 5). Though big primary carbides of hexagonal shape are characteristic for the cast irons with over 35 % of carbide phase, they were observed also in some of our alloys, but mainly in the centre of the testing cylinders where the conditions for their formation were the most suitable (Fig. 6).

The portions of carbide phase in the microstructure was for some alloys evaluated by the equation (1):

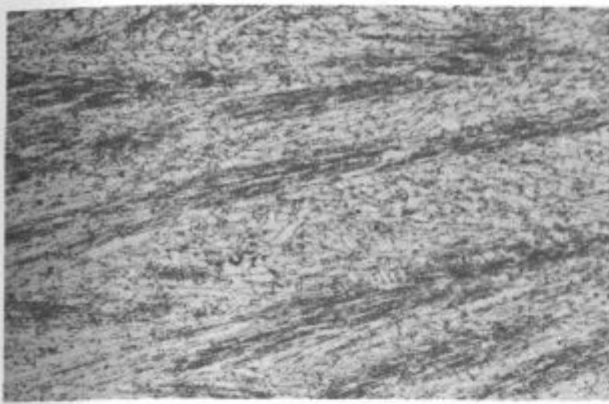
$$\% K = 12,33 (\% C) + 0,55 (\% Cr) - 15,2$$

The obtained values are in a good agreement with the values which were obtained by the measurements in optical microscope by the intercept method (Table 2). Contents of Mo and W are low and they do not influence essentially the portion of carbide phase.



Sl. 4:  
Eutektični karbidi rastejo iz sredine meddendritskih prostorov, lito stanje (3,21 % C, 15,42 % Cr, 0,53 % Mo, Cr/C 4,80). Pov. 100 x

Fig. 4  
Eutectic carbides grow from the centre of interdendritic spaces, as cast (3.21 % C, 15.42 % Cr, 0.53 % Mo, Cr/C 4.80). Magn. 100 x



Sl. 5:

Lamelarni eutektični karbidi, lito stanje (3,20 % C, 17,95 % Cr, 0,63 % Mo, Cr/C 5,61). Pov. 100×

Fig. 5

Lamellar eutectic carbides, as cast (3.20 % C, 17.95 % Cr, 0.63 % Mo, Cr/C 5.61). Magn. 100×

Preiskovane zlitine so legirane z Mo in preizkusni valjčki imajo na presekih, ulitih v kokilo pri razmerjih Cr/C nad 5,5, popolnoma avstenitno matico (sl. 5). Le v večji oddaljenosti od površine smo pri nekaterih vzorcih opazili v mikrostrukturi manjša perlitra zrna. S padojočo vrednostjo razmerja Cr/C narašča v matici delež perlitrne faze. Avstenitno perlitra mikrostruktura matice je prikazana na sliki 4.

Perlitra matico lahko reavsternitiziramo in tako zagotovimo, da ima litina po destabilizaciji in transformaciji s stališča mehanskih lastnosti ustrezejšo mikrostrukturo matice (martenzit). Menimo, da z ogrevanjem avstenitno perlitrnih litin 50 °C pod solidus temperaturo dobimo avstenitno mikrostrukturo matice. Za natančnejše pogoje reavsternitizacije so v literaturi podani diagrami (1, 2). Vsekakor pa je ugodnejše, da z razmerjem Cr/C, legiranjem z Mo in pogojih strjevanja že v litem stanju zagotovimo litini avstenitno mikrostrukturo matice (9).

#### Kemična sestava karbidov in matice

Koncentracije Cr, Mo, Mn in W v primarnih in eutektičnih karbidih in v matici, izmerjene v elektronskem mikroanalizatorju, so podane v tabeli 3. Meritve smo naredili na vzorcih ulitih v kokilo.

Tabela 3: Vsebnosti Cr, Mo, Mn in W v karbidih in matici

Zlitina	Cr/C	% C	% Cr	Mo	Karbidi primarni	Karbidi eutek.	Matica perlit	Matica austenit
7	3.62	3.31	11.97	0.58	38.3 Cr	32.9 Cr	6.7 Cr	—
				0.55 Mo	0.45 Mo	0.26 Mo	—	
				0.8 Mn	0.7 Mn	0.6 Mn	—	
6	4.80	3.21	15.42	0.53	42.4 Cr	37.0 Cr	7.7 Cr	7.0 Cr
				0.44 Mo	0.46 Mo	0.26 Mo	0.34 Mo	
3	5.48	2.72	14.90	0.56	44.8 Cr	39.9 Cr	—	10.5 Cr
				0.97 Mn	0.92 Mn	—	0.13 Mn	
5	5.61	3.20	17.95	0.63	48.4 Cr	43.8 Cr	—	10.2 Cr
				0.42 Mo	0.42 Mo	—	0.23 Mo	
				0.95 Mn	0.9 Mn	—	0.8 Mn	
2	7.39	2.62	19.43	0.52	50.7 Cr	49.0 Cr	—	10.8 Cr
				0.83	0.49 Mo	0.46 Mo	—	0.3 Mo
				W	0.59 W	0.61 W	—	0.44 W
				0.9 Mn	0.9 Mn	—	0.7 Mn	
1	7.76	2.49	19.31	0.54	51.2 Cr	49.0 Cr	—	10.5 Cr
				0.41 Mo	0.44 Mo	—	0.31 Mo	

V diagramu na sliki 7 je prikazana odvisnost med razmerjem Cr/C v zlitinah in razmerjem Fe/Cr v karbidih

Table 2 Portion of Carbide Phase (% K) in the Microstructure

Alloy	Cr/C	% C	% Cr	calculated	% K measured
7	3.62	3.31	11.97	32.2	30
6	4.80	3.21	15.42	32.9	29
3	5.48	2.72	14.90	26.5	26
5	5.61	3.20	17.95	34.1	35
2	7.39	2.62	19.43	27.9	28
1	7.76	2.49	19.31	26.1	25

Microstructure of matrix depends on the Cr/C ratio, amount of Mo, and conditions of solidification. Matrix as cast has austenitic microstructure, or a partial or complete transformation of austenite into pearlite occurred during the solidification. Solidification and cooling are faster in casting into moulds than in casting into sand, and pearlitic transformation is retarded. In alloys without Mo fully austenitic matrix can be expected at the Cr/C ratios higher than 7.2 (1, 2). Alloying with Mo shifts the Cr/C ratio at which fully austenitic matrix is obtained towards lower values. This means that cast iron can contain at the same Cr more C, and thus a greater portion of carbide phase can be in the microstructure.

Investigated alloys were alloyed with Mo, and the testing cylinders exhibit on the cross sections cast into mould a fully austenitic matrix if Cr/C ratio was over 5.5 (Fig. 5). Only at a greater distance from the surface smaller pearlitic grains were observed in the microstructure of some samples. The reduced Cr/C ratio causes an increased amount of pearlitic phase in the matrix. The austenitic-pearlitic microstructure of the matrix is shown in Fig. 4.

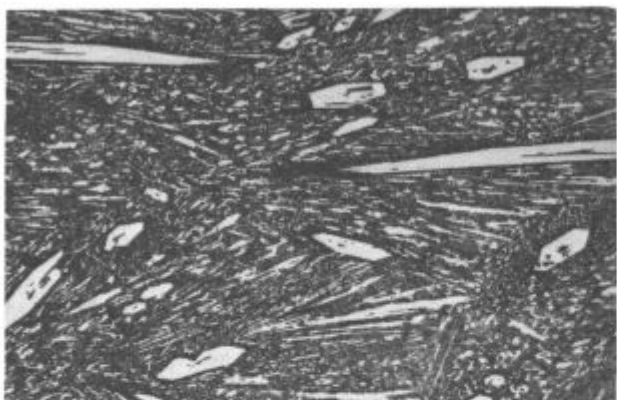
Pearlitic matrix can be reaustenitized, and thus it is ensured that the cast iron has a more suitable microstructure of matrix (martensite) from the viewpoint of mechanical properties after the destabilization and the transformation. It is supposed that heating austenitic-pearlitic cast iron at 50 °C below the solidus temperature gives austenitic microstructure of the matrix. More detailed conditions of reaustenitization are given in graphs in references (1, 2). Anyhow, it is more favourable to ensure the austenitic microstructure of the matrix in the as cast alloy by the Cr/C ratio, alloying with Mo, and the conditions of solidification.

#### Chemical Composition of Carbides and of Matrix

Concentrations of Cr, Mo, Mn, and W in the primary and the eutectic carbides, and in the matrix, measured by the electron microanalyzer are presented in Table 3.

Table 3 Contents of Cr, Mo, Mn, and W in Carbides and in the Matrix

Alloy	Cr/C	% C	% Cr	Mo	Carbides		Matrix	
					Primary	Eutec.	Pearlite	Austen.
7	3.62	3.31	11.97	0.58	38.3 Cr	32.9 Cr	6.7 Cr	—
				0.55 Mo	0.45 Mo	0.26 Mo	0.26 Mo	—
				0.8 Mn	0.7 Mn	0.6 Mn	0.6 Mn	—
6	4.80	3.21	15.42	0.53	42.4 Cr	37.0 Cr	7.7 Cr	7.0 Cr
				0.44 Mo	0.46 Mo	0.26 Mo	0.34 Mo	—
3	5.48	2.72	14.90	0.56	44.8 Cr	39.9 Cr	—	10.5 Cr
				0.97 Mn	0.92 Mn	—	0.13 Mn	
5	5.61	3.20	17.95	0.63	48.4 Cr	43.8 Cr	—	10.2 Cr
				0.42 Mo	0.42 Mo	—	0.23 Mo	
				0.95 Mn	0.9 Mn	—	0.8 Mn	
2	7.39	2.62	19.43	0.52	50.7 Cr	49.0 Cr	—	10.8 Cr
				0.83	0.49 Mo	0.46 Mo	—	0.3 Mo
				W	0.59 W	0.61 W	—	0.44 W
				0.9 Mn	0.9 Mn	—	0.7 Mn	
1	7.76	2.49	19.31	0.54	51.2 Cr	49.0 Cr	—	10.5 Cr
				0.41 Mo	0.44 Mo	—	0.31 Mo	



SL. 6:  
Primarni karbidi heksagonalne oblike. Pov. 100×  
**Fig. 6**  
Primary carbides of hexagonal shape. Magn. 100×

$M_7C_3$ . Z razmerjem  $Fe/Cr$  je podana sestava karbidov  $M_7C_3$ , ki se sicer lahko spreminja od  $(Cr_2Fe_5)C_3$  do  $(Cr_5Fe_2)C_3$ . Primarni in evtektični karbidi imajo v naših zlitinah sestavo od malo nad stehiometričnim razmerjem  $(Cr_3Fe_4)C_3$  do  $(Cr_4Fe_3)C_3$ . Krivulja za evtektične karbide leži nad krivuljo za primarne karbide, ker imajo evtektični karbidi pri istih vrednostih  $Cr/C$  manjšo vsebnost Cr. Razlika v vsebnosti Cr med primarnimi in evtektičnimi karbidi je največja pri najnižjem razmerju  $Cr/C$ . Z naraščajočo vsebnostjo tega razmerja proti 8 se vsebnost Cr v primarnih in evtektičnih karbidih približuje isti vrednosti.

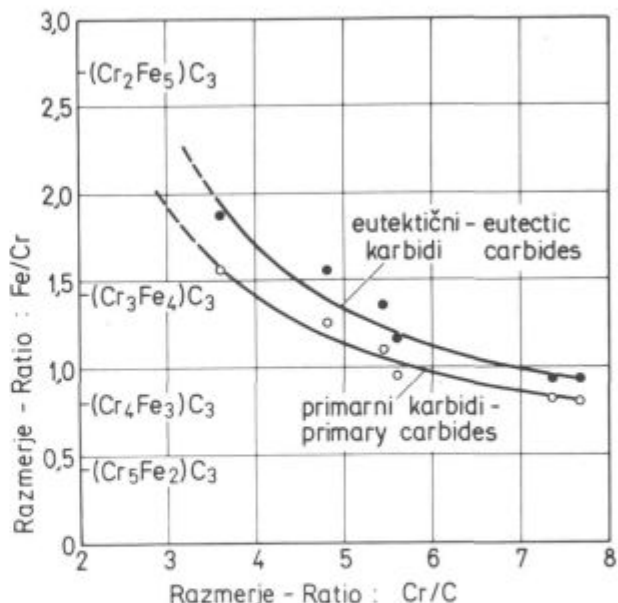
Poleg Cr, ki v kristalni mreži karbidov nadomešča atome Fe, smo v karbidih izmerili tudi določene koncentracije Mo, Mn in W. Vsebnost Mo v zlitinah je majhna, zato je v mikrostrukturi malo karbidov  $Mo_2C$ . Ti karbidi so drobni, vendar smo jih lahko določili v elektronskem mikroanalizatorju, kot tudi karbide W v zlitinah, legiranih s tem elementom.

Vsebnost Cr v matici narašča z vrednostjo razmerja  $Cr/C$ . Meritve koncentracij Cr in Mo v matici so pokazale, da je ta zelo nehomogena (5). Odstopanja od povprečnih vrednosti so pri Cr v mejah  $\pm 20\%$ . Bistveno večje je izcejanje Mo, in sicer večinoma v mejah  $\pm 50\%$ . V nekaterih primerih pa smo v izcejah izmerili tudi do 2 % Mo. Podobno smo ugotovili, da tudi karbidi nimajo homogene sestave. Pri večjih, predvsem primarnih karbidih, je koncentracija Cr največja v sredini in se zmanjšuje proti robu karbidnega zrna.

V karbidih smo merili koncentracije Cr, Mo in W tudi na vzorcih, žarjenih 2, 4 in 8 ur na temperaturi 1050 °C. Pri tej temperaturi poteka izločanje sekundarnih karbidov in s tem destabilizacija avstenitne maticice. Izmerjene razlike v koncentraciji omenjenih elementov med litim in žarjenim stanjem niso sistematične in so odstopanja v mejah merilnih napak.

#### Diagram izotermne destabilizacije avstenita

Sistematične preiskave destabilizacije avstenita, izoterna transformacijska diagrama za nedestabiliziran in destabiliziran avstenit (TTT) in kontinuirni transformacijski diagram za destabiliziran avstenit (CTT) smo naredili za zlitino 5 z naslednjo kemično sestavo: 3,2 % C, 1,22 % Si, 0,86 % Mn, 0,035 % S, 0,030 % P, 17,95 % Cr, 0,63 % Mo, 0,69 % Ni, 0,08 % Ti in 0,095 % V. Zlita ima razmerje  $Cr/C$  5,61 in vitem stanju avstenitno matico (sl. 5). Izoterna transformacijska diagrama smo naredili na osnovi metalografskih



SL. 7:  
Ovisnost med razmerjem  $Cr/C$  in razmerjem  $Fe/Cr$  v karbidih  $M_7C_3$

**Fig. 7**  
Relation between the  $Cr/C$  ratio and  $Fe/Cr$  ratio in  $M_7C_3$  carbides

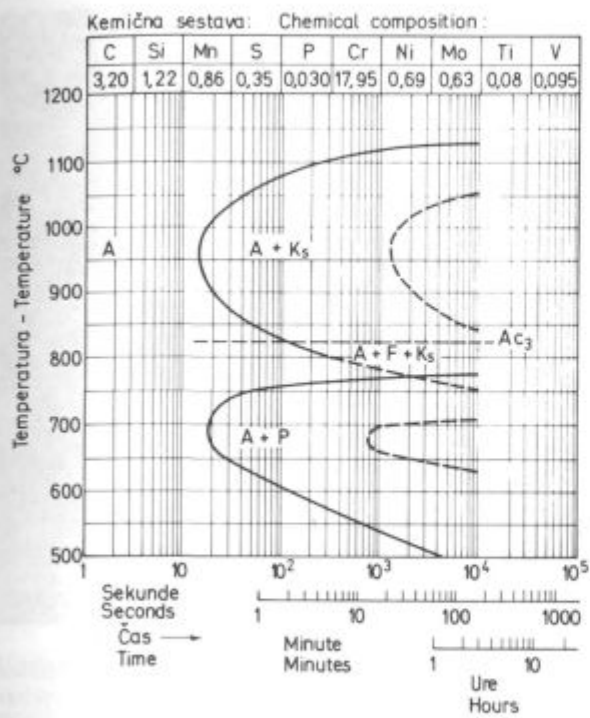
Measurements were made on the samples cast into mould.

Plot in **Fig. 7** gives the relationship between the  $Cr/C$  ratio in alloys and the  $Fe/Cr$  ratio in  $M_7C_3$  carbides. The  $Fe/Cr$  ratio defines the composition of  $M_7C_3$  carbides which varies between  $(Cr_2Fe_5)C_3$  and  $(Cr_5Fe_2)C_3$ . Primary and eutectic carbides in our alloys have the composition between the composition which is slightly above the stoichiometric one of  $(Cr_3Fe_4)C_3$ , and the composition of  $(Cr_4Fe_3)C_3$ . The curve for eutectic carbides is above the curve for primary carbides since eutectic carbides at equal  $Cr/C$  ratios have smaller contents of Cr. The difference in Cr content between the primary and the eutectic carbides was the highest at the lowest  $Cr/C$  ratio. If this ratio goes towards 8, the Cr content in primary and eutectic carbides approaches to the same value.

Beside Cr which in crystal lattice of carbides substitutes Fe atoms, certain concentrations of Mo, Mn, and W were found in carbides. Mo content in alloys is small therefore the microstructure contains small amount of  $Mo_2C$ . These carbides are fine but they were determined by the electron microanalyzer, as well as the tungsten carbides in the alloys alloyed with that element.

Cr content in matrix is increased with the increased  $Cr/C$  ratio. Measurements of Cr and Mo concentrations in the matrix showed that matrix is very unhomogeneous (5). Deviations from the mean values are for Cr in the limits  $\pm 20\%$ . Essentially greater are segregations of Mo, mainly in limits  $\pm 50\%$ . In some cases in segregations, even up to 2 % Mo was found. Similarly, it was found that also carbides do not have a homogeneous composition. In bigger, mainly primary carbides the concentration of Cr is the greatest in the centre and it is reduced towards the edge of the carbide grain.

In carbides, the concentrations of Cr, Mo, and W were measured also in the samples annealed 2, 4 and 8 hours at 1050 °C. At this temperatures secondary carbides are precipitated and thus the austenitic matrix is



Sl. 8:

Diagram izotermne destabilizacije avstenita (A — austenit, F — ferit, P — perlit, K<sub>s</sub> — sekundarni karbidi)

Fig. 8

Diagram of isothermal destabilization of austenite (A — austenite, F — ferrite, P — pearlite, K<sub>s</sub> — secondary carbides)

preiskav. Mikrostrukturne spremembe smo opredelili v optičnem mikroskopu in v SEM. V nekaterih primerih, ko je bilo težko določiti mikrostrukturne komponente, smo si pomagali še z meritvami mikrotrdot in selektivnim jedkanjem (15, 16).

Za izdelavo diagrama izotermne destabilizacije avstenita smo vzorce izotermno žarili različno dolgo časa v temperaturnem področju med 500 in 1150°C. Razpad avstenita poteka v dveh temperaturnih področjih, ki se v ozkem področju prekriva (sl. 8). Za topotorno obdelavo zlitin je pomembna destabilizacija avstenita z izločanjem sekundarnih karbidov (K<sub>s</sub>), ki poteka v višjem temperaturnem področju. Izločanje sekundarnih karbidov je najhitrejše med 940 in 990°C. Nad temperaturo Ac<sub>3</sub> poteka transformacija  $\gamma = \gamma + K_s$  in pod to temperaturo  $\gamma = \gamma + \alpha + K_s$ .

Nad temperaturo Ac<sub>3</sub> se iz avstenita izločajo karbidi M<sub>7</sub>C<sub>3</sub>. V temperaturnem področju med Ac<sub>3</sub> in Ac<sub>1</sub> pa se iz avstenita izločajo tudi karbidi M<sub>23</sub>C<sub>6</sub> (10). Izločanje sekundarnih karbidov je za nadaljnjo topotorno obdelavo bistvenega pomena. Brez predhodne destabilizacije, pri kateri se zaradi izločanja sekundarnih karbidov v avstenitu zmanjša vsebnost Cr in C, transformacija avstenita v martenit, kot tudi v bainit, niti ni mogoča. Perlitna transformacija pa poteka v destabiliziranem avstenitu počasneje.

V nižjem temperaturnem področju razpada poteka transformacija avstenitne matice v perlit. Transformacija poteka najhitrejše med 670 in 710°C.

Sekundarni karbidi se začnejo izločati iz avstenita po določeni inkubacijski dobi, in to ob kristalnih mejah med avstenitnimi zrni in na meji avstenitnih zrn z evtečnimi karbidi. Proti sredini avstenitnih zrn poteka izločanje hitreje po določenih kristalografskih ravninah (sl. 9, 10, 11). V začetni faziji izločanja so karbidi drobni,

destabilized. The measured differences of concentrations of the mentioned elements between the cast and annealed state are not systematic, and the deviations are in the limits of measuring errors.

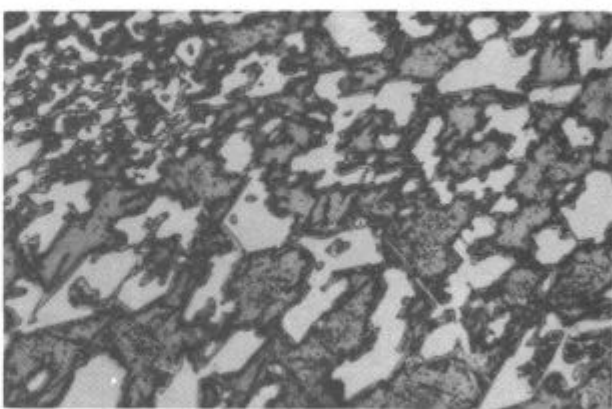
#### Diagram of Isothermal Destabilization of Austenite

Systematic investigations of the destabilization of austenite, isothermal transformation diagrams for undestabilized and destabilized austenite (TTT), and the continuous transformation diagram for destabilized austenite (CTT) were constructed for the alloy 5 with the following composition: 3.2 % C, 1.22 % Si, 0.86 % Mn, 0.035 % S, 0.030 % P, 17.95 % Cr, 0.63 % Mo, 0.69 % Ni, 0.08 % Ti, and 0.095 % V. The Cr/C ratio of the alloy was 5.61, and the as cast alloy exhibits austenitic matrix (Fig. 5). The isothermal transformation diagrams were constructed from data of metallographic investigations. Microstructural variations were determined in optical microscope and by SEM. In some cases when the microstructural components were not easy to be determined, measurements of microhardnesses, and selective etching were applied (15, 16).

To construct the diagram of isothermal destabilization of austenite, the samples were isothermally annealed for various times in the temperature interval 500 to 1150°C. Decomposition of austenite occurs in two temperature intervals which overlap in a narrow region (Fig. 8). The destabilization of austenite with precipitation of secondary carbides (K<sub>s</sub>) occurring in the higher temperature interval is important for the heat treatment of alloys. Precipitation of secondary carbides is the fastest between 940 and 990°C. Above Ac<sub>3</sub> transformation  $\gamma = \gamma + K_s$  takes place, and below that point  $\gamma = \gamma + \alpha + K_s$ .

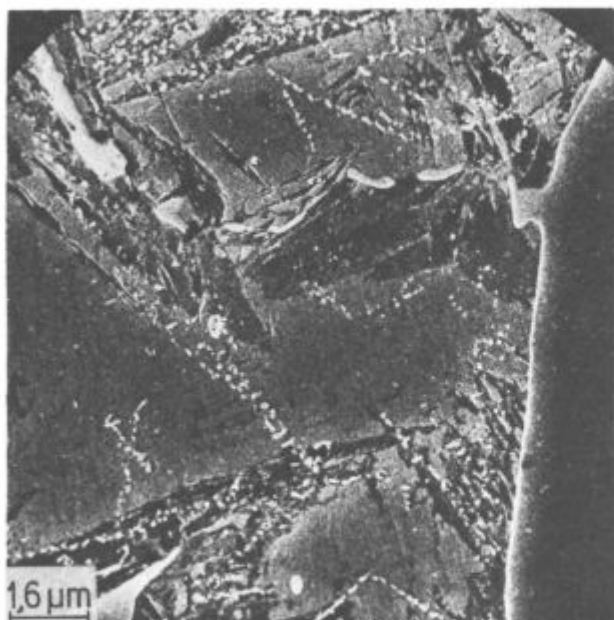
Above Ac<sub>3</sub> M<sub>7</sub>C<sub>3</sub> carbides are precipitated from austenite. In the temperature interval between Ac<sub>3</sub> and Ac<sub>1</sub> also M<sub>23</sub>C<sub>6</sub> carbides are precipitated from austenite (10). Precipitation of secondary carbides is essential for further heat treatment. Without the predestabilization when due to the precipitation of secondary carbides the concentrations of Cr and C are reduced, the transformation of austenite into martensite as well as into bainite is not possible. Pearlitic transformation is slower in the destabilized austenite.

In the lower temperature interval of the decomposition, the transformation of austenitic matrix into pearlite takes place. It is the fastest between 670 and 710°C.



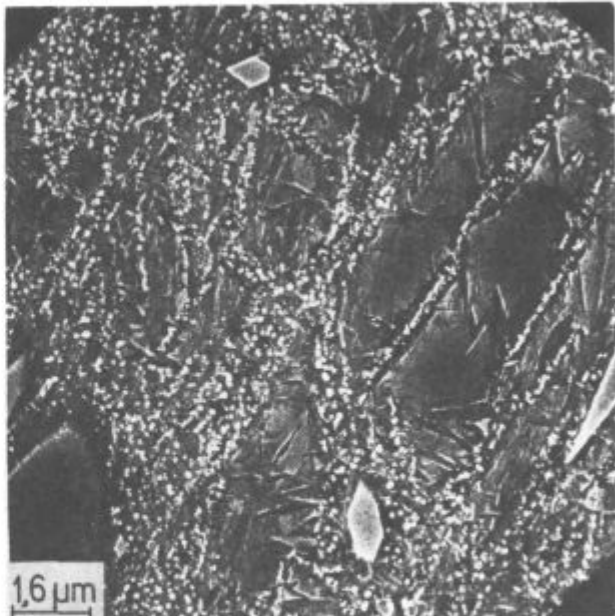
Sl. 9:  
Izločanje sekundarnih karbidov v avstenitu, 80 s žarjeno na 1050°C. Pov. 500x

Fig. 9  
Precipitation of secondary carbides in austenite, annealed 80 s at 1050°C. Magn. 500x



**Sl. 10:**  
Morfologija izločanja sekundarnih karbidov iz avstenita, 40 s žarjeno na 1050°C (matica je iz avstenita in martenzita)

**Fig. 10**  
Morphology of precipitation of secondary carbides from austenite, annealed 40 s at 1050°C (Matrix is of austenite and martensite)



**Sl. 11:**  
Morfologija izločanja sekundarnih karbidov iz avstenita, 5 min žarjeno na 950°C (matica je iz avstenita in martenzita)

**Fig. 11**  
Morphology of precipitation of secondary carbides from austenite, annealed 5 min. at 950°C (Matrix is of austenite and martensite)

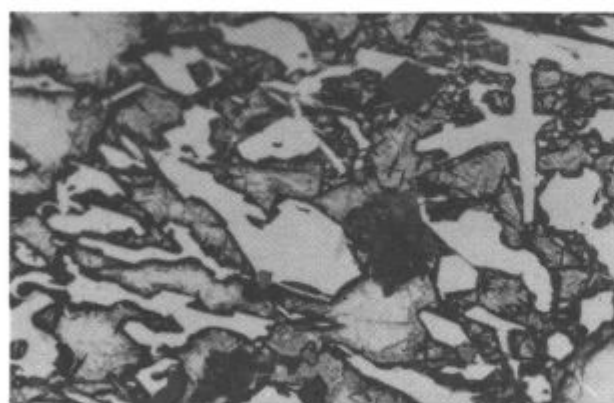
s časom izotermnega žarjenja pa rastejo. Največji vpliv na rast sekundarnih karbidov ima temperatura in nad 1050 °C je njihova rast že zelo hitra.

Inkubacijski čas za potek premete v perlitnem področju je daljši. Morfologija izločanja cementita je podobna kot pri izločanju sekundarnih karbidov, le izločanje cementita po prednostnih kristalografskih ravnih je manj izrazito. Sam potek transformacije je hitrejši kot proces destabilizacije. Na nekaterih mestih se vidi, da je transformacija potekla hitro po celiem zrnu avstenita (sl. 12). Oblika cementitnih lamel in medlamelarna razdalja v perlitu sta odvisni od temperaturo transformacije. Pri 750 °C je cementit grob in globular, le na sredini večjih zrn je nakazana lamelarna oblika. S padajočo temperaturo transformacije ima cementit vedno bolj lamelarno obliko (sl. 13, 14). Najmanjšo

Secondary carbides start to precipitate from austenite after a certain induction period, and this occurs on the grain boundaries between the austenite grains, and on the boundaries of austenite grains with eutectic carbides. Towards the centre of austenite grains the precipitation is faster on certain crystallographic planes (Figs. 9, 10, and 11). In the initial phase of precipitation, the carbides are fine, but they grow with the time of isothermal annealing. The greatest influence on the growth of secondary carbides has the temperature, and above 1050°C their growth is already very fast.

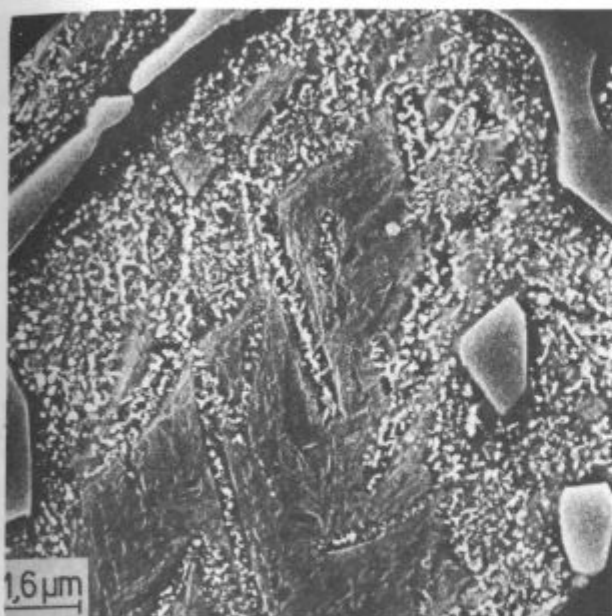
Induction period for the transformation in the pearlitic region is longer. Morphology of cementite precipitation is similar to that of the secondary carbides, only precipitation of cementite on the preferred crystallographic planes is less pronounced. Transformation itself is faster than the process of destabilization. On same spots it is evident that the transformation was fast through the whole austenite grain (Fig. 12). The shape of cementite lamellae and the interlamellar spacing in perlite depend on the transformation temperature. At 750°C cementite is coarse and globular, only in the centre of bigger grains lamellar formation is indicated. With decreasing temperature of transformation the shape of cementite is becoming more lamellar (Figs. 13 and 14). The smallest interlamellar spacing in perlite is found in the alloys at the transformation temperature around 650°C. At lower temperatures pearlitic transformation is slower, and lamellae can be observed only after longer annealing times.

The curves of the initial precipitation of secondary carbides, and of pearlitic transformation were metallographically exactly determined by optical microscopy and by SEM. Bigger problem was to determine the time when both processes are completed. Precipitation of carbides and the pearlitic transformation move from the grain boundaries into the interior of the grains. The time



**Sl. 12:**  
Perlitna transformacija, 5 min žarjeno na 690°C. Pov. 500 x

**Fig. 12**  
Pearlitic transformation, annealed 5 min. at 690°C, Magn. 500 x



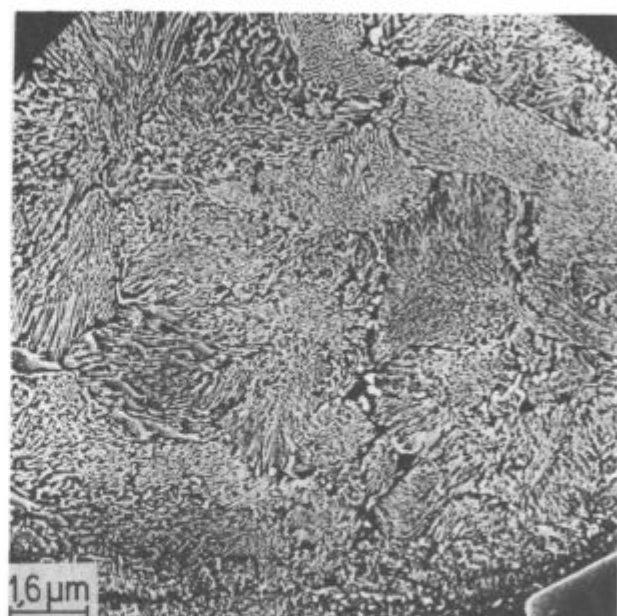
Sl. 13:

Morfologija perlitne transformacije, 10 min žarjeno na  $750^{\circ}\text{C}$   
Fig. 13

Morphology of pearlitic transformation, annealed 10 min. at  
 $750^{\circ}\text{C}$

medlamelarno razdaljo v perlitu ima zlitina v temperaturnem področju transformacije okoli  $650^{\circ}\text{C}$ . Pri nižjih temperaturah poteka perlitna transformacija počasneje in lamele opazimo le pri daljših časih žarjenja.

Krivilji začetka izločanja sekundarnih karbidov in perlitne transformacije smo lahko metalografsko točno določili z optičnim mikroskopom in v SEM. Večji problem je določiti čas, v katerem sta oba procesa končana. Izločanje karbidov in perlitna transformacija potekata s kristalnih mej v notranjost zrn. Čas, v katerem je proces končan, je zato odvisen od velikosti kristalnih zrn. V nekaterih primerih tudi sicer težko točno opredelimo konec procesa izločanja sekundarnih karbidov, ker v martenzitni osnovi težko ločimo karbidna zrna. Z meritvami trdote si prav tako težko pomagamo, saj se trdota, ko je izločenih že več kot 80 % sekundarnih karbidov, ali se perlitna transformacija približuje koncu, bistveno ne spremeni in so odstopanja v mejah merilnih napak. Na potek destabilizacije in perlitne transformacije pa vpliva tudi izcejanje legirnih elementov. Iz teh razlogov sta krivilji, ki označujeta konec obeh procesov, opredeljeni le približno.



Sl. 14:

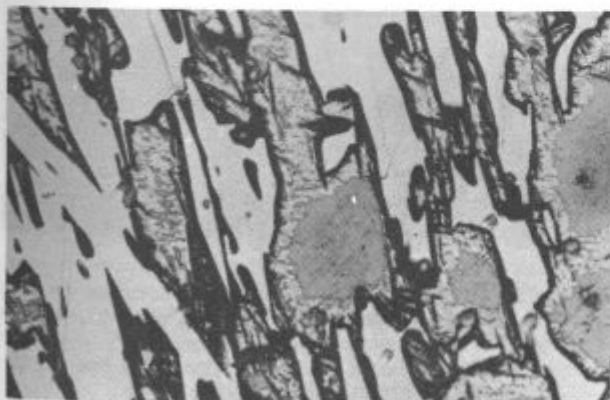
Morfologija perlitne transformacije, 120 min žarjeno na  $650^{\circ}\text{C}$   
Fig. 14

Morphology of pearlitic transformation, annealed 120 min. at  
 $650^{\circ}\text{C}$

of the process termination thus depends on the size of crystal grains. In some cases the exact determination of the end of the precipitation of secondary carbides is difficult since carbide grains can hardly be distinguished in the martensitic matrix. Measurements of hardness can also not help since the hardness changes very little when more than 80 % of secondary carbides are precipitated or the pearlitic transformation approaches to its end, and the deviations are in the limits of measuring errors. The destabilization process and the pearlitic transformation are influenced also by the segregations of alloying elements. Therefore the curves determining the completion of both processes are approximate.

In some samples being destabilized below  $900^{\circ}\text{C}$  also retained austenite was observed in the microstructure. Due to fast cooling (microstructure was stabilized by quenching) beside the stable austenite also residual austenite is present in the microstructure of the matrix in partial destabilization. The both austenites differ in the content of alloying elements (Cr, Mo, and C) (Fig. 15).

The  $\text{Ac}_3$  point was determined dilatometrically.



Sl. 15:

Delno destabiliziran avstenit ( $850^{\circ}\text{C}$ , 2 min.). V sredini zrn je stabilni avstenit. Ob kristalnih mejah, kjer so se izločili sekundarni karbidi, je med martenzitnimi iglami zaostali avstenit.  
Pov. 500 x

Fig. 15

Partially destabilized austenite ( $850^{\circ}\text{C}$ , 2 min.). In the centre of grains there is stable austenite. On grain boundaries where secondary carbides are precipitated there is residual austenite between the martensitic needles. Magn. 500 x

Pri nekaterih vzorcih, destabiliziranih pri temperaturah pod 900 °C, smo opazili v nikostruktuji tudi zaostali avstenit. Zaradi hitrega ohlajanja (mikrostruktura smo stabilizirali z gašenjem) je v mikrostrukturi matici pri delni destabilizaciji prisoten poleg stabilnega avstena še zaostali avstenit. Avstena se razlikuje po vsebnosti legirnih elementov Cr, Mo in C (sl. 15). Temperaturo  $A_{c3}$  smo določili z dilatometrom.

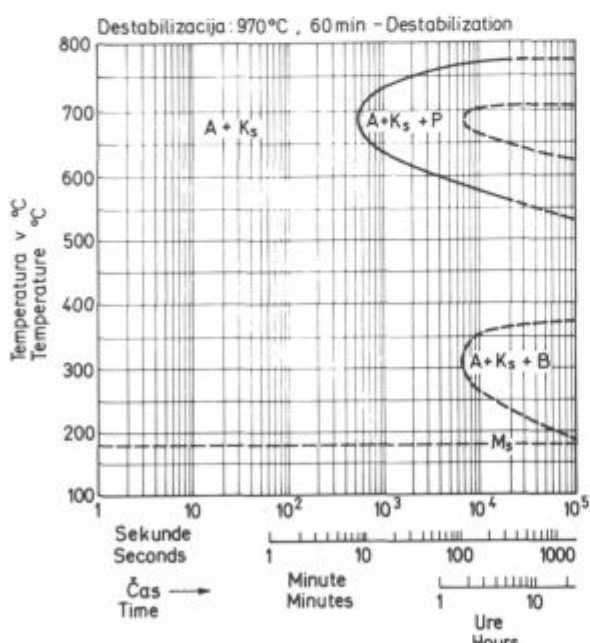
#### Izotermni transformacijski diagram za destabiliziran avstenit.

Temperatura destabilizacije 970 °C je istočasno izhodna temperatura nadaljnje toplotne obdelave.

Omenili smo že, da višje razmerje Cr/C in legiranje z Mo zavirata transformacijo avstena v perlit. Pri destabiliziranem avstenu moramo upoštevati še vpliv sekundarnih karbidov.

V primerjavi s TTT diagramom za nedestabiliziran avstenit je pri destabiliziranem avstenu področje nastajanja perlita pomaknjeno močno v desno, v temperaturah pa ni nobene razlike. Več je v avstenu izloženih sekundarnih karbidov, daljša je inkubacijska doba. Za praktično uporabo diagrama je seveda pomembna le popolna destabilizacija avstena (sl. 16).

Določena razlika je v morfološiji nastajanja perlita. V nedestabiliziranem avstenu poteka transformacija predvsem s kristalnih mej proti sredini avstentitnih zrn. Pri destabiliziranem avstenu potete premete hitro po celi, oziroma delu avstentitnega zrna. S časom žarjenja narašča število transformiranih kristalnih zrn. (sl. 17). Sekundarni karbidi delujejo kot kali in v destabiliziranem avstenu poteka kontinuirna transformacija (sl. 18). Tudi pri teh pogojih transformacije je iz omenjenih razlogov nemogoče točno opredeliti konec premene.



Sl. 16:

Izotermni transformacijski diagram za destabiliziran avstena (A — avstena, K<sub>s</sub> — sekundarni karbidi, P — perlit, B — bainit).

Fig. 16

Isothermal transformation diagram for destabilized austenite (A — austenite, K — secondary carbides, P — pearlite, B — bainite).

#### Isothermal Transformation Diagram for Destabilized Austenite

The destabilization temperature of 970 °C is simultaneously the starting temperature for further heat-treatment processes.

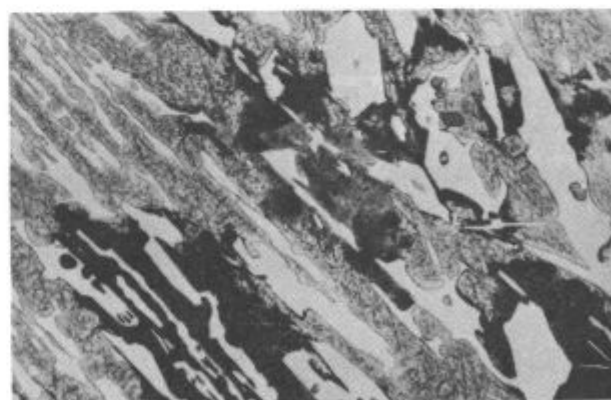
It was already mentioned that higher Cr/C ratio and alloying with Mo retard the transformation of austenite into pearlite. In destabilized austenite also the influence of secondary carbides must be taken in account.

Compared to the TTT diagram for understabilized austenite the region of formation of pearlite in destabilized austenite is shifted significantly to the right while there are no differences related to the temperatures. Amount of secondary carbides precipitated in austenite is greater, longer is also the induction period. Only the complete destabilization of austenite (Fig. 16) is certainly important for practical application of the diagram.

There is a certain difference in the morphology of pearlite formation. In unstabilized austenite the transformation goes mainly from crystal boundaries towards the centre of austenite grains. In destabilized austenite the transformation is fast over the whole or over a part of austenite grain. Longer annealing time increases the number of transformed crystal grains (Fig. 17). Secondary carbides are nuclei, and continuous transformation takes place in destabilized austenite (Fig. 18). Also in these conditions of transformation it is not possible to determine exactly the termination of the transformation due to the reasons already mentioned.

Formation of cementite is influenced also by secondary carbides beside the temperature of isothermal transformation. They are bigger in the bigger austenite grains, but their density is lower. Thus the growth of cementite in the bigger grains is less hindered than in the smaller ones.

Bainitic transformation is possible only after the destabilization of austenite and at Cr/C ratios smaller than 5.2. By alloying with Mo, bainite can be obtained also at higher concentrations of Cr (1, 6). Induction period for the bainitic transformation is long. Significant portion of bainitic phase in the microstructure is obtained only after longer times of isothermal annealing. A completely bainitic matrix can be expected only after a very long times of isothermal annealing when the alloy has a suitable Cr/C ratio and is alloyed with Mo.

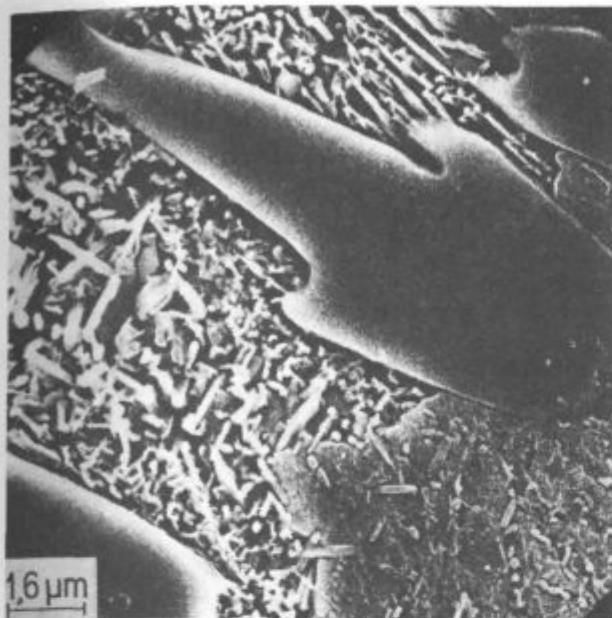


Sl. 17:

Perlita transformacija destabilizirane avstentitne matici, 60 min žarjeno na 650 °C. Pov. 500 ×

Fig. 17

Pearlitic transformation of destabilized austenitic matrix, annealed 60 min. at 650 °C. Magn. 500 ×



Sl. 18:

Meja med perlitskim zrnom (temnejše) in netransformiranim avstenitom (svetlejše) v destabilizirani matici

Fig. 18

Boundary between the perlite grain (darker) and not transformed austenite (brighter) in the destabilized matrix

Na izoblikovanje cementita vplivajo poleg temperature izotermne transformacije še sekundarni karbidi. Ti so v večjih avstenitnih zrnih večji, njihova gostota pa je manjša. Zato je v večjih zrnih rast cementita manj ovirana, kot v manjših.

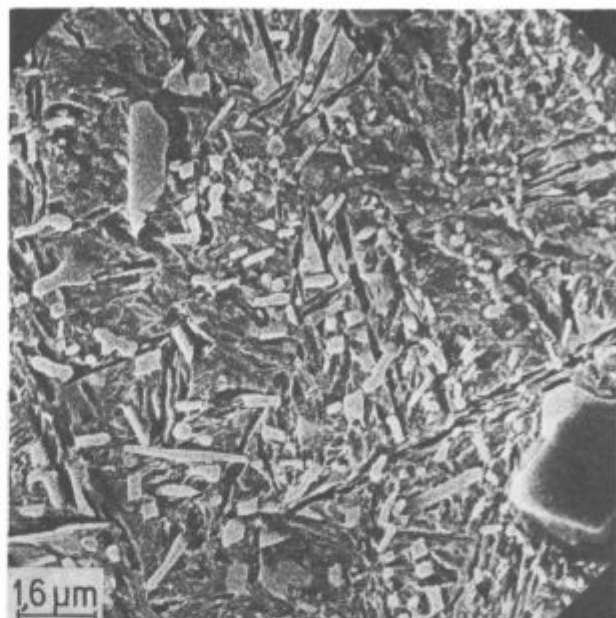
Bainitna transformacija je možna le po destabilizaciji avstenita in razmerjih Cr/C manjših od 5,2. Z legiranjem zlitin z Mo lahko dobimo bainit tudi pri višjih koncentracijah Cr (1,6). Inkubacijska doba za potek bainitne premene je dolga. Pomemben delež bainitne faze v mikrostrukturi dobimo le pri daljših časih izotermnega žarjenja. Popolnoma bainitno matico pa lahko pričakujemo po zelo dolgih časih žarjenja zlitin z ustreznim razmerjem Cr/C in legiranih z Mo.

Bainitno in martenzitno mikrostrukturo lahko ločimo le v SEM (17). Bainit stabilizira avstenit, zato je v mikrostrukturi matice še precej netransformiranega avstenita (sl. 19). To so potrdile tudi meritve mikrohardnot.

Začetek martenzitne transformacije smo določili z dilatometrom.  $M_s$  temperatura za popolnoma destabilizirano zlitino ( $970^{\circ}\text{C}$ , 60 min) je  $180^{\circ}\text{C}$ . Potek martenzitne transformacije ni odvisen le od delne ali popolne destabilizacije, temveč tudi od temperature destabilizacijskega žarjenja.  $M_s$  temperatura se znižuje z naraščajočo temperaturo destabilizacije (1, 6, 7). Pri kaljenju delno destabiliziranega avstenita je v matici poleg martenzita tudi avstenit.

#### Kontinuirni transformacijski diagram za destabiliziran avstenit

Diagram, prikazan na sliki 20 velja za popolnoma destabilizirano zlitino ( $970^{\circ}\text{C}$ , 30 min). Preizkuse smo naredili tudi pri drugih temperaturah destabilizacije in na delno destabiliziranih vzorcih, da smo dobili čim več podatkov o vplivu različnih pogojev destabilizacije na mikrostrukturne značilnosti pri kontinuirnem ohlajaju.



Sl. 19:

Morfologija bainitne transformacije v destabiliziranem avstenitu ( $300^{\circ}\text{C}$ , 4 ure). Mikrostruktura matice je iz avstenita, bainite, martenzita in sekundarnih karbidov

Fig. 19

Morphology of bainitic transformation in destabilized austenite ( $300^{\circ}\text{C}$ , 4 hours). Microstructure of matrix is of austenite, bainite, martensite, and secondary carbides

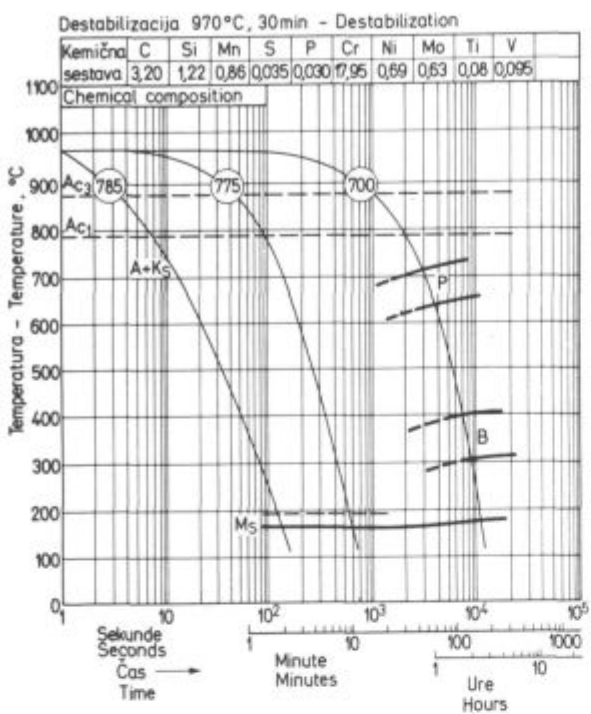
Bainitic and martensitic microstructure can be distinguished only by SEM (17). Bainite stabilizes austenite therefore a good deal of not transformed austenite can be found in the microstructure of the matrix (Fig. 19). This was confirmed also by the microhardness measurements.

The beginning of the martensitic transformation was determined by dilatometer.  $M_s$  point for a completely destabilized alloy ( $970^{\circ}\text{C}$ , 60 min.) is at  $180^{\circ}\text{C}$ . Course of martensitic transformation does not depend only on the partial or complete destabilization but also on the temperature of the destabilization annealing.  $M_s$  temperature is lowered with the increasing temperature of destabilization (1, 6, 7). After hardening the partially destabilized austenite, also austenite next to the martensite is found in the matrix.

#### Continuous Transformation Diagram for Destabilized Austenite

Diagram is presented in Fig. 20 and it is valid for a completely destabilized alloy ( $970^{\circ}\text{C}$ , 30 min.). Experiments were made also at other temperatures of destabilization, and with partially destabilized samples in order to obtain the most possible data about the influences of various conditions of destabilization on the microstructural characteristics in continuous cooling.

In slow cooling at  $300^{\circ}\text{C}/\text{h}$ , the transformation occurs at first in pearlitic stage, then also in the bainitic stage. The extent of transformation is in both stages approximately equal. Martensitic transformation is namely observed, but amount of formed martensitic phase is small. At shorter times of destabilization the extent of transformation in pearlitic stage is smaller and in the bainitic one greater, but at temperatures around  $200^{\circ}\text{C}$  also martensitic transformation is observed.



SI. 20:

Kontinuirni transformacijski diagram za destabiliziran avstenit (A — avstenit, K<sub>s</sub> — sekundarni karbidi, P — perlit, B — bainit)

Fig. 20

Continuous transformation diagram for destabilized austenite (A — austenite, K<sub>s</sub> — secondary carbides, P — pearlite, B — bainite)

Pri počasnem ohlajevanju 300 °C/h pride do premenne najprej v perlitni, nato pa v bainitni stopnji. Obseg transformacije je v obeh stopnjah približno enak. Martenzitna premena se sicer opazi, martenzitne faze pa je nastalo malo. Pri krajsih časih destabilizacije je obseg transformacije v perlitni stopnji manjši, v bainitni pa večji, s tem da se pri temperaturah okrog 200 °C opazi tudi martenzitna premena.

Pri večjih hitrostih ohlajanja (merjeno v sekundah ohlajanja med 800 in 500 °C, oznaka t8/5) dobimo pri hitrosti t8/5 = 165 s že popolnoma martenzitno premeno. V začetku martenzitne premene smo opazili anomalijo (črtkana krivulja M<sub>s</sub>). Podobni rezultati iz literature to anomalijo omenjajo, vendar brez ustrezne razlage. Ugotavljamo pa, da je anomalija pri krajsih časih destabilizacije bolj izrazita.

Naša preizkušanja so bila izvedena v omejenem obsegu, vendar se vidi, da ima čas destabilizacije, ki vpliva na obseg izločanja sekundarnih karbidov, bistveno vlogo na transformacijo avstenita pri kasnejšem ohlajevanju. Večja stopnja destabilizacije avstenita pospešuje obseg transformacije v perlitni stopnji. Anomalija pri martenzitni premeni, ki je večja pri manjši destabilizaciji avstenita, je verjetno povezana z nehomogenostjo avstenita. Ta je vsekakor večja pri nepopolni destabilizaciji.

Premenske točke, ki so vrisane na diagramu, smo določili na podlagi dilatometrskih krivulj pri kontinuirnem ogrevanju s hitrostjo 300 °C/h.

Mikrostruktura matice je odvisna od hitrosti ohlajanja. Pri delni destabilizaciji je v sredini kristalnih zrn še avstenit.

At higher cooling rates (measured in seconds for cooling from 800 to 500 °C, marked by t8/5) a complete martensitic transformation is obtained at the rate t8/5 = 165 s. In the beginning of the martensitic transformation an anomaly was observed (dashed curve M<sub>s</sub>). Similar results in references mention this anomaly but without any explanation. It was found that the anomaly is more pronounced at shorter times of destabilization.

Our testing was limited but it is evident that the time of destabilization which influences the extent of secondary-carbide precipitation has an essential role in the transformation of austenite at further cooling. Higher stage of austenite destabilization accelerates the extent of transformation in the pearlitic stage. The anomaly in the martensitic transformation which is greater at smaller destabilization of austenite is probably connected with the unhomogeneity of austenite. This is anyhow greater at uncomplete destabilization.

Transformation points being plotted into the diagram were determined from dilatometric curves in continuous heating at the rate 300 °C/h.

The microstructure of the matrix depends on the cooling rate. In partial destabilization still austenite is found in the centre of crystal grains.

Residual austenite can be obtained at harsher conditions of hardening and at higher contents of Mn and Ni.

Morphology of pearlite depends on the degree of destabilization as it was already explained at the isothermal conditions of the transformation.

### Hardness of Alloys

Corresponding applicable properties of white chromium cast irons depend on the amount of eutectic carbides in the microstructure, and on the hardness of matrix (6, 7). The best wear resistance and the hardness possess the alloys with martensitic matrix. Alloys with martensitic-pearlitic matrix are softer, their hardness depends on the portion of pearlitic phase (11, 12).

The alloy for which the transformation diagrams were constructed exhibited as cast on the cross section cast in mould the average hardness 650 HV, and on the cross section cast into sand 635 HV respectively. Destabilized samples with martensitic matrix had hardnesses between 760 and 800 HV.

The highest hardness of alloys with 15 to 18 % Cr is obtained by hardening from the temperature between 940 and 970 °C. For the alloys with higher contents of Cr (over 20 %) the temperatures of hardening are higher, up to 1010 °C. Martensite is harder if more carbon is dissolved in austenite. Solubility of carbon increases with the increased temperature of hardening (18). By hardening from higher temperatures, also residual austenite can be obtained in the microstructure, especially if alloys contain over 1 % Mn. Also Ni (Cu) acts like Mn which on the other hand improves the through-hardenability. In our alloys the residual austenite was not detected by dilatometric investigations. The residual austenite was obtained in the matrix only under harsher conditions of hardening from higher temperatures.

The samples were hardened in air from the destabilization temperature of 970 °C. Martensite is stable and the hardness starts to drop in tempering above 400 °C (Fig. 21). The hardness of alloys with sufficient portion of residual austenite increases in tempering between 450 and 550 °C due to the decomposition of residual austenite into martensite. The transformation is connected with volume changes, and it is undesired because of internal stresses. Microstructural characteristics of tempered cast iron are shown in Figs. 22 to 26.

Zaostali avstenit lahko dobimo pri ostrejših pogojih kaljenja in pri višjih vsebnosti Mn in Ni.

Morfologija perlita je odvisna od stopnje destabilizacije, kot smo to že razložili pri izotermnih pogojih transformacije.

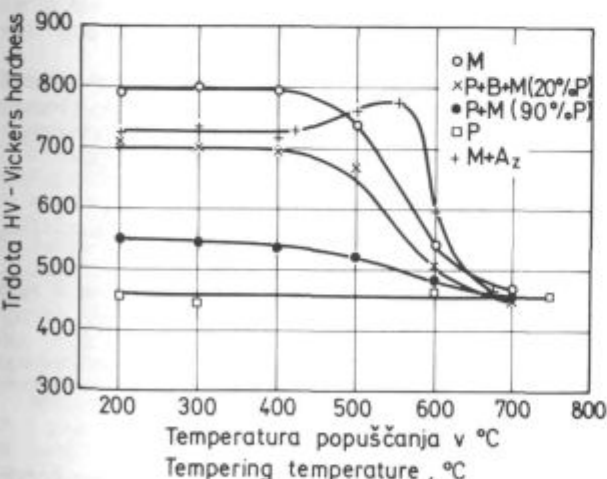
### Trdota zlitin

Ustrezne uporabne lastnosti belih kromovih litin so odvisne od deleža evtektičnih karbidov v mikrostrukturi in trdote matice (6, 7). Najboljšo obrabno obstojnost in trdoto imajo zlitine z martenzitno matico. Zlitine z martenzitno perlito matico so mehkajše, njihova trdota pa je odvisna od deleža perlite faze. (11, 12).

Zlitina, za katero so narejeni transformacijski diagrami, ima vitem stanju na preseku ulitem v kokilo, povprečno trdoto 650 HV in na preseku ulitem v pesek 635 HV. Destabilizirani vzorci z martenzitno matico imajo trdoto med 760 in 800 HV.

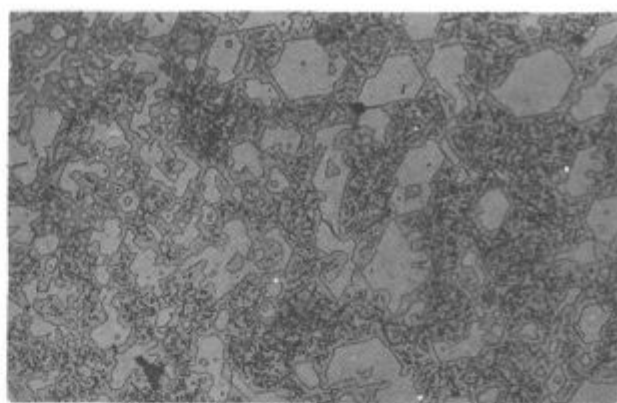
Največjo trdoto zlitin s 15 do 18 % Cr dobimo pri kaljenju s temperaturom med 940 in 970 °C. Za zlitine z višjo vsebnostjo Cr (nad 20 %) so temperature kaljenja višje, do 1010 °C. Martenzit je trši, čim več C je raztopljenega v avstenitu. Topnost C narašča z naraščajočo temperaturo kaljenja (18). Pri kaljenju z višjimi temperaturami pa lahko dobimo v mikrostrukturi še zaostali avstenit, zlasti še, če vsebujejo zlitine nad 1 % Mn. Podobno kot Mn učinkuje tudi Ni (Cu), ki sicer izboljša prekaljivost. V naših zlitinah zaostalega avstenita z dilatometrikskimi preiskavami nismo zasledili. Zaostali avstenit smo dobili v matici le pri ostrejših pogojih kaljenja z višjimi temperaturami.

Vzorce smo kalili na zraku s temperaturom destabilizacije 970 °C. Martenzit je stabilen in trdota prične pada pri popuščanju nad 400 °C (sl. 21). Trdota zlitin z zadostnim deležem zaostalega avstenita pri popuščanju med 450 in 550 °C naraste zaradi razpada zaostalega avstenita v martenzit. Premera je povezana z volumskimi spremembami in je zaradi notranjih napetosti nezažljena. Mikrostrukturne značilnosti popuščene litine so prikazane na slikah 22, 23, 24, 25 in 26.



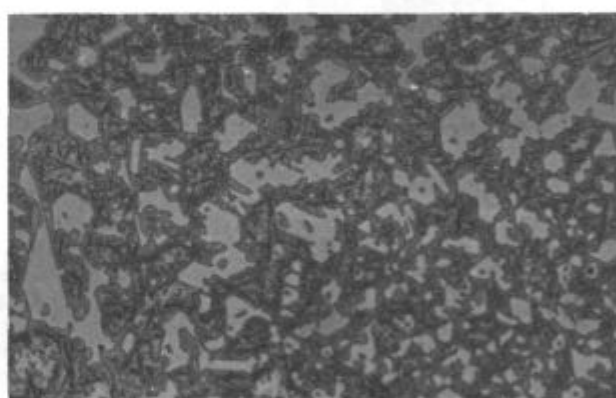
Sl. 21:  
Vpliv temperature popuščanja na trdoto destabilizirane litine z različno mikrostrukturo matice (M — martenzit, B — bainit, P — perlit, A<sub>z</sub> — zaostali avstenit)

Fig. 21  
Influence of temperature of tempering on the hardness of destabilized cast iron with various microstructures of matrix (M — martensite, B — bainite, P — pearlite, A<sub>z</sub> — residual austenite)



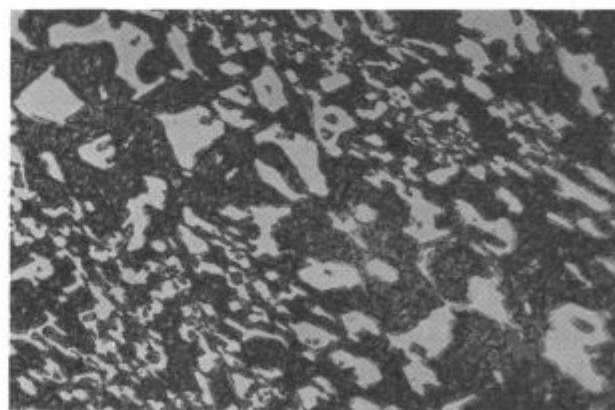
Sl. 22:  
Mikrostruktura destabilizirane litine kaljene na zraku. Matica je iz sekundarnih karbidov in martenzita. Pov. 500 ×

Fig. 22  
Microstructure of destabilized cast iron hardened in air. Matrix is of secondary carbides and martensite. Mag. 500 ×



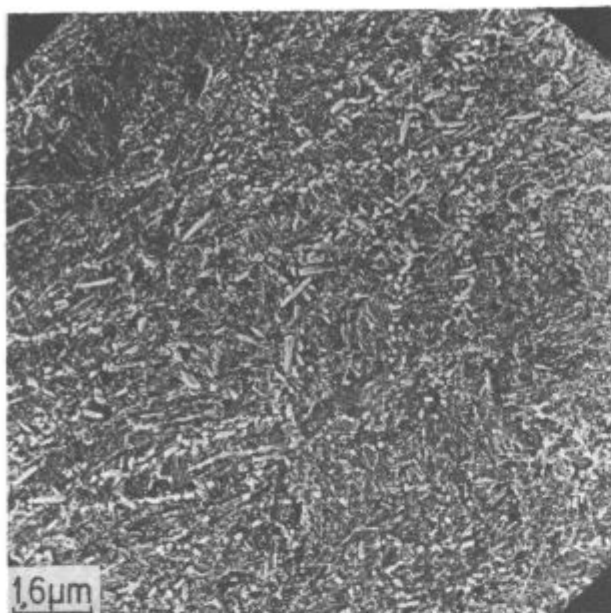
Sl. 23:  
Mikrostruktura kaljene litine 2 uri popuščane na 400 °C. Pov. 500 ×

Fig. 23  
Microstructure of hardened cast iron, tempered 2 hours at 400 °C. Magn. 500 ×



Sl. 24:  
Mikrostruktura kaljene litine 2 uri popuščane na 600 °C. Pov. 500 ×

Fig. 24  
Microstructure of hardened cast iron, tempered 2 hours at 600 °C. Magn. 500 ×



Sl. 25:  
SEM posnetek na zraku kaljene litine. Mikrostruktura matice je iz sekundarnih karbidov in martenzita.

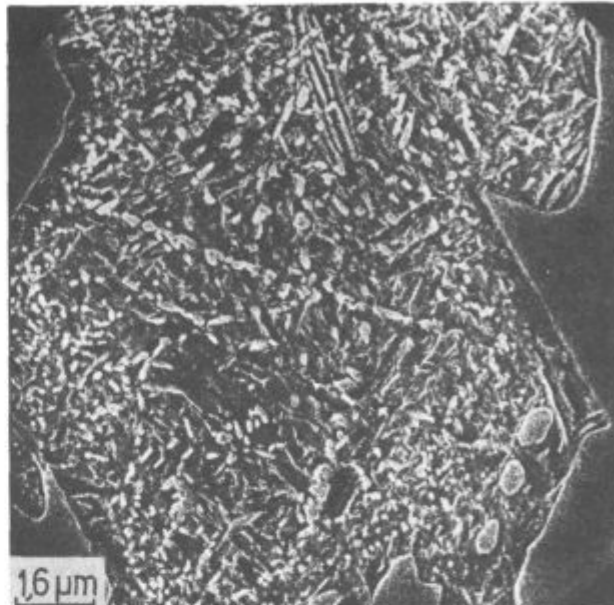
Fig. 25  
SEM picture of air-hardened cast iron. Microstructure of matrix is of secondary carbides and martensite.

S kontinuirnim ohlajanjem smo pripravili vzorce z mešano perlitno-bainitno-martenzitno mikrostrukture. Potez trdote v odvisnosti od temperature popuščanja je podoben kot pri vzorcih z martenzitno matico, le izhodna trdota je nižja. Trdota vzorcev s perlitno matico se pri popuščanju ne spremeni.

Trdote ostalih preiskovanih zlitin z avstenitno matico v litem stanju so podobne, tiste z avstenitno-perlitno ali popolnoma perlitno matico pa so mehkje in je njihova trdota med 480 in 550 HV. Temu ustreze so tudi trdote po topotni obdelavi. Trdota je pri zlitinah z avstenitno matico v litem stanju enaka po celiem preseku preizkusnih valjčkov.

Mikrotrdote posameznih mikrostrukturnih faz so podane v tabeli 4. Pri karbidih  $M_7C_3$  moramo upoštevati, da je njihova trdota odvisna od kristalografske smeri, v kateri jo merimo (6).

Tabela 4: Mikrotrdote mikrostrukturnih faz	HV
Primarni in evtektički karbidi $M_7C_3$	900—1300
Martenzit, sekundarni karbidi	650—700
Avstenit	400—520
Perlit, sekundarni karbidi	360—420



Sl. 26:  
SEM posnetek kaljene litine 2 uri popuščane na 300°C

Fig. 26  
SEM picture of hardened cast iron, tempered 2 hours at 300°C

By continuous cooling the samples with mixed pearlite-bainitic-martensitic microstructure were prepared. The variation of hardness depending on the tempering temperature is similar to that in the samples with martensitic matrix, only the initial hardness is lower. Hardness of samples with pearlitic matrix does not change in tempering.

Hardnesses of the other investigated as cast alloys with austenitic matrix are similar to that of alloys with austenitic-pearlitic matrix, but the alloys with fully pearlitic matrix are softer and their hardnesses varied between 480 and 550 HV. Similar relationship remains also after the heat treatment. Hardness of the as cast alloys with austenitic matrix is practically equal through the whole cross section of testing cylinders.

Microhardnesses of single microstructural phases are given in Table 4. It is necessary to take into account that the hardness of  $M_7C_3$  carbides depends on the crystallographic direction in which it is measured (6).

Table 4 Microhardnesses of Microstructural Phases

Phase	HV
$M_7C_3$ primary and eutectic carbides	900 ... 1300
Martensite, secondary carbides	650 ... 700
Austenite	400 ... 520
Pearlite, secondary carbides	360 ... 420

## ZAKLJUČEK

Opisane so nekatere mikrostrukturne značilnosti in pogoji topotne obdelave belih kromovih litin, legiranih z Mo in z Ni, Si, Mn, V, Ti, in W, namenjenih za centrifugalno dvošlojno lite valje. Iz preiskav se vidi, da so mehanske lastnosti odvisne od mikrostrukturnih značilnosti in s tem od kemične sestave, pogojev strjevanja in ohlajanja ter topotne obdelave.

Z ustreznim razmerjem Cr/C, legiranjem z Mo in hitrim strjevanjem dobimo v litem stanju drobne evtek-

## CONCLUSIONS

Some microstructural characteristics and the conditions for heat treatment of white chromium cast irons alloyed with Mo, and with Ni, Si, Mn, V, Ti, and W which are intended for centrifugal compound casting of rolls, are presented in the paper. The investigations show that mechanical properties depend on the microstructural characteristics, and thus on the chemical composition, conditions of solidification and cooling, and on the heat treatment.

tične karbide in avstenitno matico, ki je s stališča nadaljnje toplotne obdelave najustreznejša. Sicer pa je matica lahko tudi avstenitno-perlitna ali perlitra.

Dlež karbidne faze je odvisen predvsem od vsebnosti C. Primarni heksagonalni karbidi, ki nastajajo pri počasnem ohlajanju ali pri deležu karbidne faze, večjem od 35 %, so nezaželeni, ker bistveno poslabšajo žilavost litin. Po kemični sestavi ustrezajo karbidi stechiometričnemu razmerju od  $(Cr_3Fe_4)C_3$  do  $(Cr_4Fe_3)C_3$ . Z naraščajočo vrednostjo razmerja Cr/C narašča vsebnost Cr v karbidih. Karbidi  $M_7C_3$  z več Cr so trši. V evtektičnih karbidih je pri istem razmerju Cr/C manj Cr kot v primarnih karbidih.

Trdota litin je odvisna od deleža evtektičnih karbidoval in trdote mikrostrukture, ki jo dobimo po toplotni obdelavi. Osnova za toplotno obdelavo litin sta TTT diagrama za destabilizacijo avstenita in za destabiliziran avstenit in CTT diagram za destabiliziran avstenit.

Morfologija izločanja sekundarnih karbidoval (destabilizacija avstenita) in perlitrne transformacije nedestabiliziranega avstenita je podobna. Oba procesa potekata s kristalnih mej proti sredini kristalnih zrn, in to hitreje po določenih kristalografskih ravninah. V destabiliziranem avstenitu poteka kontinuirna perlitrna transformacija.

Izločanje sekundarnih karbidoval, ki poteka najhitreje med 940 in  $990^{\circ}C$ , je bistvenega pomena za nadaljnjo toplotno obdelavo litin. Le v destabilizirani matici je mogoča martenzitna in tudi bainitna transformacija. Bainitna transformacija poteka počasi in je za prakso manj pomembna. Najtrše so litine z martenzitno matico. Z ustrezno toplotno obdelavo pa lahko dobimo zlitine z martenzitno-perlitno ali perlitno matico, ki so mekejše. Pri popuščanju litin z martenzitno ali martenzitno-perlitno matico prične trdota padati pri temperaturah popuščanja nad  $400^{\circ}C$ .

Suitable Cr/C ratio, alloying with Mo, and fast solidification enable the formation of fine eutectic carbides in the austenitic matrix in cast state which is the most desired from the viewpoint of further heat treatment. Matrix can also be austenitic-pearlitic or only pearlitic.

Portion of carbide phase depends mainly on the carbon content. Primary hexagonal carbides formed during slow cooling or in alloys containing more than 35 % of carbide phase are undesired since they essentially reduce the toughness of alloys. According to the chemical compositions the carbides correspond to stoichiometric ratios from  $(Cr_3Fe_4)C_3$  to  $(Cr_4Fe_3)C_3$ . The increasing value of the Cr/C ratio causes the increased content of Cr in carbides.  $M_7C_3$  with higher Cr content are harder. Eutectic carbides at the same Cr/C ratio contain less Cr than the primary ones.

Hardness of cast irons depend on the amount of eutectic carbides and on the hardness of the microstructure obtained by the heat treatment. Basis for the heat treatment of cast irons are the TTT diagrams for the destabilization of austenite, and for destabilized austenite, beside the CTT diagram for the destabilized austenite.

Morphologies of precipitation of secondary carbides (destabilization of austenite), and of pearlitic transformation of undestabilized austenite are similar. Both processes start on the crystal boundaries and proceed towards the centre of grains, and the process is faster along certain crystallographic planes. In destabilized austenite continuous pearlitic transformation takes place.

Precipitation of secondary carbides which is the fastest between 940 and  $990^{\circ}C$  is essential for further heat treatment of cast irons. Only in destabilized matrix the martensitic and also bainitic transformation is possible. Bainitic transformation is slow and it is less important for practical applications. The hardest are the alloys with martensitic matrix. By a suitable heat treatment the alloys with martensitic-pearlitic or pearlitic matrix can be obtained, but they are softer. In tempering the cast irons with martensitic or martensitic-pearlitic matrix, their hardness begins to decrease at the tempering temperatures above  $400^{\circ}C$ .

#### LITERATURA/REFERENCES

1. F. Maratray, R. Usseglio-Nanot: Factors Affecting the Structure of Chromium and Chromium-Molybdenum White Irons, Climax Molybdenum, 1979
2. F. Maratray, R. Usseglio-Nanot: Atlas, Transformation Characteristics of Chromium and Chromium-Molybdenum White Irons, Climax Molybdenum, 1979
3. Metals Handbook: Metallography, Structures and Phase Diagrams, vol. 8, American Society for Metals, 1973
4. R. S. Jackson: Journal of the Iron and Steel Institute, 1970, febr., 163—167
5. J. D. B. DeMello, M. Durand-Charre, S. Hamar-Thibault: Metallurgical Transactions, 1983, sept., 1793—1801
6. W. Fairhurst, K. Röhrlig: Foundry Trade Journal, 1974, May, 685—698
7. J. Drabina, A. Mazur: Giesserei Praxis, 1981, 6, 108—112
8. Centrifugally Cast High-chromium Rolls, Transactions ISIJ, 1986, pp. 168
9. T. Minemura, A. Inoue, T. Masumoto: Transactions ISIJ, vol. 21, 1981, pp. 649—655
10. J. T. H. Pearce, D. W. L. Elwell: Journal of Materials Science Letters, 5, 1986, pp. 1063—1064
11. L. H. Price: Metal Progress, 1983, aug., 21—27
12. R. W. Durman: Journal of Mechanical Working Technology, 8, 1983, 217—223
13. I. Katavić: Ljevarstvo (Foundry), 28, 1981, 2, 3—6
14. J. Honda: Transactions ISIJ, vol. 24, 1984, 85—100
15. D. Kmetič et alt.: Development of cast irons for rolls with high content of chromium (Razvoj valjčnih litin z visoko vsebnostjo kroma) — Part I. Report of The Institute of Metallurgy, Ljubljana, 1983
16. D. Kmetič et alt.: Development of cast irons for rolls with high content of chromium (Razvoj valjčnih litin z visoko vsebnostjo kroma) — Part II. Report of The Institute of Metallurgy, Ljubljana, 1984
17. D. Kmetič et alt.: Development of cast irons for rolls with high content of chromium (Razvoj valjčnih litin z visoko vsebnostjo kroma) — Part III. Report of The Institute of Metallurgy, Ljubljana, 1985
18. F. Henke: Giesserei-Praxis, 1975, 23—24, 377—407
19. F. Mlakar, V. Tucić, B. Mlač: Optimal parameters in manufacturing indefinite chill rolls (Optimalni parametri izdelave indefinitne chill valjev). Report of The Institute of Metallurgy, Ljubljana, 1980



# Osnovni koncept numerične simulacije radialnega kovanja

## Basic Concepts of Numerical Simulation of a Radial Forging Process

T. Rodič\*, D. R. J. Owen\*\*

UDK: 621.73.045:519.6  
ASM/SLA: F22, Q24, 1—66, U4g, U4k

### 1. UVOD

S spoznaji splošnih principov fizikalne metalurgije<sup>1</sup> postajajo preoblikovalni procesi v vročem pomembnejši. Preoblikovanje v vročem že dolgo ni več samo spremiščanje oblike preoblikovanca, temveč termomehanska obdelava materiala, ki naj privede do ugodnih strukturnih sprememb. Pri upoštevanju medsebojnih odvisnosti med strukturo, lastnostmi in obnašanjem materiala med plastičnim preoblikovanjem so deformacija, hitrost deformacije in temperatura tiste fizikalne večine, ki imajo odločilni vpliv. Nadzorovana porazdelitev teh termomehanskih parametrov med preoblikovanjem je potrebna pri optimirjanju preoblikovalne operacije. Preoblikovalni procesi v vročem so zahtevni za eksperimentalna opazovanja zaradi visokih temperatur in preoblikovalnih hitrosti. Od tod tudi potreba po matematičnih in numeričnih modelih, ki pripomorejo k boljšemu razumevanju eksperimentalnih rezultatov ali celo delno nadomeščajo draga preizkušanja. Tri klasične metode za analizo preoblikovalnih procesov so bile pogosto uporabljane v preteklosti<sup>2</sup>:

- metoda elementarne plastomehanike
- metoda drsnih linij
- metoda zgornje in spodnje meje.

Analiza preoblikovalnih procesov je zahtevna in mnogo poenostavljena predpostavka je bilo vpeljanih v klasičnih metodah, da bi se izognili matematičnim težavam, kar je seveda zmanjševalo njihovo uporabnost. Napredek numeričnih metod v zadnjem času, posebej metode končnih elementov<sup>3</sup> (MKE) in vzporedno zmanjševanje cen računalniških obdelav, ponuja možnost za realnejše simulacije preoblikovalnih procesov.

### 2. MATEMATIČNI MODEL

Za analizo porazdelitev napetosti, deformacij in temperature, ki se spreminja znotraj deformacijske cone med preoblikovanjem, je nujna uporaba numeričnih metod. Razvoj MKE na področju plastomehanike<sup>4</sup> in prenosa toplote ponuja zadovoljivo orodje za računalniško simulacijo preoblikovalnih procesov v vročem.

Simulacijo preoblikovalnega procesa v vročem lahko idealiziramo<sup>5</sup>, kot je to prikazano na sliki 1.

### 1. INTRODUCTION

Since the general principles of physical metallurgy were recognised<sup>1</sup>, the hot working processes are no longer only concerned with shape changes but also consider the thermomechanical treatment which contributes to beneficial structural changes within the material. In considering the interaction between the structure, properties and performance of the material under plastic deformation, the strain, strain rate and temperature are quantities which have a fundamental influence and a controlled variation of these thermomechanical parameters is essential for optimising the forming operation. The nature of hot working processes makes experimental observations difficult, due to the high temperatures and speeds involved. Therefore mathematical and numerical models have a role to play in either improving the interpretation of experimental results or even replacing, in part, an expensive testing programme. Three classical methods for analysing metal forming problems have been widely used in the past<sup>2</sup>:

- elementary plasticity
- the slip line method
- the upper and lower bound method.

Metal forming processes are complex and many simplifying assumptions have been introduced to these classical methods in order to avoid mathematical difficulties. This, however, limits their applicability. Recent developments of numerical methods, in particular the Finite Element Method<sup>3</sup> (FEM), and a parallel reduction in unit computing costs offer an opportunity for a more realistic simulation of working processes.

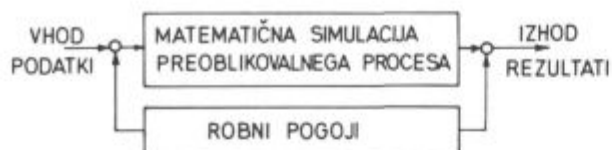
### 2. MATHEMATICAL MODEL

The complex stress-strain and temperature distributions which vary across the deformed region during the deformation process require the use of numerical methods. Developments in the FEM in the field of plastomechanics<sup>4</sup> and heat transfer offer a satisfactory tool for computer simulation of hot working processes.

The numerical simulation of the hot working process can be idealised<sup>5</sup> as shown in Fig. 1.

\* FNT — Odsek za metalurgijo, Univerza E. Kardelja, Ljubljana

\*\* Dept. of Civil Engineering, University of Wales, Swansea, U. K.



**Slika 1:**  
Simulacija preoblikovalnega procesa.

*Vhodni podatki* predstavljajo lastnosti in začetno stanje preoblikovanca, kot so: oblika, porazdelitev temperature, sestava in mikrostruktura materiala.

*Matematična simulacija preoblikovalnega procesa:* Pri MKE razdelimo preoblikovanec na manjša območja, imenovana elementi. Togost vsakega elementa je določena z njegovo geometrijo in lastnostmi materiala, ki jih elementu pripisemo. Oba vpliva obravnavamo ločeno in zato relativno enostavno vgrajujemo različne *materialne modele*. Model preoblikovanca dobimo s sestavljanjem togostnih matrik elementov. Takšen pristop omogoča analizo različnih geometrijsko zahtevnih preoblikovalnih procesov.

Z *robnnimi pogoji* simuliramo različne pogoje, v katerih poteka proces.

*Izhodni rezultati.* Po obdelavi rezultatov numerične analize določimo optimalne tehnološke pogoje. Nazoren grafični prikaz rezultatov je pomemben sestavni del analize z MKE.

### 3. MATERIALNI MODEL

Pri modeliranju obnašanja materiala med plastično deformacijo je potrebno poznavanje ustreznih napetosti tečenja. V splošnem je ta odvisna od sestave in mikrostrukture materiala in od hitrosti deformacije, temperaturе ter deformacijskega stanja, povzročenega s plastično deformacijo. Napetost tečenja določimo z nateznim, tlachnim ali torzijskim preizkusom<sup>6</sup>. Pogosto napetosti tečenja niso dosegljive za specifične kombinacije termome-

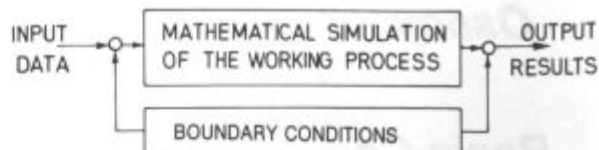


**Fig. 1:**  
Simulation of the working process.

*Input data* represent the material properties and initial state of the workpiece; such as shape, temperature distribution, composition and microstructure of the material.

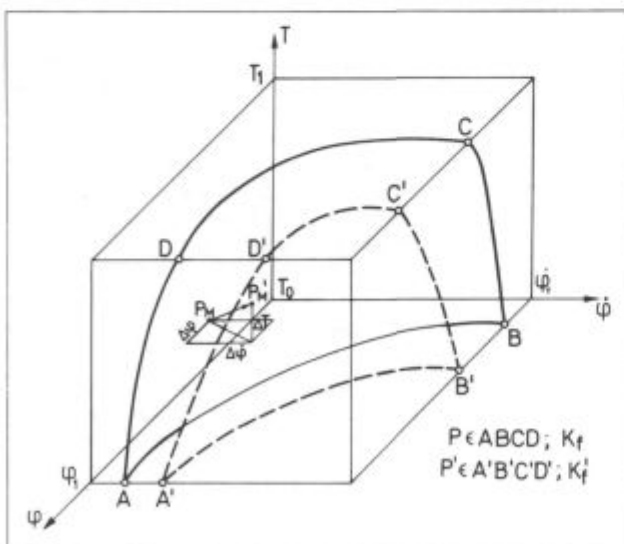
*Mathematical simulation of the working process:* In FEM the workpiece is divided into small regions termed elements. The stiffness of each element is determined by its geometry and material properties. Both effects are considered separately and therefore it is relatively simple to incorporate different *material models*. The workpiece model is obtained by combining the stiffness contribution of each element. Thus any complex shape of the workpiece model can be analysed using the FEM.

*Boundary conditions* are applied to simulate different conditions under which the process is to operate.

*Output results:* A decision on the most suitable set of operating conditions can be made by postprocessing the numerical results. Graphical representations play an integral part in the interpretation of the numerical results of a FEM analysis.

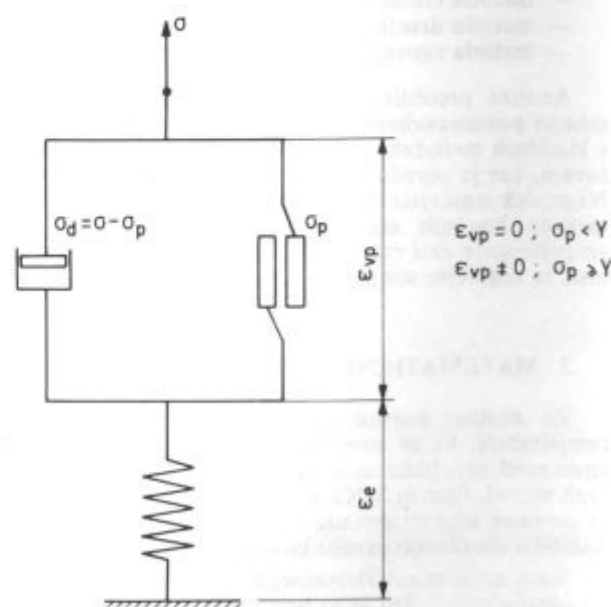
### 3. MATERIAL MODELS

In the modelling of material behaviour during metalworking processes a knowledge of the appropriate flow stress for the material is essential. In general this will depend on the composition and microstructure of the material and on the strain rate, temperature and deformation modes imposed by the working process. The flow



**Slika 2:**  
Ploskve napetosti tečenja v prostoru termomehanskih parametrov.

**Fig. 2:**  
Flow stress surfaces in the space of the thermomechanical parameters.



**Slika 3:**  
Osnovni enodimensionalni elasto-viskoplastični reološki model.

**Fig. 3:**  
Basic one-dimensional elasto-viscoplastic rheological model.

hanskih parametrov in jih ocenimo s pomočjo poznanih podatkov. Znane so različne interpolacijske enačbe, kot na primer Hajdukova<sup>7</sup> ali Sellars-Tegartova enačba<sup>8</sup>. Na podlagi teh enačb lahko določimo potencial napetosti tečenja v prostoru deformacije, hitrosti deformacije in temperature<sup>9</sup> (Sl. 2). Ploskev A-B-C-D je določena z  $\varphi$ ,  $\dot{\varphi}$ ,  $T$ , ki povzročajo enako napetost tečenja  $K_f$  pri določenem stanju mikrostrukturi materiala. V splošnem se v delcu materiala med preoblikovanim procesom termomehanski parametri spreminjajo iz  $\varphi$ ,  $\dot{\varphi}$ ,  $T$  v  $\varphi'$ ,  $\dot{\varphi}'$ ,  $T'$  in temu ustrezno se spremeni napetost tečenja iz  $K_f$  v  $K'_f$ , ki je določena s ploskvijo A'-B'-C'-D'. Za napovedovanje sprememb termomehanskih parametrov med preoblikovalnim procesom v vročem uporabljamo elasto-viskoplastični materialni model, združen s prenosom toplote.

#### 4. OSNOVNE ENAČBE ELASTO-VISKOPLASTIČNOSTI

Osnovni enodimensionalni elasto-viskoplastični reološki model, ki je predstavljen na sliki 3, lahko razširimo za primer splošnega kontinuma. Postopek je podrobno opisan v literaturi [4]. Na tem mestu bodo predstavljene le najosnovnejše enačbe (Sl. 4).

Hitrost deformacije je razdeljena na elastično  $\dot{\varepsilon}_e$  in visokoplastično  $\dot{\varepsilon}_{vp}$  komponento (En. 1). Elastična hitrost deformacije je določena s Hookeovim zakonom, medtem ko  $\dot{\varepsilon}_{vp}$  izrazimo z ustreznim zakonom tečenja. S tem dobimo enačbo (En. 2), kjer je  $\gamma$  parameter tečenja in  $\Phi$  je funkcija, ki je različna od nič samo za pozitivne vrednosti funkcije F. Začetek visokoplastičnega obnašanja določa pogoj, izražen s skalarno enačbo (En. 3), kjer je  $K_f$  napetost tečenja pri enoosnem preizkusu in  $\chi$  parameter utrjevanja. Enočbi (En. 1) in (En. 2) lahko zapišemo v inkrementalni obliku in tako dobimo izraz (En. 4), ki določa spremembo napetosti v časovnem koraku  $\Delta t_n = t_{n+1} - t_n$ . Z uporabo implicitne časovno integracijske sheme (En. 6), kjer je hitrost viskoplastične deformacije na koncu časovnega intervala izražena s pomočjo prvih dveh članov Taylorjeve vrste (En. 7), dobimo končni izraz za inkrement napetosti. (En. 8, 9). Plastično delo se med preoblikovanjem spreminja v toploto, kar povzroča prirastek temperature. Povprečno hitrost generacije toplote v časovnem koraku izračunamo s pomočjo izrazov (En. 10, 11), kjer je f frakcija plastičnega dela, ki jo akumulira material.

Analiza nestacionarnega prenosa toplote z MKE je opisana v literaturi [9].

#### 5. ROBNI POGOJI

Z robnimi pogoji simuliramo pogoje, v katerih poteka preoblikovalni proces. V splošnem ločimo mehanske in termalne robne pogoje.

##### 5.1. Mehanski robni pogoji

Mehanski robni pogoji so odvisni od oblike in gibanja orodja ter od trenjskih razmer med orodjem in preoblikovancem.

Med preoblikovanjem se preoblikovalni stroj elastično deformira. Problem poenostavimo, če privzamemo, da je stroj tog. Tako je gibanje orodja popolnoma opisano z gibanjem ene točke, ki ga izračunamo iz kinematike stroja<sup>10</sup>. Ti podatki so del vhodnih podatkov in so lahko časovno odvisni.

stress is determined from true stress — true strain data obtained from tension, compression or torsion tests<sup>5</sup>. Frequently stress — strain data are not available for specific combinations of the required conditions and they must be estimated from data that are available. Various expressions have been suggested for the interpolation of high temperature data, for example Hajduk's<sup>7</sup> relation or the Sellars — Tegart expression<sup>8</sup>. On the basis of these expressions the material flow stress surface in the strain, strain rate and temperature space can be represented<sup>5</sup> (Fig. 2). Surface A-B-C-D is defined by the  $\varphi$ ,  $\dot{\varphi}$ ,  $T$  required to give the same flow stress  $K_f$  for a particular state of the microstructure of the material. In a part of the deformed material the thermomechanical parameters  $\varphi$ ,  $\dot{\varphi}$ ,  $T$  will change to  $\varphi'$ ,  $\dot{\varphi}'$ ,  $T'$  during the forming process and the flow stress will be changed from  $K_f$  to  $K'_f$  defined by surface A'-B'-C'-D'. To predict the change of the thermomechanical parameters during the hot working operation an elasto-viscoplastic material model coupled with heat transfer is used.

#### 4. BASIC CONCEPTS OF ELASTO-VISCOPLASTICITY

The basic one dimensional elasto-viscoplastic rheological model shown in Fig. 3 can be extended to the case of general continua. Details of this approach are provided in Ref. 4 and only essential expressions are reproduced in Fig. 4.

The total strain rate is separated into elastic  $\dot{\varepsilon}_e$  and viscoplastic  $\dot{\varepsilon}_{vp}$  components (Eq. 1). The elastic strain rate obeys Hooke's law and  $\dot{\varepsilon}_{vp}$  is expressed by the appropriate viscoplastic flow rule. This gives the governing equation (Eq. 2) where  $\gamma$  is fluidity parameter and  $\Phi$  is taken as non-zero for positive values of the yield function, F, only. The onset of viscoplastic behaviour is governed by a scalar yield condition (Eq. 3) where the uniaxial yield stress is denoted by  $K_f$  and  $\chi$  is a hardening parameter. The rate equations (Eq. 1, 2) can be written in an incremental form to give the stress increment occurring in time step  $\Delta t_n = t_{n+1} - t_n$  (Eq. 4). Use of the implicit time integration scheme (Eq. 6) where the viscoplastic strain rate at the end of the time step is predicted by a limited Taylor series expansion (Eq. 7) results in (Eq. 8, 9) for the stress increment. Most of the plastic work done during the time step is converted into heat and gives an increase of temperature. The average rate of heat generation within the time step which enters the thermal analysis is calculated according to (Eq. 10, 11) where, f, is a fraction of the plastic work stored in material.

Thermal transient finite element analysis is described in Ref. 9.

#### 5. BOUNDARY CONDITIONS

The boundary conditions represent the conditions under which the process is to operate. Generally we distinguish between mechanical and thermal boundary conditions.

##### 5.1. Mechanical boundary conditions

The mechanical boundary conditions depend on the shape and movement of the die and the friction at the die — workpiece interface.

During the course of the forming process the forming machine undergoes elastic deformation. To simplify the problem the forming machine is assumed to be rigid. Therefore the motion of the die can be completely described by specifying a velocity at one point which can be calculated from the kinematics of the forging ma-

**OSNOVNE ENAČBE ELASTO-VISCOPLASTIČNOSTI  
BASIC EQUATIONS OF ELASTO-VISCOPLASTICITY**

$$\{ \dot{\epsilon} \} = \{ \dot{\epsilon}_e \} + \{ \dot{\epsilon}_{vp} \} \quad \dots \dots \dots \quad (1)$$

$$\{ \dot{\epsilon} \} = [E]^{-1} \{ \dot{\sigma} \} + \gamma \langle \Phi(F) \rangle \frac{\partial F}{\partial(\sigma)} \quad \dots \dots \dots \quad (2)$$

$$F(\{\sigma\}, \chi) = f(\{\sigma\}) - K_f(\chi) = 0 \quad \dots \dots \dots \quad (3)$$

Inkrementalna oblika osnovnih enačb:  
Incremental form of the basic equations:

$$\{ \Delta\sigma^n \} = [E] \{ \Delta\epsilon_e^n \} - [E] \left[ \{ \Delta\epsilon^n \} - \{ \Delta\epsilon_{vp}^n \} \right] \quad \dots \quad (4)$$

$$\{ \Delta\epsilon^n \} = [B^n] \{ \Delta U^n \} \quad \dots \dots \dots \quad (5)$$

$$\{ \Delta\epsilon_{vp}^n \} = \Delta t_n \left[ (1-\theta) \dot{\epsilon}_{vp}^n + \theta \dot{\epsilon}_{vp}^{n+1} \right] ; \quad 0 \leq \theta \leq 1 \quad \dots \quad (6)$$

$$\{ \dot{\epsilon}_{vp}^{n+1} \} = \{ \dot{\epsilon}_{vp}^n \} + \frac{\partial(\dot{\epsilon}_{vp})}{\partial(\sigma^n)} \Delta\sigma^n \quad \dots \dots \dots \quad (7)$$

$$\{ \Delta\sigma^n \} = [\hat{D}^n] \left[ [B^n] \{ \Delta U^n \} - \{ \dot{\epsilon}_{vp}^n \} \Delta t_n \right] \quad \dots \quad (8)$$

$$[\hat{D}^n] = \left[ [E]^{-1} - \theta \Delta t_n \left[ \frac{\partial(\dot{\epsilon}_{vp})}{\partial(\sigma^n)} \right] \right]^{-1} \quad \dots \dots \dots \quad (9)$$

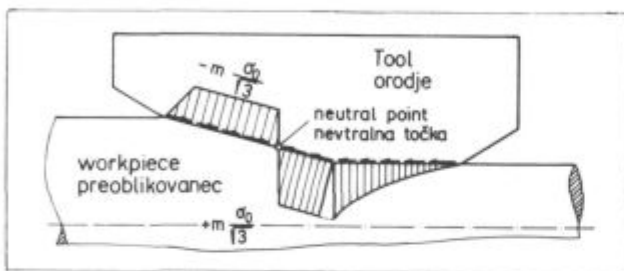
Povprečna hitrost generacije toplotne v časovnem koraku  
Average rate of heat generation within the time step:

$$\dot{Q}^n = (1-f) \{ \sigma^{n+\alpha} \}^T \frac{1}{\Delta t_n} \left[ \{ \dot{\epsilon}_{vp}^{n+1} \} - \{ \dot{\epsilon}_{vp}^n \} \right] \quad \dots \dots \dots \quad (10)$$

$$\{ \sigma^{n+\alpha} \} = \{ \sigma^n \} + \alpha \{ \Delta\sigma^n \} ; \quad 0 \leq \alpha \leq 1 \quad \dots \dots \dots \quad (11)$$

Slika 4:  
Pregled osnovnih enačb.  
Fig. 4:  
Overview of basic equations.

Proces radialnega kovanja v vročem poteku brez maziv pri visokih temperaturah, zato so trenjske razmere v stiku med orodjem in preoblikovancem zahtevne za numerično obravnavo. Porazdelitev strižnih napetosti v kontaktu lahko ustreza Coulombovemu zakonu, pravilu o konstantni strižni napetosti ali lepljenju. Smer strižnih napetosti je odvisna od relativnega gibanja med orodjem in preoblikovancem. Ker je relativno gibanje materiala odvisno od trenjskih razmer, je problem očitno nelinearen. Mesto neutralne točke, kjer ni relativnega gibanja, najdemo z iteracijskim procesom. Ko najdemo pozicijo neutralne točke, lahko trenjske razmere predpišemo, kot je to prikazano na sliki 5.



## 5.2. Termalni robni pogoji

Med preoblikovanjem preoblikovanec izgublja toploto zaradi stika s hladnejšim orodjem in s sevanjem. Za opisovanje teh pogojev uporabljamo standardne matematične robne pogoje.

- predpisano temperaturo na stični površini
- predpisani topotni tok skozi stično površino
- Newtonov zakon o prenosu toplote

## 6. ILUSTRATIVNI PRIMER

Z MKE smo analizirali proces radialnega kovanja na kovaškem stroju z zaokroženimi kladivi, ki je shematično prikazano na sliki 6. Napetostno-deformacijsko stanje pri takšnem kovanju je kvaziaksimetrično. Geometrijo delovnih površin kovaškega kladiva razdelimo na tri dele:<sup>11, 12</sup>

- I — vhodno cono
- II — kalibrirno cono in
- III — izhodno cono.

Skoraj vsa plastična deformacija nastopi v vhodni coni. Glavna parametra vhodne cone sta kot  $\alpha$  na kladivu ter povprečna vhodna hitrost  $V_{inp}$  materiala. Za kovanje z redukcijo  $\varnothing 120/\varnothing 80 \text{ mm}$ , ki smo ga analizirali, je bil kot  $\alpha = 10^\circ$  in  $V_{inp} = 45 \text{ mm/s}$ . Iz teh podatkov in iz poznane kinematike stroja lahko izračunamo:

$L_d$	projekcijo vhodne dotikalne površine na os simetrije (113.4 mm)
$U_{inp}$	pomik vhodnega materiala v smeri simetrijske osi po vsakem udarcu (10 mm)
$W_{rad}$	delovni hod kladiva v radialni smeri (1.76 mm)
$t_{ud}$	čas trajanja udarca (0.018 s)

Uporabljeni podatki o materialu<sup>13</sup>:

Material: X5CrNi18.8

Začetna temperatura 1000°C

chine.<sup>10</sup> These velocity data are part of the input and can be varied with time.

Since the radial forging operation is carried out at high temperatures without lubrication the friction conditions at the tool-workpiece interface face are complex. The distribution of the shear stress at the interface may obey either Coulomb's law, the constant shear rule or sticking friction conditions. However, the direction of the shear stress is unknown due to relative movement of the material at the interface. Since the relative movement is friction dependent the problem clearly becomes nonlinear. The position of the neutral point, where relative sliding is zero must be found by an iterative procedure. After the position of neutral point is established the friction conditions can be prescribed as presented in Fig. 5.

Slika 5:

Predpostavljeni trenjski razmere.

Fig. 5:

Assumed friction conditions.

## 5.2. Thermal boundary conditions

During the forming process the workpiece loses heat due to contact with the colder die and also by radiation. To model these effects, standard mathematical boundary conditions are used:

- prescribed temperature at the contact surface
- prescribed flux across the contact surface
- Newton's law of heat transfer

## 6. ILLUSTRATIVE EXAMPLE

A roundfaced die radial forming proces which is schematically presented in Fig. 6, has been analysed using FEM. The stress-strain field is assumed to be quasi-axisymmetric in this case. The geometry of the working surfaces of the radial forging die is divided into three parts:<sup>11, 12</sup>

- I — the inlet cone
- II — the sizing cone
- III — the outlet cone

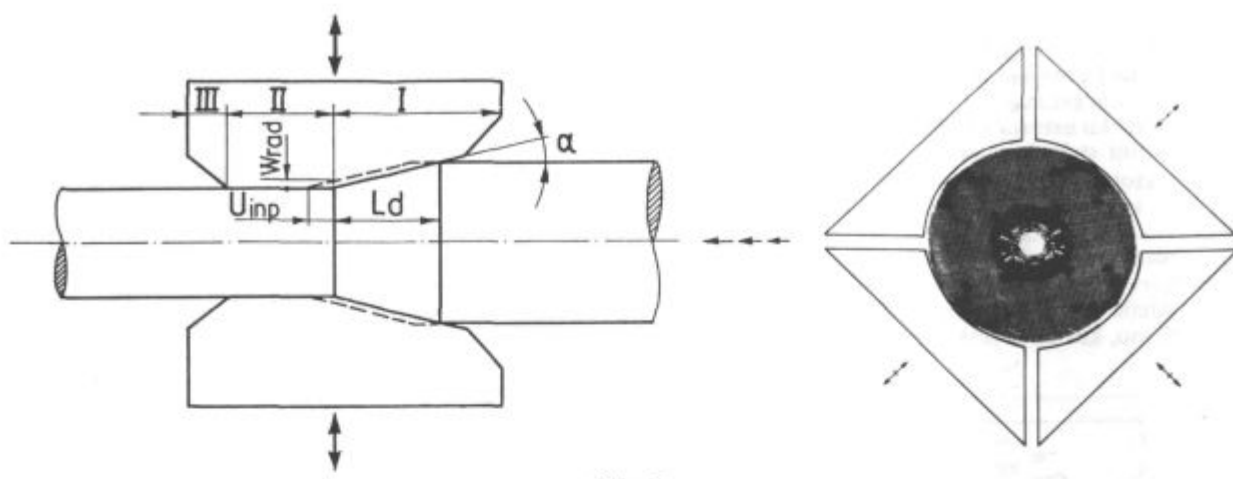
Nearly all the plastic deformation occurs in the inlet cone. The main parameters of the inlet cone are the angle  $\alpha$  of the die and the average speed  $V_{inp}$  of the input material. In the present example the reduction was  $\varnothing 120/\varnothing 80 \text{ mm}$  and the inlet cone angle  $\alpha$  and speed  $V_{inp}$  were  $10^\circ$  and  $45 \text{ mm/s}$  respectively. From this data and kinematics of the machine the following boundary conditions are evaluated:

$L_d$	projection of the inlet cone contact area on to the centreline axis (113.4 mm)
$U_{inp}$	displacement of the input material along the centralline axis after each punch (10 mm)
$W_{rad}$	displacement of the die in the radial direction while in contact with the workpiece (1.76 mm)
$t_{ud}$	duration of the punch (0.018 s)

The material properties used in this example are given below:

Material: X5CrNi18.9

Initial temperature 1000°C



Slika 6:  
Shematični prikaz procesa radialnega kovanja.  
Fig. 6:  
Schematical view of the radial forging process.

Lastnosti materiala pri začetni temperaturi kovanja:<sup>13</sup>

— modul elastičnosti	120 kN/mm <sup>2</sup>
— Poissonov količnik	0.34
— gostota	7430 kg/m <sup>3</sup>
— specifična toplotna kapaciteta	650 J/kg K

Interpolacijska funkcija za napetost tečenja:

$$K_t = K_{t_0} \cdot A_1 \cdot e^{-m_1 T} \cdot A_2 \cdot \varphi^{m_2} \cdot A_3 \cdot \dot{\varphi}^{m_3}$$

kjer je

$$K_{t_0} = 189.5 \text{ N/mm}^2$$

$$A_1 = 12.997 \quad m_1 = 0.00258$$

$$A_2 = 1.570 \quad m_2 = 0.196$$

$$A_3 = 0.740 \quad m_3 = 0.128$$

Uporabljeni so bili 8-vozliščni Serendipity aksialno simetrični končni elementi z reducirano ( $2 \times 2$ ) numerično integracijsko shemo<sup>14</sup> ter von Misesovim kriterijem tečenja z izotropnim modelom utrjevanja materiala.<sup>4</sup> Nelinearni elasto-viskoplastični problem smo reševali z metodo tangencialnih togosti. Pri tem smo uporabili implicitno časovno integracijsko shemo s korekcijo napetosti na koncu vsakega časovnega koraka<sup>15</sup>. Sistem linearnih enačb smo reševali s frontalno metodo<sup>16</sup>.

## REZULTATI

Na slikah 7, 8 in 9 so prikazane posamezne faze razvoja prirastka plastičnih deformacij v preoblikovalni coni med udarcem kladiva. S pomočjo rezultatov MKE lahko na enak način predstavimo prostorsko in časovno porazdelitev ostalih termomehanskih parametrov med preoblikovanjem. To so temperatura ter vse komponente in primerjalne vrednosti tenzorjev napetosti, deformacij in hitrosti deformacij. Določevanje sil, momentov in energije, potrebne za preoblikovanje, je z MKE natančnejše kot pri klasičnih metodah. V mnogih primerih nas zanima tok materiala. Pri kovaško-valjavski liniji, na primer, je glavna naloga kovaškega stroja zapiranje notranjih napak v materialu. Simulacija zapiranja notranjih poroznosti v materialu z MKE je grafično prikazana na sliki 10.

Material properties at the initial temperature:<sup>13</sup>

— Young's modulus	120 kN/mm <sup>2</sup>
— Poisson's ratio	0.34
— density	7430 kg/m <sup>3</sup>
— specific heat capacity	650 J/kg K

Interpolation function for high temperature data:<sup>7</sup>

$$K_t = K_{t_0} \cdot A_1 \cdot e^{-m_1 T} \cdot A_2 \cdot \varphi^{m_2} \cdot A_3 \cdot \dot{\varphi}^{m_3}$$

with:

$$K_{t_0} = 189.5 \text{ N/mm}^2$$

$$A_1 = 12.997 \quad m_1 = 0.00258$$

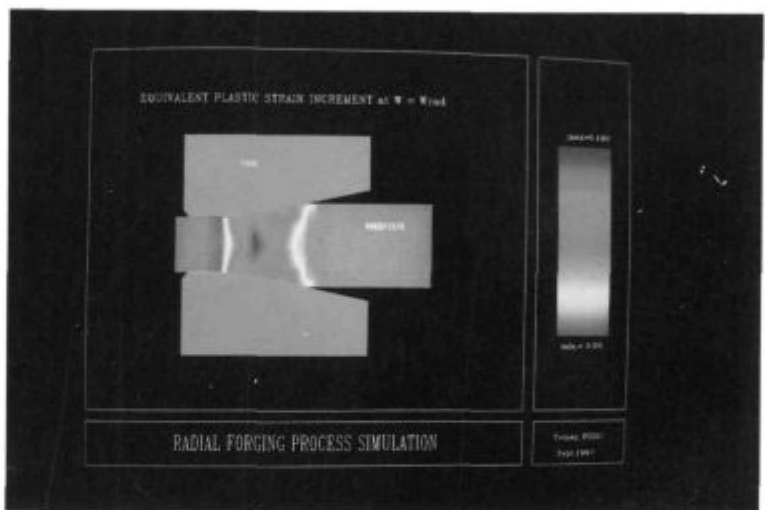
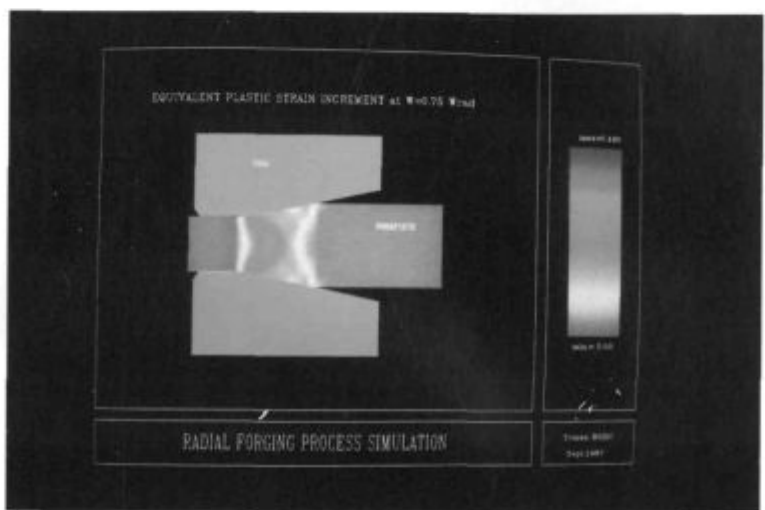
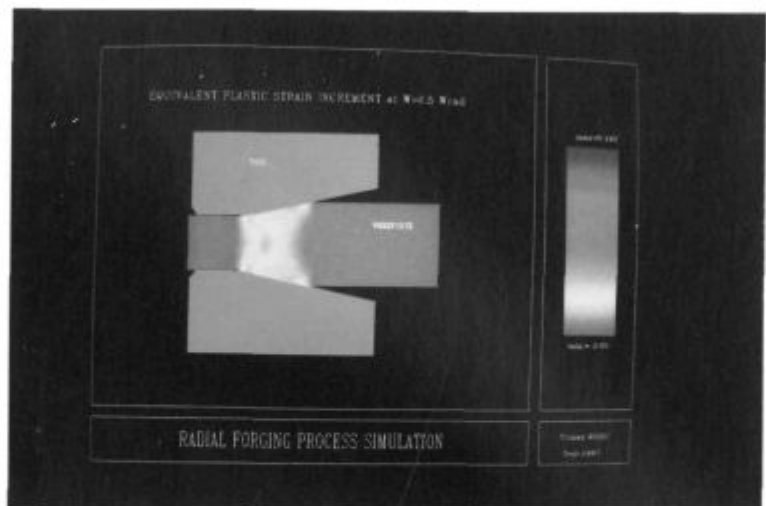
$$A_2 = 1.570 \quad m_2 = 0.196$$

$$A_3 = 0.740 \quad m_3 = 0.128$$

The 8-noded Serendipity axisymmetric elements with reduced ( $2 \times 2$ ) numerical integration scheme<sup>14</sup> were used. A von Mises yield function with isotropic strain hardening was employed.<sup>4</sup> The nonlinear viscoplastic problem was solved by tangential stiffness solution algorithm. An implicit time integration scheme with the stress correction at the end of each time step was performed.<sup>15</sup> The resulting set of linear equations were solved by the frontal technique.<sup>16</sup>

## RESULTS

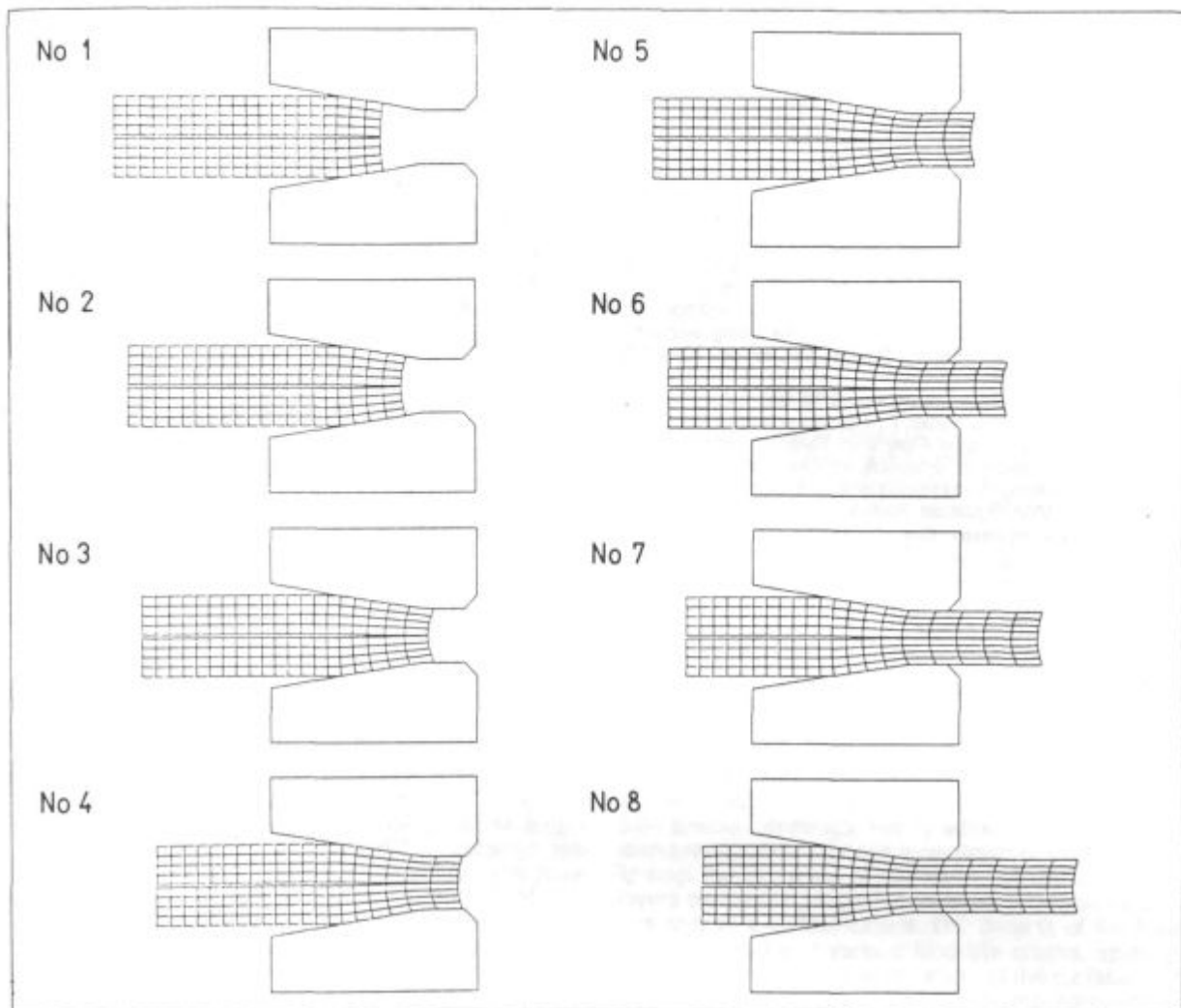
Figures 7, 8 and 9 show the distribution of the increment of the equivalent plastic strain developed at three positions of the die during one stroke of the forging machine. The distribution and history of the other thermomechanical parameters can be similarly represented. These parameters are temperature and all components and equivalent values of the stress, strain and strain rate tensors. Calculation of forces and energy consumption during the forming process by FEM is more accurate than by classical methods. In many cases the material flow is of great interest. In the forging-rolling production line, for example, the main purpose of the forging machine is to close the internal rupture. Modelling of the closure of an internal rupture in a continuous cast billet by the radial-forging process is illustrated in Fig. 10.



**Slike 7, 8 in 9:**  
Prirastek plastičnih deformacij v preoblikovalni coni med udarcem kladiva.

**Fig. 7, 8 and 9:**  
Increment of the equivalent plastic strain developed at three positions of the die during one stroke of the forging machine.





Slika 10:

Modeliranje zapiranja notranih odprtin v konti-liti gredici z radialnim kovanjem.

Fig. 10:

Modelling the closure of an internal rupture in a continuous cast billet by the radial-forging process.

## 7. ZAKLJUČEK

MKE je pogosto uporabljena metoda za analizo preoblikovalnih procesov. V primerjavi s klasičnimi metodami ima naslednje prednosti: z MKE lahko rešujejo primere z zahtevno geometrijo preoblikovanca; problem lahko rešujemo z različnimi materialnimi modeli; možno je obravnavanje nestacionarnih napetostno-deformacijskih in temperaturnih polj. V prihodnje pričakujemo vgrajevanje novih spoznanj s področja fizikalne metalurgije v numerične modele. Prvi koraki v tej smeri so bili že storjeni.<sup>17, 18</sup>

## 6. CONCLUSIONS

The FEM is now widely used for the analysis of metal forming processes. In comparison with classical methods the FEM has certain advantages: various complex shapes can be considered, it enables implementation of different material models and treatment of transient stress-strain and temperature fields. In the future the inclusion of the metallurgical development in the numerical modelling of hot working processes is expected. The first steps toward this goal have already been made.<sup>17, 18</sup>

## LITERATURA/REFERENCES

1. Sellars C. M.: *The Physical Metallurgy of Hot Working The Working and Forming Processes* (edited by Sellars C. M. and Davies G. J.) The Metals Society, London, U. K., (1979)
2. Mahrenholz D. and Dung N. L.: *Mathematical Modeling of Metal Forming Processes by Numerical Methods*. Advanced Technology of Plasticity 1987 (edited by K. Lange), Vol. 1, pp. 3–10, Springer-Verlag, Berlin Heidelberg New York Tokyo, (1987)
3. Zienkiewicz O. C.: *The Finite Element Method* (The third edition) McGRAW-HILL Book Company, London, U. K., (1977)
4. Owen D. R. J., Hinton E.: *Finite Elements in Plasticity*. Pineridge Press Limited, Swansea, U. K., (1980)

5. Rodić T., Štok B., Gologranc F., Owen D. R. J.: Finite Element Modelling of a Radial Forging Process. Advanced Technology of Plasticity 1987 (edited by K. Lange), Vol. 2, pp. 1065—1072, Springer-Verlag, Berlin Heidelberg New York Tokyo, (1987)
6. Richardson G. J., Hawkins D. N., Sellars C. M.: Worked Examples in Metalworking. The Institute of Metals, London, (1985)
7. Hensel A., Spittel T.: Kraft und Arbeitsbedarf Bildsamer Formgebungsverfahren. Deutscher Verlag für Grundstoffindustrie, Leipzig, (1978)
8. Krengel R.: Anpassung von Warmwalzstichplanen . . . Institut für Werkstoffumformung, T. U. Clausthal, (1985)
9. Damjanović F., Owen D. R. J.: Practical Considerations for Thermal Transient Finite Element Analysis Using Isoparametric elements. Nucl. Engng. Design, Vol. 69, pp. 109—126, (1982)
10. Hein O.: Private communications. GFM, Steyr, Austria
11. Lahoti G. D., Liuzzi L., Altan T.: Computer-Aided Analysis of Stresses, Loads, Metal Flow and Temperatures in Radial Forging of Tubes. 1st. International Conference on Rotary Metal — Working Processes, London, (1979)
12. Hojas H.: GFM Precision Radial — Forging Machine. FIA Equipment Symposium, Chicago, (1973)
13. Richter F.: Die Wichtigsten Physikalischen Eigenschaften von 52 Eisenwerkstoffen. Stahleisen-Sonderberichte Heft 8 (1973)
14. Crook A. J. L., Hinton E.: Comparison of 2 D Quadrilateral Finite Elements for Plasticity Problems. Proceedings of the International Conference held in Barcelona, Computational Plasticity, Spain, 6—10th April, 1987
15. Rodić T., Owen D. R. J., Damjanović F.: An approach to correct Elasto-Viscoplastic Stress Predictions. NUMETA 87. Proceedings of the International Conference on Numerical Methods in Engineering, NUMETA 87 Vol. 1, pp. D55/1—9, Swansea, 6—10 July 1987.
16. Hinton E., Owen D. R. J.: Finite Element Programming Academic Press, London, (1977)
17. Beynon J. H., Brown P. R., Mizban S. I., Ponter A. R. S., Sellars C. M.: Inclusion of Metallurgical Development in the Modelling of Industrial Hot Rolling of Metals. Proceedings of the NUMIFORM '86 Conference, Gothenburg, (1986)
18. Huang-Vu Kh., Birch D. W.: Integration of CAD/CAM/CAE in an Aerospace forging Company. Advanced Technology of Plasticity 1987 (edited by K. Lange), Vol. 1, pp. 161—170, Springer-Verlag, Berlin Heidelberg New York Tokyo, (1987)

# Nastanek in rast utrujenostne razpoke v koroziskem mediju

## Occurrence and Growth of Fatigue Cracks in Corrosion Environment

L. Kosec\*, F. Kosel\*\*

UDK: 620.193.01

ASM/SLA: R1h, R1e, R2j, Q26p

*V prispevku obravnavamo nastanek in razvoj poškodb kovinskih materialov v obliki klinov iz koroziskih produktov. Analizirali smo pogoje rasti in motenj v rasti klinov, vpliv števila in velikosti klinov na intenzivnost napetosti v sistemu kovina-klin. Rezultate analize smo posplošili s tremi primeri poškodb delov orodij in naprav.*

### 1. UVOD

V kemično aktivnih okoljih nastanejo na površini kovin koroziski produkti, ki so različno trdno povezani s kovinsko osnovo. Temperaturne ali mehanske napetosti lahko poškodujejo plasti koroziskih produktov. Teno oprijete in goste plasti koroziskih produktov upočasnijo ali povsem zavro potek koroziskih procesov. Poškodovane plasti pa te zaščite ne nudijo ali pa zgolj v omejenem obsegu. Poškodbe so različne: razpoke, luščenje koroziskih produktov na posameznih delih površine ob meji s kovino ali znotraj koroziskih produktov.

V prispevku obravnavamo vplive temperaturnih napetosti in oksidacije kovine na razvoj in obliko poškodb, ki pripeljejo do porušitve. Analiziran je primer, ko se je zaradi mehanske nestabilnosti porušila oksidna plast na površini in je skozi nastale razpoke prišel koroziski medij v stik s kovino. Na takih mestih je prišlo do pospešene oksidacije. Zaradi posebnega načina dostopa oksidanta so na teh mestih koroziski produkti zrasli v obliki klinov. Koroziski produkti se v fizikalnih in mehanskih lastnostih bistveno razlikujejo od kovine. Zato pride pri temperaturnih spremembah do napetostno deformacijskih stanj, ki vplivajo na morfologijo ter deformacijo koroziskskega produkta in kovine.

Rezultate analize modela ilustriramo s tremi primeri: z elementom orodja za tlačno litje medi, cevmi pregrevalnika pare iz termoelektrarne in anodnimi palicami akumulatorja, ki naj pokažejo relativno razširjenost pojava.

O pojavu oksidnega klina in njegovem vplivu na porušitev kovine je malo strokovnih referenc. Vpliv oksidnega klina na širjenje razpok je analiziral P. T. Heald<sup>1</sup> in ugotovil, da razpoka samo zaradi oksidnega klina ne more preiti v nestabilno rast, če sistem ni obremenjen. Razprave o pomenu oksidnega klina na razvoj poškodb strojnih delov in naprav pa najdemo tudi v naši strokovni literaturi<sup>2, 3, 4, 5, 6</sup>.

The contribution treats the occurrence and growth of defects in metal materials in the form of corrosion product wedges. The conditions of wedge growth and crack growth retardation, and the effect of the number and size of wedges on the stress intensity in the metal/oxide system were analyzed. The results of the analysis were illustrated by three examples of this kind of defects on certain tool parts and equipment components.

### 1. INTRODUCTION

In chemically active environment metal surfaces get covered by corrosion product coatings whose adhesion to the base metal is variously firm. High thermal or mechanical loads of metal/oxide systems can impair corrosion product coatings. Firmly adhered and thick corrosion product coatings can slow down or even completely stop the progress of corrosion, whereas the injured layers can no longer protect against corrosion or can do this only to a certain extent. The defects of the injured coatings can be of various kind like cracks, splitting of corrosion products on some areas of the surface, on the boundary to the base metal, inside the corrosion product layer etc.

This contribution treats the effects of thermal stresses and metal oxidation on the occurrence and development of defects leading to failure. An analysis is made of a case where due to mechanical instability, the oxide surface coating broke, and through the created cracks the corrosion medium came into contact with the metal. On such places an intensified oxidation took place. Due to the special way of transfer of the oxidizing agent through the broken oxide layer, on these places the oxides grew in the form of wedges. Corrosion products differ essentially from metals so by their physical as well as their mechanical properties. As a result the properties inside such a system are very non-uniform, so the stress-strain states which occur at temperature changes, cause the deformation of the corrosion products, and change their geometric characteristics.

The results of a general analysis of the model representing the discussed system are illustrated by three examples: an element of tool for die casting of brass, pipes of a steam superheater from a thermal power plant, and anode rods of a car battery. These examples

\* Univerza Edvarda Kardelja v Ljubljani, FNT, VTOZD Montanistika

\*\* Univerza Edvarda Kardelja v Ljubljani, Fakulteta za strojništvo

\* E. Kardelj University of Ljubljana, Faculty of Natural Sciences, Dept. of Metallur.

\*\* E. Kardelj University of Ljubljana, Faculty of Mechanical Engineering

Visokotemperaturna oksidacija je eden od pogostih načinov korozije kovin (suha korozija). Povišane in višoke temperature in nihanje temperature še dodatno močno obremenjujejo kovino, zato so poškodbe v takih okoljih še bolj pogoste in usodne. Take pogoje bomo upoštevali pri nastanku in rasti oksidnega klina.

## 2. NASTANEK IN RAST OKSIDNEGA KLINA

Nastanek oksidnega klina sledi predhodni enakomerni oksidaciji površine kovine na primerno visoki temperaturi. Na površini nastali oksid ima različen temperaturni razteznostni koeficient od kovine. Prav tako je pomembno, da ima nastali koroziski produkt tudi znatno večji specifični volumen. Fizikalne in mehanske lastnosti oksida in kovine se s temperaturo spreminja. Na obravnavanih pojavih pa vpliva tudi trdnost vezi med oksidom in kovino.

### 2.1 Nastanek oksidnega klina

Obravnavali bomo primer, kjer sta nastanek in širjenje oksidnega klina možna zaradi menjajočih se temperaturnih obremenitev. Na primerno visoki temperaturi nastane na površini kovine v določenem času zvezna plast oksida. Pri ohlajanju sistema kovina — oksid se zaradi različnih temperaturnih razteznostnih koeficientov v oksidu pojavijo tlačne napetosti. Zaradi njih se pri višjih temperaturah kovina v oksidu plastificira; ko pa se temperatura zniža in preide sistem iz plastičnega v elastično območje, začno v oksidu naraščati tlačne napetosti. Oksidni sloj na površini se elastično deformira. Z ohlajanjem lahko tlačne napetosti v oksidu dosežejo mejo plastičnosti. Če je trdnost vezi s kovino dovolj velika, prične oksid ponovno plastično teči. Drugače pa se lahko lokalno ukloni ali pa lušči, če je zrušilna strižna trdnost na meji s kovino manjša od tangencialnih napetosti. Ponavadi potekata oba pojava istočasno.

Pri ponovnem segrevanju sistema se pri določeni temperaturi eventuelne preostale tlačne napetosti v oksidu izničijo zaradi različnega širjenja kovine in oksida. Nato se s segrevanjem v oksidu pojavi in narašča natezna napetost. Zaradi mehanskih poškodb, ki so nastale med ohlajanjem, se v oksidu pojavijo koncentracije napetosti. Na teh mestih se pri nadaljnem segrevanju še razmeroma krhek oksid lahko poruši z razpoko, ki je pravokotna na površino kovine. Nastane lahko več takih razpok. Te razpoke omogočajo prost in hiter dostop zraka do kovine, zaradi česar pride do omejene, lokalne oksidacije. Ta drobna oksidna zajeda je začetek oz. zaredek oksidnega klina.

### 2.2 Rast oksidnega klina

Nastali oksid ima znatno večjo prostornino od kovine. Volumska deformacija zaradi oksidacije je tolikšna, da bi napetostno stanje daleč preseglo porošno trdnost kovine in oksida. Zato se oba (sistem) plastificira. Napetostno stanje je v oksidni zajedi (zaredu klina) enako manjši meji tečenja ene od obeh sestavin sistema  $\sigma_{T \min}$ , kot je:

$$\sigma_T = \min (\sigma_{T \min}^{\text{OK}}, \sigma_{T \min}^M)$$

Pri ohlajanju s  $T_{\max}$  bi se v oksidu pojavile tlačne napetosti, zaradi katerih sistem plastično teče. Plastično tečenje poteka vse do temperature prehoda sistema v elastično stanje pri  $T_p$  (temperatura prehoda sistema v

should point to the relative frequency of the phenomenon. In literature very few references can be found about the phenomenon of an oxide wedge. The effect of the oxide wedge on crack propagation was analysed by P. T. Heald (1) who proved that a crack cannot start growing unstably only because of an oxide wedge if no load is applied. Some investigations about the importance of an oxide wedge for the development of defects on various machine parts can also be found in our professional literature<sup>2, 3, 5, 6</sup>.

High temperature corrosion is one of the most frequently found types of metal corrosion (dry corrosion). High temperatures, raised temperatures and high temperature cycles represent an additional load for metal, making the defects in these environments even more frequent and fatal. These very conditions will be considered in our investigation of the occurrence and growth of an oxide wedge.

## 2. OCCURRENCE AND GROWTH OF OXIDE WEDGE

And oxide wedge occurs after a previous uniform oxidation of a metal surface at a correspondingly high temperature. The newly formed oxide has a different thermal expansion coefficient than the metal. It is also important that this new corrosion product has a considerably larger specific volume than the metal. The physical and mechanical properties of the oxide and the metal are changing with temperature. Besides this, the discussed phenomenon is affected also by the strength of the oxide adhesion to the metal.

### 2.1. Oxide Wedge Occurrence

We will discuss a case where the occurrence and growth of the oxide wedge are possible because of changing thermal loads. At a correspondingly high temperature and within a certain time a continuous oxide layer occurs on the metal surface. During the cooling process of the metal/oxide system compressive stresses arise in the oxide due to the different thermal expansion coefficients. At higher temperatures the oxide and the metal become plastic because of the compressive stresses, but when the temperature lowers, and the system passes from the plastic into elastic region, the compressive stresses in the oxide start increasing. Now, the oxide layer on the surface undergoes elastic deformation. During the process of cooling the compressive stresses in the oxide can reach the plastic limit. If the strength of the adhesion to the metal is strong enough, the oxide starts flowing plastically. Otherwise, it can bend locally or split in case that the breaking shear strength on the metal boundary is smaller than the tangential stresses. Generally, however, both these two processes are going on simultaneously.

During reheating of the system, at a certain temperature the possible remaining compressive stresses in the oxide become eliminated because of the different expansion of the metal and the oxide. If heating is continued, tensile stresses appear and increase in the oxide. Due to mechanical defects that occurred in the oxide during the process of cooling, different stress concentration areas can be found. With continued heating on these areas, a relatively brittle oxide can break with a crack running rectangularly to the metal surface. Several such cracks might occur. These cracks enable a free and fast transfer of the oxidant (air) to the metal, indu-

elastično stanje pri tlaku). Napetostno stanje v oksidni zajedi je pri tej temperaturi enako:

$$\sigma_{T \min} (T_p) = \sigma_{\min} (\sigma_T^{OK} (T_p), \sigma_T^M (T_p))$$

Z ohlajenjem pa tlačne napetosti naraščajo. Če dosegajo mejo tečenja  $\sigma_{T \max}$ , pride do ponovnega plastičnega tečenja sistema.

Naslednja stopnja v spremenljivem temperaturnem režimu je segrevanje sistema od  $T_{\min}$  na  $T_{\max}$ . Pri tem se v začetku tlačne napetosti, nastale pri ohlajanju, zmanjšujejo in pri določeni temperaturi je sistem brez napetosti. S segrevanjem se v zajedi pojavi natezne napetosti, ki s temperaturo rastejo. Če napetost preseže trdnost zajeda pod temperaturo prehoda iz elastičnega v plastično področje ( $T_p^+ -$  pri natezni obremenitvi), se zajeda poruši. Razpoka je nadaljevanje razpoke v zvezni površinski plasti oksida. S tem se ponovno odpre hitra pot za dostop oksidanta do kovine ter se tako pospeši rast zajeda v smeri razpoke. Po večkratni ponovitvi temperaturnega cikla ( $T_{\max} - T_{\min} - T_{\max}$ ) se zajeda izoblikuje v obliko klinov mikroskopskih razsežnosti.

### 3. NAPETOSTI ZARADI OKSIDNEGA KLINA

Rast oksidnega klinov v kovini uravnava predvsem hiter prenos kisika po razpoki do kovine, v smeri normalno na steno klinov, pa difuzija skozi oksid. Na ta način nastane in se ohranja trikotna oblika klinov. Vsaka razpoka skozi primarni oksidni sloj je lahko začetek oksidne zajede oz. klinov. Zato je na kovinskih delih, ki so izpostavljeni menjajočim se temperaturam, veliko mikroskopskih poškodb v obliki oksidnih klinov.

Napetostno stanje, ki se pojavi v sistemu med rastjo oksidnega klinov, raziskujemo na poenostavljenem modelu, tako da izberemo tanek sloj polprstora, ki ga predstavlja polravnina z več oksidnimi klini. Napetostno stanje je odvisno od temperaturnih obremenitev in ga bomo analizirali pri treh značilnih mejnih temperaturah.

#### 3.1 Napetostno stanje pri najvišji temperaturi, $T_{\max}$ .

Pri tej temperaturi oksidni klin najhitreje raste. V njem se pojavijo tlačne napetosti, ki dosežejo minimalno mejo tečenja ene od sestavin sistema  $\sigma_{T \min}$ . Ker pa se oksid in kovina razlikujeta tudi v drugih lastnostih, se pojavijo še dodatne temperaturne napetosti. Te napetosti so v temenu klinov, to je na meji polravnine razmeroma velike tlačne napetosti in so vzporedne z mejo polravnine. Pod mejo polravnine delujejo na klin znatne strižne in normalne napetosti pravokotno na smer polravnine<sup>5</sup>. Primerjalna napetost v sistemu kovina-oksid je znatno večja od meje tečenja, zato je hitrost plastične deformacije velika in napetostno stanje ne preseže  $\sigma_{T \min}$ . Rezultant sil zaradi tlačne napetosti na plašču klinov ( $\sigma_{T \min}$ ) deluje proti meji polravnine. Zaradi nje in temperaturnih napetosti se sistem značilno deforma. Teme oksidnega klinov se pri tem zoži, kovina pa s plastičnim tečenjem zavzame ta prostor. Posledica rezultirajočih napetosti je izbočitev meje polravnine okoli temena oksidnega klinov (sl. 1). Zelo izraziti primeri plastične deformacije sistema so takrat, ko na temenih oksidnih klinov izpade del oksida in se poruši ravnotežno napetostno stanje na tem delu polravnine (sl. 2, 3).

Oksidni klin vpliva na stabilno oz. nestabilno rast razpokane v kovini zaradi tlačnih napetosti, ki so enake mejo tečenja  $\sigma_{T \min} (T_{\max})$ . Dejanska širina korena razpokane je (2):

cinc a limited local oxidation. This tiny oxide flaw represents the beginning of an oxide wedge.

### 2.2. Oxide Wedge Growth

The newly formed oxide has a much larger volume than the metal. The volume deformation due to oxidation is so extensive that the stress state exceeds by far the rupture strength of the metal and the oxide. Therefore both of them (the metal/oxide system) become plastic. The stress state in the oxide flaw (wedge embryo) is equal to the lower yield point of one of the system's components as follows:

$$\sigma_{y \min} = \sigma_{\min} (\sigma_y^{OK} (T_p), \sigma_y^M (T_p)) \quad (1)$$

During cooling from  $T_{\max}$ , compressive stresses appear in the oxide due to which the system exceeds the yield point. The plastic flow continues down to the temperature of the transition of the system from the plastic into elastic state,  $T_p$  (temperature of the system's transition into elastic state under pressure). The stress state in the oxide flaw at this temperature is:

$$\sigma_{y \min} (T_p) = \sigma_{\min} (\sigma_y^{OK} (T_p), \sigma_y^M (T_p)) \quad (2)$$

With continued cooling the compressive stresses increase. If they attain the yield point  $\sigma_{y \min}$ , this induces a repeated plastic flow of the system.

In changing temperature conditions, the next stage is heating up the system from  $T_{\min}$  onto  $T_{\max}$ . Here, at the beginning, the compressive stresses induced by cooling, are reduced and at a certain temperature the system is free of stress. With heating up the system, tensile stresses appear in the flaw, increasing with temperature. If the stress exceeds the strength of the flaw below the temperature of the transition from the elastic into plastic state ( $T_p^+ -$  under tensile load), the flaw breaks. The newly occurred crack continues the crack in the primary surface layer of the oxide. In this way, the oxidant has again a fast access to the metal reopened, stimulating the growth of the flaw in the direction of the crack. After several repetitions of the temperature cycle ( $T_{\max} - T_{\min} - T_{\max}$ ), the flaw grows into a wedge of microscopic dimensions.

### 3. STRESSES INDUCED BY OXIDE WEDGES

The growth of the oxide wedge into the metal depends especially on how rapid is the access of the oxidant to the metal along the crack, and in the direction normally to the wedge face, on how strong is the diffusion through the oxide. In this way the wedge grows in the form of a triangle and keeps this form. Any crack through the primary oxide layer can mean the onset of an oxide flaw or wedge. As a result, on metal parts which are exposed to changing temperature conditions, a great number of microscopic defects in the form of oxide wedges can be found.

The stress state occurring in the system during the process of oxide wedge development, is investigated on a simplified model by choosing a thin layer of semi-space, representing the semi-plane with several oxide wedges. The stress state as function of thermal loads will be analysed only for three extreme temperatures.

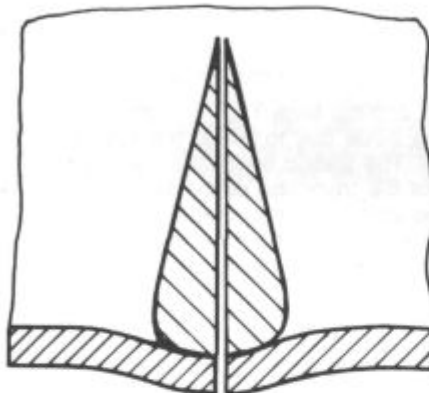
#### 3.1. Stress State at the Highest Temperature ( $T_{\max}$ )

At this temperature the oxide wedge grows the most rapidly. Compressive stresses appear in it, attaining the

$$\varphi(C) = \frac{C(1-v)}{4\pi\mu\sigma_{yz}(T_{max})} \left[ \frac{\mu}{1-v} \tan \Theta + \pi \sigma_{ymin}(T_{max}) \right],$$

kjer je  $\Theta$  kot klinja razpoke v kovini, v Poissonovo število in  $\mu$  strižni modul.

Kritična širina korena razpoke pri nestabilni razpoke pa je:  $\varphi_c = 2\gamma/\sigma_{yz}(T_{max})$ , kjer je  $\gamma$  površinska napetost. Razpoke je stabilna, če je  $\varphi_c > \varphi(C)$ . Če pa je  $\varphi_c < \varphi(C)$ , je nestabilna in vodi k porušitvi.

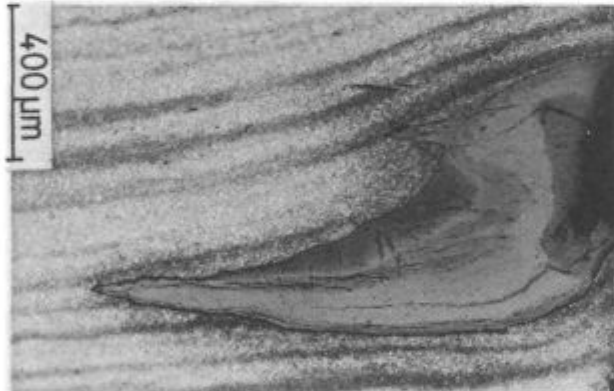


Slika 1

Razpoke skozi oksidno plast in klin do kovine na vrhu klinja.

Fig. 1

A crack running through the oxide layer and the wedge right to the metal at the wedge tip



Slika 2

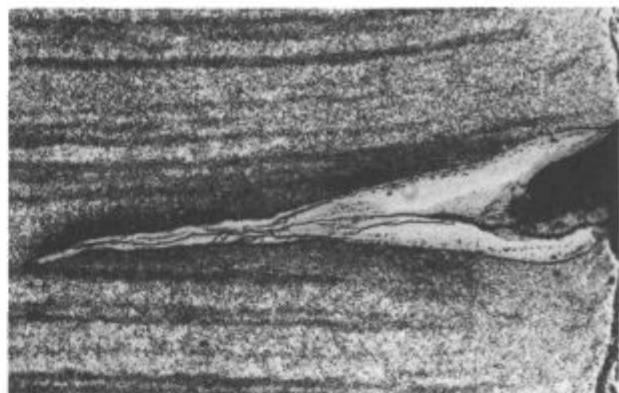
Deformacija kovine v okolici klina. Razpoke v smeri osi klina; 50 x

Fig. 2

Deformation of the metal in the vicinity of the wedge. Cracks in the direction of the wedge axis; 50 x

### 3.2 Napetostno stanje pri temperaturi prehoda iz plastičnega v elastično področje sistema, $T_p$

Tlačne napetosti v oksidnem klinu se povečajo, vendar ne čez mejo tečenja. V tem primeru lahko določimo največje napetostno stanje v kovini ob korenu oksidnega klina, prav tako pa faktor koncentracije napetosti<sup>4</sup>. Napetost v oksidnem klinu je enaka  $\sigma_{Tmin}(T_p)$ , faktor koncentracije napetosti pa:  $K_1 = 1,1209 \cdot \sigma_{Tmin}(T_p) / c$ , kjer je  $c$  dolžina oksidnega klina. Če pa je na površini več klinov, je faktor koncentracije napetosti v kovini ob



Slika 3

Deformacija kovine in oksidnega klina zaradi odluščenja oksida na temenu klina; 40 x

Fig. 3

Deformation of the metal in the oxide wedge due to oxide splitting on the wedge back face; 40 x

minimum yield point of one of the system's components  $\sigma_{ymin}$ . But since the oxide and the metal differ also in other properties, additional thermal stresses appear too. On the back face of the oxide wedge, i. e. on the semi-plane boundary, these stresses are compressive, and relatively high, acting in the direction parallel to the semi-plane. Under the semi-plane boundary considerable shear and normal stresses act on the wedge in the direction rectangular to the semi-plane (5). The comparative stress in the metal-oxide system is considerably higher than the yield point, therefore, the rate of plastic deformation is high, and the stress state does not exceed the  $\sigma_{ymin}$ . The resultant of the forces arising from compressive stress on the wedge faces ( $\sigma_{ymin}$ ), acts in the direction towards the semi-plane boundary. Because of this and due to temperature stresses, the system undergoes a typical deformation.

The back face of the oxide wedge narrows, its place being taken by the plastically flowing metal. The consequence of the stresses resulting from this is the buckling of the semi-plane boundary around the oxide wedge, (Fig. 1). Very distinct cases of plastic deformation of the system can be observed if on the back face of the wedge a tiny piece of the oxide splits off and destroys the equilibrium stress-state in this part of the semi-plane (Fig. 2, 3).

The oxide wedge has an influence on the stable or unstable crack growth in the metal owing to compressive stresses being equal to the yield point  $\sigma_{ymin}(T_{max})$ .

The actual width of the crack tip is (2)

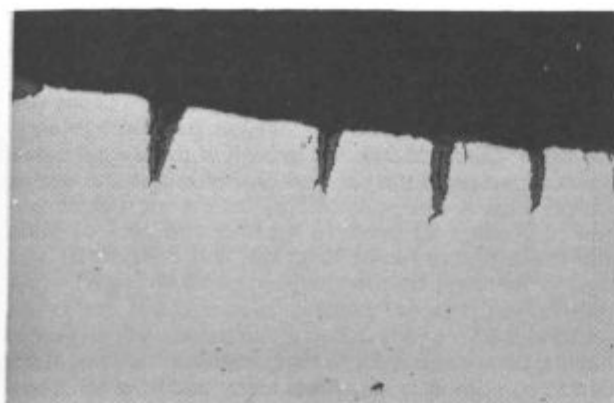
$$\theta(c) = \frac{c(1-v)}{4\pi\mu\sigma_u(T_{max})} \left[ \frac{\mu}{1-v} \tan \Theta + \pi \sigma_{ymin}(T_{max}) \right] \quad (3)$$

where  $\Theta$  is the wedge angle of the crack in the metal,  $v$  Poisson's number and  $\mu$  shear module.

And the critical width of the crack tip at unstable growth is:  $\varphi_c = 2\gamma/\sigma_{yz}(T_{max})$  where  $\gamma$  is the surface stress. Crack growth is stable if  $\varphi_c > \theta(c)$  and unstable and leading to failure if  $\varphi_c < \theta(c)$ .

### 3.2. Stress State at the Transition Temperature from the Plastic into Elastic State ( $T_p$ )

In this case the compressive stresses in the oxide wedge are increased, however not beyond the yield



Slika 4  
Skupine oksidnih klinov; 50 x  
Fig. 4  
Groups of oxide wedges; 50 x

korenih klinov manjši (sl. 4, 5). Če je v polravnini več klinov dolžine c, ki so med sabo oddaljeni z d, je faktor koncentracije napetosti  $K_1 = \beta_1 \cdot \sigma_{T_{\min}} (T_p) / c$ .

$\lambda$	0	0,2	0,4	0,6
$\beta_1$	1,1209	0,87186	0,62536	0,51046
	0,8	1,0	2,0	3,0
	0,4446	0,39866	0,282206	0,2303

kjer je  $\lambda = c/d$ .

Sistem z več enako velikimi oksidnimi klini v polravnini je odpornejši proti porušitvi v primerjavi s sistemom, ki ima le enega samega iste dolžine.

### 3.3 Napetostno stanje pri najnižji temperaturi, $T_{\min}$

Tlačne napetosti v oksidnem klinu se povečujejo in dosežejo pri neki  $T_{\min}$  vrednost, ki presega napetostno stanje pri vseh višjih temperaturah. Faktor koncentracije napetosti se zato poveča in je določen na enak način kot zgoraj.

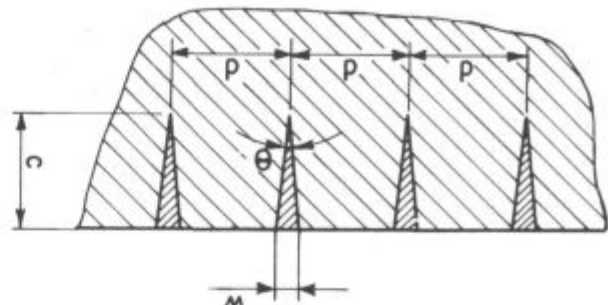
Tako kot pri najvišji, je tudi pri najnižji temperaturi zanimiv odgovor na vprašanje o stabilnosti razpoke v kovini. Hitrost širjenja razpoke  $c(t)$  je:

$$c(t) = \frac{\mu \omega(t)}{\pi(1-\nu)} \left\{ \left[ 1 - \frac{\omega(t)\sigma}{2\gamma} \right]^{-0.5} - 1 \right\}$$

Odtod sledi pogoj za nestabilno rast razpoke:  $\omega = 2\gamma/\sigma$ , kjer je  $\omega$  širina temena oksidnega klini. V tem primeru je hitrost širjenja razpoke neskončno velika.

### 4. MOTNJE V RASTI OKSIDNEGA KLINA

Motnje v rasti oksidnega klini se pojavijo takrat, ko se v določenih razmakih ne obnavlja razpoka v oksidni plasti ali klinu kot hitra pot za prenos kisika do kovine na vrhu klini. V nekaterih primerih se lahko zgodi, da oksid zapre zunanj stran razpoke, tako da se tudi pri nihanju temperature zapreka ne poškoduje oz. ne poči. Takrat je oksidacija vezana zgolj na transport skozi oksid. Rast klini se tedaj upočasni, posebej še na koren, zato se mu spremeni tudi oblika. Zelo trdno zaporo



Slika 5  
Shema sistema kovina-oksidni klini.  
Fig. 5  
Scheme of the metal/oxide wedge system

point. We can define the maximum stress state as well as the stress concentration factor in the metal around the oxide wedge tip<sup>4</sup>. The stress in the oxide wedge is equal to  $\sigma_{T_{\min}} (T_p)$  and the stress concentration factor is  $K_1 = 1,1209 \cdot \sigma_{T_{\min}} (T_p) / c$ , where  $c$  represents the length of the oxide wedge. In case of several wedges on the surface, the stress concentration factor in the metal around the wedge tips is smaller (Fig. 4, 5). If there are several wedges in the semi-plane of various lengths ( $c$ ) and distances ( $d$ ), then the stress concentration factor is  $K_1 = \beta_1 \cdot \sigma_{T_{\min}} (T_p) / \bar{c}$ .

$\lambda$	0	0,2	0,4	0,6
$\beta_1$	1,209	0,87186	0,62535	0,51046
	0,8	1,0	2,0	3,0
	0,4446	0,39866	0,28206	0,2303

where  $\lambda = c/d$

A system with several equally sized oxide wedges in the semi-plane is more resistant to rupture than a system with only one wedge of the same length.

### 3.3. Stress State at the Lowest Temperature ( $T_{\min}$ )

The compressive stresses in the wedge increase, and at a certain minimum temperature ( $T_{\min}$ ), attain the value which exceeds the stress state at all higher temperatures. The stress concentration factor is therefore increased, and can be defined in the same way as above.

Similarly as for  $T_{\max}$ , we are also for  $T_{\min}$  interested in the answer to the question of stable or unstable crack growth.

The rate of crack propagation  $c(t)$  (2) is:

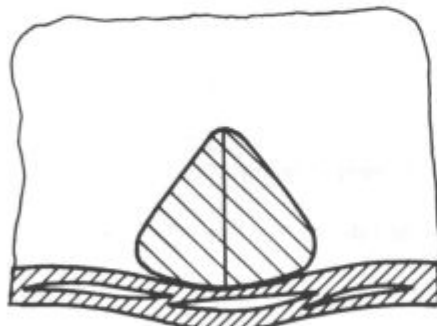
$$c(t) = \frac{\mu w(t)}{\pi(1-\nu)\sigma} \left\{ \left[ 1 - \frac{w(t)\sigma}{2\gamma} \right]^{-0.5} - 1 \right\} \quad (4)$$

Therefrom the condition for the unstable crack growth is obtained:  $w = 2\gamma/\sigma$  where  $w$  is the width of the oxide wedge back face. In this case the rate of crack propagation is infinite.

### 4. RETARDATION IN GROWTH OF AN OXIDE WEDGE

Retardation in the growth of an oxide wedge takes place when from time to time a crack enabling a fast

za dostop kisika predstavlja npr. kompozitna plast oksida in kovine, ki lahko nastane v določenih delovnih okoljih oz. pogojih. Ta je odporna na menjajoče se temperaturne obremenitve, posebej v fazi ogrevanja (nateg) in je vzrok dolgotrajni motnji v rasti oksidnega klinja. Taka kompozitna zapora je manj odporna na tlačne oz. strižne obremenitve, zaradi katerih se lahko odlušči s površine in motnja preneha (sl. 6, 7, 8).

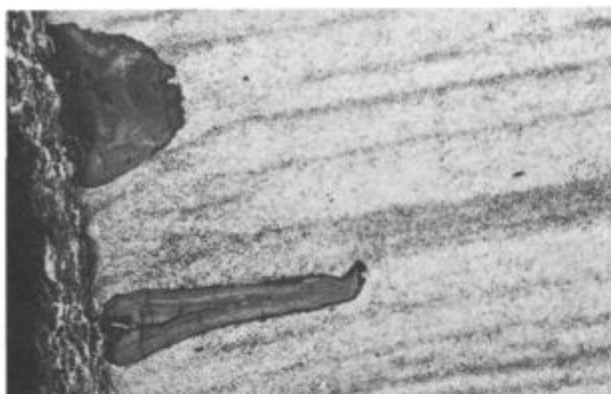


Slika 6

Mehanske stabilne pregrade (komposit oksid-kovina) nad oksidnim klinom.

Fig. 6

Stable mechanical closure barrier (an oxide/metal composite) above the oxide wedge



Slika 7

Mehanske stabilne pregrade (komposit kovina-oksid) nad dvema degeneriranimi oksidnimi klinoma; 50 x

Fig. 7

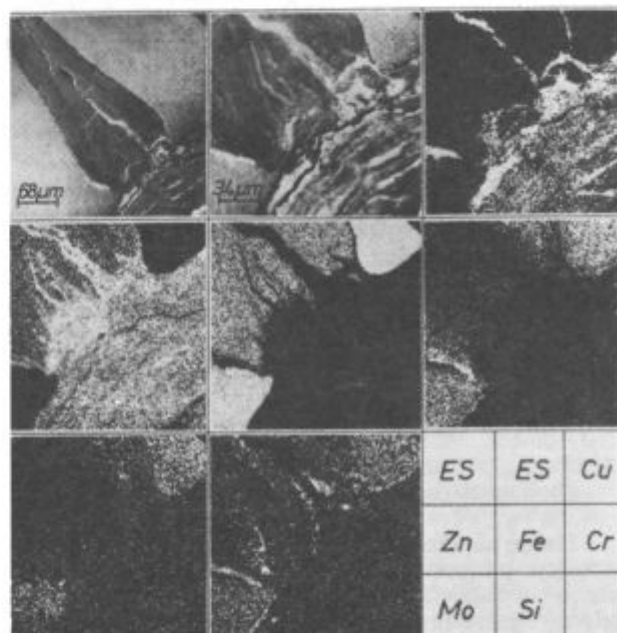
Stable mechanical barrier (an oxide/metal composite) above two degenerated oxide wedges; 50 x

## 5. PRIMERI NASTAJANJA OKSIDNIH KLINOV

### 5.1

Bat stroja za tlačno litje medi je izdelan iz orodnega jekla za delo v vročem (0,4 % C, 5 % Cr, 1,3 % Mo in 0,4 % V)<sup>5</sup>. V stacionarnih pogojih dela je nihala temperatura na površini bata v približno 11 sekundah od 780 °C ( $T_{\max}$ ) do 600 °C ( $T_{\min}$ ), ob prekinitvah pa se površina bata ohladi pod 200 °C ali celo na temperaturo okolice. Po določenem času dela se je bat poškodoval zaradi t. i. toplotnega razpokanja na delovni površini. Te poškodbe se kažejo v mreži bolj ali manj globokih razpok-kanalov, ki se širijo v kovino v obliki oksidnih klinov. Na osnih presekih bata je tako moč opaziti

transfer of oxygen to the metal does not reopen. In some cases it can happen that corrosion products close the crack from the outside so that even at varying temperature this closure does not break. In these cases oxidation depends only on the oxygen transport through the oxide. Owing to this, the growth of the wedge slows down especially at the tip, thus changing also the wedge morphology. A very solid closure for the transfer of oxygen represents for example a composite layer of oxide and metal created in specific working conditions. This layer is resistant to changing temperature loads, especially in the phase of heating (tension), and this is the reason for a long retardation in the oxide wedge growth. Such a composite closure can, however, be less resistant to compressive and shear loads due to which it can peel off the surface, and the wedge starts growing again (Fig. 6, 7, 8).



Slika 8

Kemična sestava oksidnega klinja in stabilne pregrade.

Fig. 8

Chemical composition of the oxide wedge and the stable barrier

## 5. SOME EXAMPLES OF OXIDE WEDGE OCCURRENCE

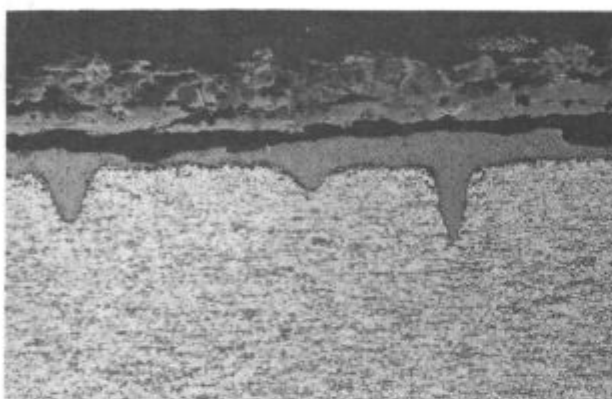
### 5.1.

The plunger of a die casting machine for brass is made from hot-working tool steel (0.4 % C, 5 % Cr, 1.3 % Mo and 0.4 % V) (5). At stable operating conditions the temperature on the plunger surface varies in approx. 11 seconds from 780 °C ( $T_{\max}$ ) to 600 °C, while at work stoppage, the plunger surface cools down below 200 °C, or even down to the ambient temperature ( $T_{\min}$ ). After a certain time of operation, heat cracking occurs on the working surface of the plunger. These defects can be seen as a network of more or less deep cracks — channels — extending into the metal in the form of oxide wedges. On the axial cross section of the plunger it is thus possible to observe practically all the above de-

praktično vse prej opisane pojave: razpoke v klinih, deformacije klinov in okolišne kovine, zaprtje razpok in motnje v rasti oksidnega klinja (sl. 2, 3, 6, 7, 8).

## 5.2

Na zunanjih stenah cevi pregrevalnika pare, ki dela pri nižjem temperaturnem nivoju kot bat, so se pod relativno tanko plastjo škajajo pojavili oksidni klini. V nekaterih primerih se je iz teh klinov razvila poškodba do porušitve stene cevi. Poleg agresivnega delovanja okolice (dimni plini) je sistem cevi podvržen tudi obremenitvam zaradi nihanja temperature (sl. 9).



Slika 9

Oksidni klini z zunanje stene cevi pregrevalnika pare; 100 x  
Fig. 9

Oxide wedges from the outer side of the steam superheater tube; 100 x

## 5.3

Povsem enake poškodbe, v obliki klinov koroziskih produktov, so nastale na pozitivnih elektrodaх akumulatorskih baterij in so pripeljale do lokalnih zlomov palic in uničenja baterije. Palice iz malolegorane svinčeve zlitine so obešene v bateriji in zato so ves čas zaradi lastne teže obremenjene na nateg. Pri polnjenju in praznjenju baterije poteka kemična reakcija, katere produkti se močno razlikujejo v gostoti. Trdnost sulfata PbSO<sub>4</sub> je manjša od napetosti zaradi teže palice in se poruši. Menjajoči se ciklusi praznjenja in polnjenja pri stalni natezni obremenitvi omogočajo rast koroziskskega produkta v obliki klinov (sl. 10). Ko seže poškodba zadosti globoko v kovino, se palica nenadno poruši (krhko).

## 6. ZAKLJUČEK

Kovinski deli orodij in naprav, ki delajo v agresivnih okoljih, se prekrijejo s plastmi koroziskih produktov. Zaradi mehanskih ali temperaturnih obremenitev so koroziski produkti pogosto mehansko nestabilni, kar pripelje do lokalnih porušitev. Skozi razpove prihaja medij zelo hitro do kovine in na teh mestih začno rasti koroziskski produkti v obliki klinov.

Ce so izpolnjeni pogoji trajne mehanske nestabilnosti koroziskskih produktov, klin raste in pripelje do porušitve sistema. V sistemih s koroziskskimi klini nastanejo značilna napetostno deformacijska stanja. Ta vplivajo na oblikovanje sistema in eventualno porušitev. Mot-

scribed phenomena: cracks in the wedges, deformation of wedges and the surrounding metal, crack closure and retardation in the growth of the oxide wedge etc. (Fig. 2, 3, 6, 7, 8).

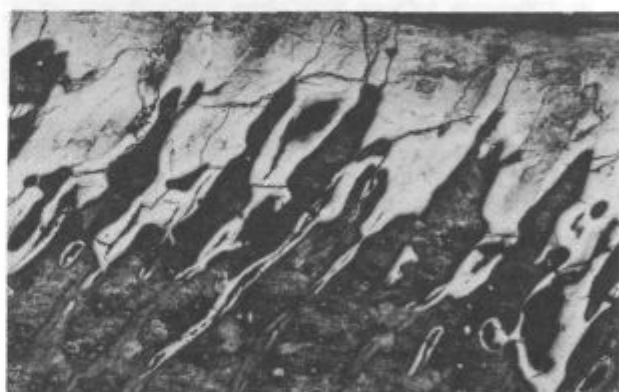
## 5.2

On the outer wall of a steam superheater, operating at a lower temperature level than the plunger, oxide wedges were observed under a relatively thin layer of oxide scale. In some cases the defects arising from these wedges developed into total failure of the pipe wall. Besides the aggressive effect of the environment (flue gases), the piping system is subjected also to loads arising from temperature variation (Fig. 9).

## 5.3

The same kind of defects in the form of corrosion product wedges were found on positive electrodes of a car battery.

These defects resulted in local breaking of anode rods and total failure of the battery. The anode rods, which are made of a low-alloyed Pb-alloy, are hung onto the battery boxing and thus constantly under tension load. During battery charging and discharging a chemical reaction takes place. Its products differ very much in specific volume, so the PbSO<sub>4</sub> probably cannot bear the weight of the anode rod and breaks. The exchanging cycles of discharging and charging at constant tensile load enable the growth of corrosion products in the form of wedges (Fig. 10). When the crack reaches a certain critical point deep enough in the metal, the rod undergoes a sudden brittle failure.



Slika 10

Klin v anodni palici akumulatorske baterije; 100 x

Fig. 10

A wedge in the anode rod of a car battery; 100 x

## 6. CONCLUSION

Metal parts of tools and machines, operating in aggressive environment, get covered with corrosion product layers. Due to mechanical and thermal loads corrosion products are subject to mechanical instability, leading to local failures. Through cracks the oxidant rapidly reaches the metal and on these places corrosion products start growing in the form of wedges.

In the conditions of permanent mechanical instability of corrosion products, a wedge grows and causes a fail-

nje, ki preprečujejo hiter dotok koroziskskega medija do kovine na vrhu klinov, zavro njihovo rast in spremene njihovo obliko. Ugotovljeno je tudi, da je rast skupine oksidnih klinov v enakih pogojih počasnejša kot pa takrat, če je v sistemu en sam klin.

V prispevku smo obravnavali rast klinov v kemično in mikrostrukturno homogenem kovinskem materialu.

V kemično nehomogenih materialih so s potekom koncentracije legirnih elementov določena prednostna mesta nastanka in rasti klinov. Če je medsebojna orientacija nehomogenosti in komponent temperaturnih napetosti ugodna, potekajo razpoke oz. oksidni klini vzdolž negativnih izcej. Na teh mestih so razlike v razteznostnih koeficientih kovine in oksida največje; oksid nad negativno izcejo je med nihanjem temperature znatno bolj obremenjen kot nad pozitivno, zato večina razpok v oksidu nastane nad negativnimi izcejami. Analiza takega primera je zahtevnejša in bo vsebina samostojnega prispevka.

lure of the system. In corrosion wedge systems very typical stress-strain states occur, affecting the morphology of the system and inducing a possible failure. Closures preventing a rapid access of the oxidant to the metal at the wedge tip, retard the growth of the wedge and change its morphology. The authors also found out that the growth of a group of oxide wedges is slower than that of only one wedge in the system.

This contribution treats oxide wedge growth in a homogeneous metal material. In metal materials with non-homogeneous chemical composition and microstructure the places likely for the occurrence and growth of wedges are defined from the concentration distribution of the alloying elements. If the interorientation of non-homogeneities and thermal load components is favorable, cracks or wedges run along the negative segregations. On these places the differences in thermal expansion coefficients between the metal and the oxide are the greatest; the oxide above the negative segregation is during temperature variation under much greater load than above the positive segregation, therefore the major part of cracks in the oxide are to be found above the negative segregations. The analysis of such a case demands special attention and efforts, and will be the subject of a separate investigation.

#### LITERATURA/REFERENCES

1. Heald P. T.: The Oxide Wedging of Surface Cracks, Material Science and Engineering, 35, 1978, 165—169, Lausanne, Swiss.
2. Kosel F. in Kosec L.: Toplotno razpokanje orodij za delo v vročem, Strojniški vestnik, 1983, 7—9., 151—159, Ljubljana, Yugoslavia
3. Vodopivec F., Ralić B. in Dobovišek B.: Poškodbe na ceveh visokotlačnega parnega kotla zaradi kombiniranega vpliva mehanske in kemijske obremenitve, Strojniški vestnik, 1985, 1—3, 6—12, Ljubljana, Yugoslavia
4. Berežnickij L T., Pansjuk V. V. in Staščuk N. G.: Vzaimodejstvie žestkih linearnih uključenij i treščin, Naukova Dumka, 1983, Kiev, USSR.
5. Kosel F. in Kosec L.: High Temperature Fatigue in Nonhomogeneous Continuum, Fatigue and Fatigue Thresholds, 1, 1984, 613—623, Birmingham, England.
6. Kosel F., Kosec L.: Occurrence and Growth of Fatigue Cracks in Corrosion Environment, Fatigue 87, 3, 1987, 1201—1210, Virginia, USA.

# Zapozneli lom jekla z visoko trdnostjo

## Delayed Fracture of High-strength Steel

B. Ule\*, F. Vodopivec\*, J. Žvokelj\*, M. Grašič\* in L. Kosec\*\*

UDK: 669.14.018.2:539.56:620.192.3  
ASM/SLA: Q26s, SG Ba, ST, 2—60, EGn, 3—66

V članku so opisane teoretične osnove, potrebne za razumevanje napetostno induciranega segregiranja vodika v jeklu z visoko trdnostjo. Opisano je merjenje kritičnega in mejnega napetostnega intenzitetnega faktorja ter na tej osnovi analiziran vpliv malih mikrostrukturnih variacij jekla na njegovo občutljivost k zapoznemu lomu.

### 1. UVOD

Ena od znanih oblik porušitve jekla z visoko mejo plastičnosti ter trdnostjo nad  $1200 \text{ Nmm}^{-2}$  je zapozneli lom, ki nastane zaradi napetostno induciranega segregiranja vodika v jeklu.

Raziskave zapoznelega loma, ki jih je opravil G. L. Hanna s sodelavci<sup>1</sup>, kažejo, da obstaja inkubacijski čas do nastanka prve mikrorazpoke; ta počasi raste, vse dokler ne doseže kritične velikosti, kar privede do hipne porušitve. Tako inkubacijski čas, kot tudi čas do loma se podaljšuje z zmanjševanjem obremenitve, vse dokler pri neki dovolj nizki obremenitvi zapozneli lom sploh izostane. A. R. Troiano<sup>2</sup> je odkril, da nukleacija mikrorazpok izostane tudi v primeru pravočasne razbremenitve, vendar pa se mikrorazpoke pojavi potem, ko je jeklo ponovno daljši čas mehansko obremenjeno. To vodi do sklepa, da je nukleacija mikrorazpok posledica elastične interakcije med mobilnimi atomi vodika v jeklu ter polji troosnih napetosti ob različnih diskontinuitetah kovine.

Lokalno kopičenje vodika v zadostni količini pa poslabša kohezivnost mreže ter olajša nukleacijo mikrorazpok.

### 2. TEORETIČNI DEL

Atomarni vodik v železu je bodisi na intersticijskih mrežnih mestih, bodisi ujet na različnih napakah kristalne mreže, ki jih imenujemo pasti. Nekaj vodika najdemo vedno tudi v molekularni obliki v porah.

Koncept pasti sta predlagala Darken in Smith<sup>3</sup>, da bi pojasnila vpliv temperature in koncentracije vodika v železu na njegovo difuzivnost. Oriani<sup>4</sup> je kasneje na osnovi različnih eksperimentalnih podatkov izračunal vezavno energijo, s katero je vodik vezan v pasteh. Skoraj v vseh primerih je dobil vrednosti okrog 27 kJ na mol vodika. Podobne vrednosti so navedene tudi v referencah 5,6 in 7, čeprav sta Kumnick in Johnson<sup>5</sup> odkrila tudi pasti z vezavno energijo približno 60 kJ na mol vodika. Gostoto teh pasti, vejetno so bili to dislokacijski pragovi, sta ocenila na  $10^{23} \text{ m}^{-3}$  v močno deformiranem železu.

Danes je znano, da kot pasti delujejo skoraj vse nepravilnosti kristalne mreže kovin, tako dislokacije<sup>9,10</sup>,

The paper presents theoretical fundamentals to understand the stress-induced hydrogen segregation in high-strength steel.

Measurements of the critical and of the threshold stress intensity factor are presented which represent the basis for analysing the influence of small microstructural variations of steel on its sensitivity to the delayed fracture.

### 1. INTRODUCTION

Delayed fracture caused by stress-induced hydrogen segregation is one of the known types of failure of steel with high yield strength and tensile strength above  $1200 \text{ N mm}^{-2}$ .

Investigations of the delayed fracture by G. L. Hanna and coworkers<sup>1</sup> showed an incubation period before the nucleation of the first microcrack, a slow growth of the microcrack and an instantaneous failure when a critical size was reached. The incubation period as well as the time till failure occurs are prolonged with the decreased load until at a sufficiently low load the delayed fracture does not occur at all.

A. R. Troiano<sup>2</sup> found that nucleation of microcracks does not appear if the unloading took place in the due time, but microcracks occur after steel was again mechanically loaded for a longer time. This leads to the conclusion that the nucleation of microcracks is a consequence of elastic interaction between the mobile hydrogen atoms in steel and the triaxial stress fields at different discontinuities in the metal. Local accumulations of hydrogen at a sufficient level diminish the cohesive forces in the lattice and facilitate the nucleation of cracks.

### 2. THEORY

Atomic hydrogen in iron is found either in interstitial sites of the lattice or it is as trapped hydrogen bound on different imperfections of the crystal lattice, being called "traps". Some hydrogen in molecular form is found always in the microvoids too.

Darken and Smith<sup>3</sup> suggested the concept of traps to explain the influence of temperature and of concentration on the diffusivity of hydrogen in iron. Later, on basis of experimental data, Oriani<sup>4</sup> calculated the trap binding energy of hydrogen and obtained value of about 27 kJ/mole hydrogen in almost all the cases. Similar values are quoted also in refs. 5, 6 and 7, while Kumnick and Johnson<sup>5</sup> discovered traps with the binding energy of about 60 kJ/mole hydrogen too. The density of traps, probably dislocation jogs, were estimated to  $10^{23} \text{ m}^{-3}$  in a heavily deformed iron.

\* Metalurški inštitut, Lepi pot 11, Ljubljana

\*\* Univerza Edvarda Kardelja, FNT — Montanistika, Aškerčeva 20, Ljubljana

pore<sup>11, 12</sup>, meje zrn<sup>13</sup>, mejne površine kovina-karbidi delci<sup>14</sup>, kot tudi površine nekovinskih vključkov<sup>15, 16</sup>.

Matematični model za opis vodika v pasteh sta razvila Foster in McNabb<sup>17</sup>. Po njunem modelu je v pasteh ujeti vodik v lokalnem ravnotežu z interstičijskim vodikom. Interakcija med vodikom in pastmi je termično aktiviran proces z aktivacijsko energijo, ki jo sestavljata vezavna energija pasti ter aktivacijska energija za difuzijo vodika v idealni mreži železa, ki dosega vrednost 12 kJ na mol vodika.

Gonila sila za interstičijsko difuzijo raztopljenega vodika v kovinah je gradient kemičnega potenciala vodika. K temu gradientu prispevajo koncentracijske razlike ter učinki polj elastičnih napetosti. Termodynamični učinek polj elastičnih napetosti je utemeljen z reverzibilno dilatacijo kristalne mreže kovin ter pozitivno spremembo volumna, ki spremi vgnezdjenje vodikovih intersticij v področja pozitivne deformacije, medtem, ko se področja s tlačno deformacijo z vodikom osirošajo. Na ta način je z nehomogeno prerazporeditvijo vodika dosežen krajevno neodvisen kemični potencial vodika v nehomogenem polju elastičnih napetosti.

Li, Oriani in Darken<sup>19</sup> so s termodynamično analizo problema, pri čemer so vodik v železu obravnavali kot povsem mobilno komponento, izpeljali naslednjo enačbo:

$$\mu_H = \mu_H^0 + RT \ln[H] - \sigma_h \bar{V}_H \quad (1)$$

v kateri prva dva člena določata kemični potencial vodika v odvisnosti od njegove koncentracije,  $\bar{V}_H$  je fenomenološki parcialni atomski volumen vodika v železu,  $\sigma_h$  pa je hidrostatična komponenta napetostnega tenzorja, s katerim popišemo troosno napetostno stanje. Ob predpostavki, da je v ravnotežju kemični potencial vodika krajevno neodvisen, z enačbo (1) izračunamo koncentracijo vodika v področju maksimalne hidrostatične komponente napetostnega tenzorja v razdalji r pred korenem zareze:

$$[H]_r = [H] \exp(\sigma_h \bar{V}_H / RT), \quad (2)$$

kjer je  $[H]$  povprečna koncentracija vodika v preizkušnici.

Za ravninsko deformacijsko stanje, način obremenitve I ter za ravnino napredovanja razpok iz korena zareze uporabimo naslednjo enačbo<sup>20</sup>:

$$\sigma_h = 2(1+v) K_I / 3\sqrt{2\pi r} \quad (3)$$

Iz enačb (2) in (3) dobimo:

$$[H]_r = [H] \exp \frac{2(1+v) K_I \bar{V}_H}{3RT\sqrt{2\pi r}} \quad (4)$$

Enačba (4) povezuje napetostni intenzitetni faktor  $K_I$  ter koncentracijo vodika v razdalji r pred korenem zareze.

Dejstvo, da pri apliciranem napetostnem intenzitetnem faktorju  $K_I$ , ki je nižji od mejnega napetostnega intenzitetnega faktorja  $K_{TH}$  zapozneli lom sploh izostane, je Beachem<sup>21</sup> zapisal v obliki kriterija, ki določa pogoje pojavljanja tega loma:

$$K_{TH} < K_I < K_{Ic} \quad (5)$$

kjer je  $K_{Ic}$  kritični napetostni intenzitetni faktor.

Gerberich<sup>22</sup> je na osnovi bodisi mehanizma Troiano-Oriani<sup>2, 23</sup> bodisi Beachemove hipoteze<sup>24</sup> postuliral kritično koncentracijo vodika  $[H]_r^{cr}$ , ki v razdalji r pred korenem zareze povzroči nukleacijo mikrorazpok. Predpostavil je, da je kritična koncentracija vodika lahko dosežena le, ako deluoča mehanska obremenitev preseže neko mejno vrednost, kar lahko zapišemo kot:

$$K_I \geq K_{TH} \Rightarrow [H]_r = [H]_r^{cr} \quad (6)$$

At present, it is known that almost all the kinds of imperfections in the crystal lattice of metals, both dislocations<sup>9, 10</sup>, microvoids<sup>11, 12</sup>, grain boundaries<sup>13</sup>, metal-carbide interfaces<sup>14</sup>, and the surfaces of non-metallic inclusions<sup>15, 16</sup> can act as trapping sites.

A mathematical model of hydrogen traps was developed by Foster and McNabb<sup>17</sup>. According to the model, trapped hydrogen is locally in equilibrium with the interstitial hydrogen. The interaction between hydrogen and the traps is a thermally activated process with an activation energy constituted of the binding trap energy, and the activation energy of diffusion of hydrogen in an ideal iron lattice being 12 kJ/mole hydrogen<sup>18</sup>.

The driving force for the interstitial diffusion of the dissolved hydrogen in metals is the gradient of chemical potential. This gradient is influenced by the differences in hydrogen concentrations and by the effects of elastic-stress fields. The thermodynamic effect of the elastic-stress fields is caused by the reversible dilatation of the crystal lattice of metals, and the positive volume change accompanied by the insertion of hydrogen interstitials into the areas of positive strain, while compressively strained regions are impoverished with hydrogen. Thus a locally independent chemical potential of hydrogen in an inhomogeneous elastic-stress field is obtained through an inhomogeneous redistribution of hydrogen.

The thermodynamic analysis of this process, under supposition that hydrogen is a completely mobile component, was established by Li, Oriani and Darken<sup>19</sup> who developed the following equation:

$$\mu_H = \mu_H^0 + RT \ln[H] - \sigma_h \bar{V}_H \quad (1)$$

The first two terms determine the chemical potential of hydrogen depending on its concentration,  $\bar{V}_H$  is the phenomenological partial atomic volume of hydrogen in iron, while  $\sigma_h$  is the hydrostatic component of the stress tensor describing the triaxial state of stresses. Supposing that the chemical potential of hydrogen in equilibrium is locally independent, the concentration of hydrogen in the region of the maximal hydrostatic component of stress tensor is given at a distance r from the notch root by (1):

$$[H]_r = [H] \exp(\sigma_h \bar{V}_H / RT), \quad (2)$$

with  $[H]$  as an average concentration of hydrogen in the specimen.

For a plane strain state, for a mode of loading I, and for the plane crack propagation from the notch root, the following equation is given<sup>20</sup>:

$$\sigma_h = 2(1+v) K_I / 3\sqrt{2\pi r} \quad (3)$$

From equations (2) and (3) we obtain:

$$[H]_r = [H] \exp \frac{2(1+v) K_I \bar{V}_H}{3RT\sqrt{2\pi r}} \quad (4)$$

The equation (4) connects the stress intensity factor  $K_I$  with the concentration of hydrogen at the distance r from the notch root. The fact, that the delayed fracture does not occur if the applied stress intensity factor  $K_I$  is lower than the threshold stress intensity factor  $K_{TH}$ , has been applied by Beachem<sup>21</sup> as the criterion to determine the conditions under which the delayed fracture takes place:

$$K_{TH} < K_I < K_{Ic}, \quad (5)$$

where  $K_{Ic}$  is the critical stress intensity factor.

On the basis of the Troiano-Oriani mechanism<sup>2, 23</sup> or the Beachem hypothesis<sup>24</sup>, the critical concentration of

S kombiniranjem enačb (4) in (6) dobimo:

$$K_{TH} = \frac{3 RT / 2\pi r}{2(1+v) \bar{V}_H} \ln \left\{ \frac{[H]_r^{cr}}{[H]} \right\} \quad (7)$$

**Enačba (7)** velja le v primeru, ko je plastična zona ob konici zareze omejena na manj kot eno kristalno zrno velikosti d. Če upoštevamo, da je vpletten še vodik, ujet na mejah zrn, lahko pišemo:

$$K_{TH} = \frac{3 RT / 2\pi d}{2(1+v) \bar{V}_H} \ln \left\{ \frac{[H]_r^{cr}}{[H]} \right\}; d \geq R_i, \quad (8)$$

kjer je  $R_i$  velikost plastične cone pri ravnninskem deformacijskem stanju ter načinu obremenitve I.

Z izrazom (8) ni mogoče pojasnit eksperimentalno ugotovljene odvisnosti med  $K_{TH}$  ter mejo plastičnosti.

Upoštevaje še vpliv polja drsnih linij ob korenju zareze, dobimo po Gerberichu<sup>22</sup> za  $K_{TH}$  naslednji izraz:

$$K_{TH} = \frac{RT}{\alpha \bar{V}_H} \ln \left\{ \frac{[H]_r^{cr}}{[H]} \right\} - \frac{\sigma_{ys}}{2\alpha} \quad (9)$$

Omeniti je potrebno, da pri meji plastičnosti pod  $1200 \text{ Nmm}^{-2}$  pogosto prihaja do neujemanja med enačbo (9) ter rezultati eksperimentov. Deloma lahko to neujemanje razložimo z odvisnostjo razmerja  $[H]^{cr}/[H]$  od meje plastičnosti jekla. Farrell in Quarrell<sup>23</sup> sta namerič ugotovila, da so za doseganje krhkosti v jeklih z nižjo mejo plastičnosti potrebne višje koncentracije vodika, kar sta zapisala kot  $[H]^{cr} \propto 1/\sigma_{ys}$ . Kim in Loginow<sup>27</sup> pa sta pokazala, da se v jeklih z višjo mejo plastičnosti topi več vodika, torej  $[H] \propto \sigma_{ys}$ . Končno dobimo:

$$\frac{[H]^{cr}}{[H]} = \frac{\beta}{\sigma_{ys}}, \quad (10)$$

pri čemer je  $\beta$  konstanta za posamično vrsto jekla.

### 3. EKSPERIMENTALNI DEL Z REZULTATI

#### 3.1 Izberi jekla in geometrija preizkušancev

Cilj preiskave je bila ugotovitev vpliva mikrostrukturnih variacij visokotrdnega jekla z 0,40 % C, 0,31 % Si, 0,71 % Mn, 0,019 % P, 0,006 % S, 1,03 % Cr, 0,21 % Mo, 0,26 % Cu, 0,009 % Al in 0,010 % Sn na občutljivost k z vodikom induciranimu pokanju. Jeklo je bilo izdelano po VOD postopku, zato vsebuje le malo žvepla, analize pa so pokazale, da vsebnost residualnega vodika ne presega 0,05 ppm. Navezni preizkusi so bili opravljeni s preizkušanci z zarezo, katerih geometrija je prikazana na sliki 1. Po podatkih iz literature<sup>27</sup> je za takšne preizkušance odvisnost med napetostnim intenzitetnim faktorjem  $K_i$ , njih geometrijo ter aksialno delujejočo silo P dana z izrazom:

$$K_i = \frac{P}{D^{3/2}} (-1,27 + 1,72 D/d) \quad (11)$$

pri pogoju:

$$0,5 < d/D < 0,8$$

Razmerje  $P/D$ , pri čemer je  $P$  korenski radius zareze, je bilo blizu vrednosti 0,02. Moran in Noris<sup>29</sup> sta z računalniško simulacijo nateznega preizkusa cilindričnih preizkušancev z zarezo po obodu ugotovila, da se pri razmerju  $P/D = 0,01$  do  $0,02$  pojavljajo maksimalne napetosti ob lomu preizkušanca za približno dva korenska radiusa pod površino, medtem ko so maksimalne defor-

hydrogen  $[H]_r^{cr}$  which produces crack nucleation at the distance  $r$  from the notch root was postulated by Gerberich<sup>22</sup>. He assumed that the critical concentration of hydrogen could be achieved only if the applied load exceeds a certain limiting value, which could be written as:

$$K_i \geq K_{TH} \Rightarrow [H]_r = [H]_r^{cr} \quad (6)$$

Combining Eqs. (4) and (6) we obtain:

$$K_{TH} = \frac{3 RT / 2\pi r}{2(1+v) \bar{V}_H} \ln \left\{ \frac{[H]_r^{cr}}{[H]} \right\} \quad (7)$$

The equation (7) is correct only when the plastic zone at the notch tip is limited to less than the grain diameter  $d$ . Considering that also hydrogen on the grain boundaries at the crack tip is involved, we can write:

$$K_{TH} = \frac{3 RT / 2\pi d}{2(1+v) \bar{V}_H} \ln \left\{ \frac{[H]_r^{cr}}{[H]} \right\}; d \geq R_i, \quad (8)$$

with  $R_i$  as the size of the strain plastic zone under mode of loading I.

On the basis of equation (8) it is not possible to explain the connection between the yield strength effect and  $K_{TH}$ , though it has been established by experiments.

If taking into account the influence of a slip-line field at the notch root, according to Gerberich<sup>22</sup>, we obtain for  $K_{TH}$ :

$$K_{TH} = \frac{RT}{\alpha \bar{V}_H} \ln \left\{ \frac{[H]_r^{cr}}{[H]} \right\} - \frac{\sigma_{ys}}{2\alpha} \quad (9)$$

It is necessary to mention that disagreements are often observed between Eq. (9) and experimental results at yield strength below  $1200 \text{ N mm}^{-2}$ . These disagreements were explained partly by the dependence of the  $[H]^{cr}/[H]$  ratio on the yield point. Namely Farrell and Quarrell<sup>23</sup> ascertained that larger concentrations of hydrogen are needed to produce embrittlement in steel with lower yield strength, and postulated the relationship  $[H]^{cr} \propto 1/\sigma_{ys}$ .

Kim and Loginow<sup>26</sup> suggested that the content of soluble hydrogen in steel was proportional to the yield strength, therefore  $[H] \propto \sigma_{ys}$ . Finally, we obtain:

$$\frac{[H]^{cr}}{[H]} = \frac{\beta}{\sigma_{ys}}, \quad (10)$$

with  $\beta$  as constant for a single type of steel.

### 3. EXPERIMENTS AND RESULTS

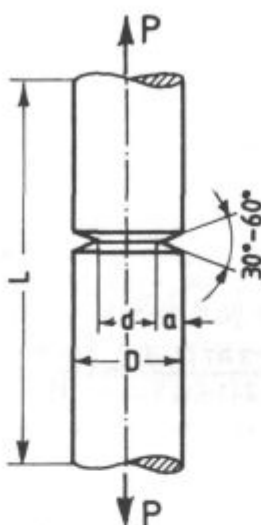
#### 3.1 Selection of Steel and the Geometry of Specimens

The aim of the investigation was to establish the influence of microstructure on the hydrogen induced susceptibility to cracking of a high-strength steel with the composition: 0.40 % C, 0.31 % Si, 0.71 % Mn, 0.019 % P, 0.006 % S, 1.03 % Cr, 0.21 % Mo, 0.26 % Cu, 0.009 % Al and 0.010 % Sn. The steel was manufactured by the VOD process, thus the content of sulphur was low and the concentration of residual hydrogen did not exceed 0.05 ppm.

Tensile tests were made on notched tensile specimens with the geometry shown in Fig. 1. For these specimens, the relationship between the stress intensity factor  $K_i$ , the geometry, and the axial force P is given by the equation<sup>27</sup>:

$$K_i = \frac{P}{D^{3/2}} (-1,27 + 1,72 D/d) \quad (11)$$

macije dosežene v samem korenju zareze, kjer se sicer pojavljajo prve mikrorazpoke.



Slika 1

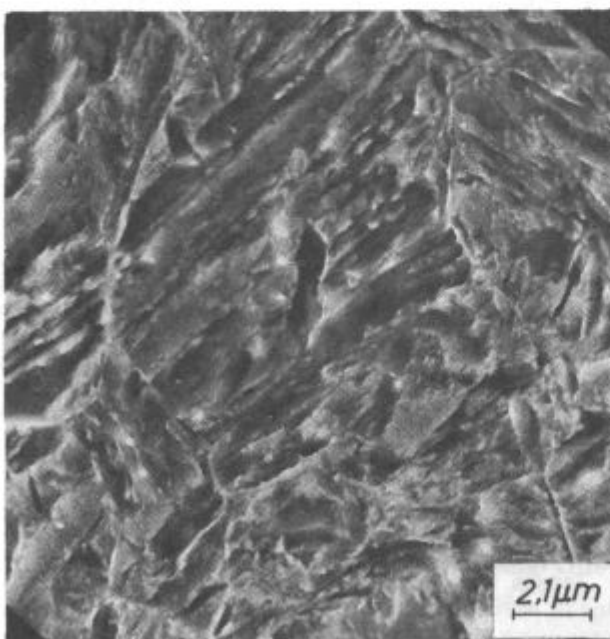
Geometrija cilindričnih nateznih preiskušancev z zarezo po obodu.

Fig. 1

Geometry of cylindrical round notched tensile specimens.

### 3.2 Toplotna obdelava

Toplotna obdelava preizkušancev je obsegala 1/2-urno avsténitizacijo pri  $850^{\circ}\text{C}$  s kaljenjem v vodi oziroma olju ter popuščanje. Slika 2 prikazuje mikrostrukturo letvastega martenzita, izoblikovanega pri kaljenju v vodi. S popuščanjem 2 ur pri  $480^{\circ}\text{C}$  oziroma  $420^{\circ}\text{C}$  je bila dosežena meja plastičnosti  $1185$  oziroma  $1290 \text{ Nmm}^{-2}$ .



Slika 2

Avsténitizirano pri  $850^{\circ}\text{C}$  in kaljeno v vodi. Letvasti martenzit.

Fig. 2

Austenitized at  $850^{\circ}\text{C}$ , and quenched in water. Lath-shaped martensite.

under condition that:

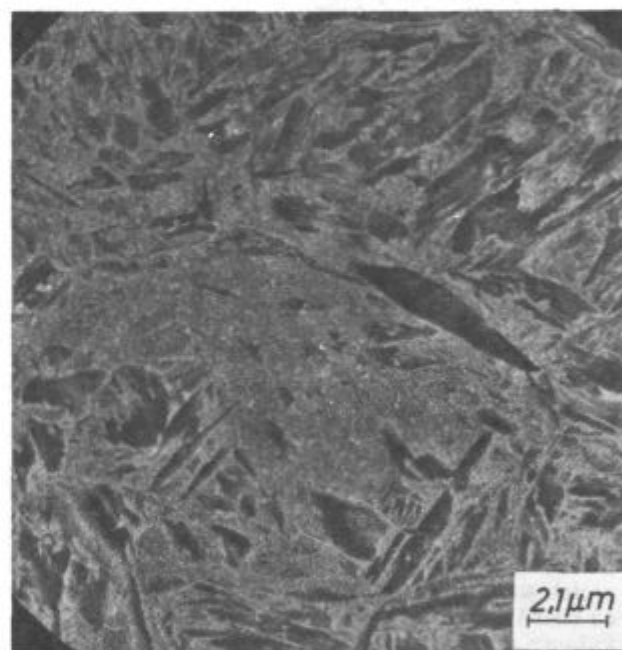
$$0.5 < d/D < 0.8$$

The ratio  $p/D$ , with  $p$  as the notch root radius, was close to the value 0.02. Moran and Noris<sup>28</sup> found by the computer simulation of the tension test with cylindrical, peripherally notched specimens, that the maximum stresses at fracture occur at about two notch-root radii below the surface when the  $p/D$  ratio is 0.01 to 0.02. On the other hand the maximum strain occurs at the notch root where also the first microcracks appear.

### 3.2 Thermal Treatment

Thermal treatment of specimens consisted of a 30 mins. austenitisation at  $850^{\circ}\text{C}$ , quenching in water or in oil, and tempering.

Fig. 2 shows the microstructure of the lath-formed martensite in the steel quenched in water. After tempering 2 hrs. at  $480^{\circ}\text{C}$  or  $420^{\circ}\text{C}$  yield strengths of  $1185$  and  $1290 \text{ N mm}^{-2}$  respectively were obtained. The hardness of oil quenched specimens was between 52 and 53.7 HRC. This means, that the predominantly martensitic microstructure of oil quenched specimens (Fig. 3) still contains up to 3 % of bainite. After tempering specimens quenched in oil 2 hrs. at  $450^{\circ}\text{C}$ , a yield strength of  $1230 \text{ N mm}^{-2}$  was obtained.



Slika 3

Avsténitizirano pri  $850^{\circ}\text{C}$  in kaljeno v olju. Spodnji bainit v martensiti osnovi.

Fig. 3

Austenitized at  $850^{\circ}\text{C}$ , and quenched in oil. Lower bainite in the martensitic matrix.

### 3.3 Hydrogen Charging

After thermal treatment, the specimens were charged with hydrogen by etching 24 hrs. in a  $0.1 \text{ N}$  aqueous solution of hydrochloric acid.

Chemical analysis of specimens immediately after the removal from the acid solution showed a hydrogen concentration of  $2.9 \pm 0.1 \text{ ppm}$  independently upon the yield

Trdota v olju kaljenih preizkušancev je dosegala vrednosti med 52 in 53,7 HRc. Pomeni, da je v pretežno martenzitni mikrostrukturi tovrstnih preizkušancev po kaljenju v olju (sl. 3) še tudi do 3 % bainita. S popuščanjem v olju kaljenih preizkušancev 2 ur pri 450°C je bila dosegrena meja plastičnosti 1230 Nmm<sup>-2</sup>.

### 3.3 Navodičenje

Toplotni obdelavi je sledilo navodičenje preizkušancev z jedkanjem 24 ur v 0,1 N vodni raztopini solne kisline.

Kemične analize vzorcev neposredno po odstranitvi iz kisline kažejo, da dobljena koncentracija vodika 2,9±0,1 ppm praktično ni odvisna od meje plastičnosti jekla. Z drugimi besedami: s 24-urnim jedkanjem še ni dosegena stacionarna koncentracija nasičenja jekla z vodikom. Zaključujemo, da del pasti še ni zaseden, saj bi v takšnem primeru bila koncentracija vodika različna v preizkušancih z različno mejo plastičnosti<sup>26, 29</sup>.

24 ur po odstranitvi iz raztopine je koncentracija vodika v preizkušancih padla na 0,82±0,1 ppm ter 48 ur po odstranitvi na 0,58±0,08 ppm.

Ob predpostavki, da je hitrost uhajanja vodika iz cilindričnih preizkušancev majhnega premera (D je približno 7 mm) premo sorazmerna razlike med trenutno ter residualno koncentracijo vodika v njih, dobimo za koncentracijo vodika v odvisnosti od časa po jedkanju (v urah) naslednji izraz:

$$[H] = 0,55 + 2,35 \exp(-0,09 t) \quad (12)$$

Polempiričen izraz (12) je uporaben za fenomenološki opis uhajanja vodika iz cilindričnih preizkušancev in ugotovljeno je bilo<sup>30</sup>, da v navodičenih preizkušancih ostaja še okrog 0,55 ppm vodika tudi dolgo časa po končanem jedkanju.

### 3.4 Določevanje kritičnega ter mejnega napetostnega intenzitetnega faktorja

Razvit je bil eksperimentalni sklop za registriranje inkubacijskega časa, to je časa do porajanja prve mikrorazpoke ter za registriranje počasnega napredovanja mikrorazpok do hipnega loma statično obremenjenih preizkušancev z zarezo po obodu. Sestavljen je bil iz polovičnega Wheatstonevega mostička z variabilnim uporom, ki ga je predstavljal uporovni listič, nalepljen preko ustja zareze. Porajanje ter napredovanje mikrorazpok je bilo registrirano posredno z odpiranjem ustja zareze, kot spremembra upornosti aktivnega uporovnega

strength of steel. In the other words, a 24 hrs. etching did not produce the saturation of steel with hydrogen. It was concluded that all the traps were not filled since in such a case the concentration of hydrogen in steel would be different in samples with different yield strengths<sup>26, 29</sup>. Twenty-four hours after removal from the acid solution, the concentration of hydrogen in specimens dropped to 0.82±0.1 ppm and after 48 hours to 0.58±0.08 ppm.

Supposing that the escape rate of hydrogen from the cylindric specimens with small diameter (D is approx. 7 mm) is proportional to the difference between the actual and the residual hydrogen concentration, the following equation can be derived for the variation of hydrogen concentration with time (hours) after the removal of samples from the acid solution:

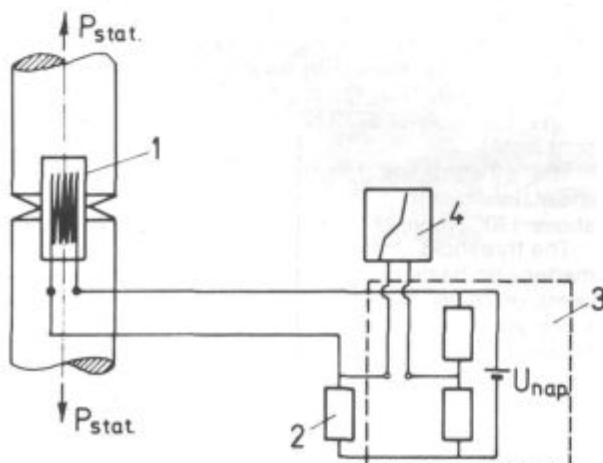
$$[H] = 0,55 + 2,35 \exp(-0,09 t) \quad (12)$$

This semiempirical equation is useful for the phenomenological description of hydrogen losses from the cylindric specimens and as it has been established<sup>30</sup> that the specimens charged with hydrogen still contain residual hydrogen of about 0.55 ppm even a long time after the etching.

### 3.4 Determination of the Critical and the Threshold Stress Intensity Factor

An experimental set-up was developed for the registration of the incubation period i.e. of the time necessary for the nucleation of the first microcrack, as well as for the registration of the slow propagation of microcracks to the instantaneous fracture of the round-notched specimens under static load. It consisted of a half-Wheatston bridge with a variable resistor represented by a strain-gauge stucked across the notch opening. Nucleation of microcracks and their propagation were indirectly registered by the displacement of the notch opening as the change of the resistance of the active strain-gauge compared with the resistance of the reference strain-gauge. This experimental set-up (schematically shown in Fig. (4)) permitted to detect the propagation steps of about 0.1 μm.

An almost similar set-up was used to measure the critical stress intensity factor i.e. fracture toughness of steel. Fig. 5 shows how the measurements were made on the "Instron" tensile machine with an accurate extensometer mounted on the notch opening of the specimen for calibration of the strain-gauges.



Slika 4

Eksperimentalni sklop za zasledovanje porajanja ter napredovanja mikrorazpok (1 — natezni preiskušec z uporovnim lističem, 2 — referenčni uporovni listič, 3 — merilna enota z izvorom napetosti, galvanometrom ter ojačevalcem, 4 — registrator).

Fig. 4

Experimental set-up for the detection of crack nucleation and propagation (1 — tensile specimen with strain-gauge, 2 — reference strain-gauge, 3 — measuring unit with power source, galvanometer and amplifier, 4 — recorder).



Slika 5

Merjenje lomne žilavosti. Ekstenzometer na preiskušanju služi kalibriraju uporavnih lističev.

Fig. 5

Measurement of fracture toughness. Extensometer on the tensile specimen used for the calibration of the strain-gauges.

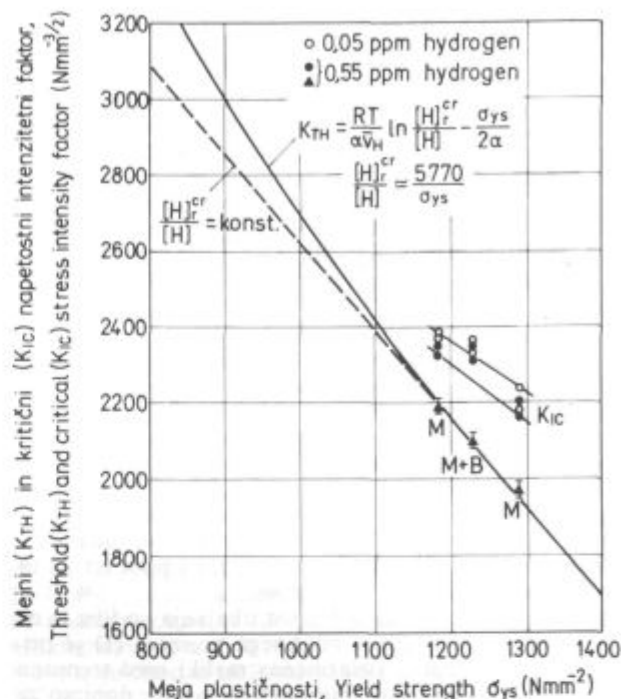
lističa glede na upornost referenčnega uporavnega lističa. Eksperimentalni sklop (shematsko prikazan na sliki 4) je dovoljeval zaznavanje koraka propagacije okrog 0,1 μm.

Skoraj podoben sklop opreme je bil uporabljen za merjenje kritičnega napetostnega intenzitetnega faktorja, t. j. lomne žilavosti jekla. Na sliki 5 je prikazana izvedba merjenja na trgalnem stroju »Instron« s preciznim ekstenzometrom, montiranim preko ustja zareze preizkušanca ter uporabljenim za kalibriranje uporavnih lističev.

Z merjenjem časa do loma preizkušancev v odvisnosti od uporabljene obremenitve je bil eksperimentalno določen mejni napetostni intenzitetni faktor  $K_{TH}$ , to je mejna statična obremenitev, pri kateri še ne pride do nukleacije mikrorazpok.

Kritični napetostni-intenzitetni faktor  $K_{Ic}$ , t. j. lomna žilavost jekla je bila izmerjena na cilindričnih preizkušancih z zarezo ter utrujenostno razpoko v korenju zareze. Tako kot za izračun mejnega, je bila tudi za izračun kritičnega napetostnega intenzitetnega faktorja uporabljena formula (11), globina utrujenostne propagacije mikrorazpok pa je bila izmerjena z optičnim mikroskopom po vsakokratnem preizkuusu.

Za preverjanje rezultatov je bila lomna žilavost izračunana še s korelacijo Rolfe-Novak<sup>31</sup> za takoimenovano upper shelf področje. Odvisnost med izmerjenimi faktorji ( $K_{TH}$ ,  $K_{Ic}$ ) ter mejo plastičnosti jekla je prikazana



Slika 6

Odvisnost med napetostnim intenzitetnim faktorjem ( $K_{TH}$ ,  $K_{Ic}$ ) in mejo plastičnosti preiskovanega jekla.

Fig. 6

Relationship between the stress intensity factor ( $K_{TH}$ ,  $K_{Ic}$ ) and the yield strength of the investigated steel.

The threshold stress intensity factor  $K_{TH}$  which represents the limiting value of static load below which micro-cracks do not appear, was experimentally determined by measuring the time till fracture occurs related to the applied load.

The critical stress intensity factor  $K_{Ic}$  i. e. the fracture toughness of steel was measured on round notched tensile specimens with fatigue crack at the notch tip. The Eq. (11) was applied to calculate both the threshold and the critical stress intensity factor. The width of the fatigue crack was measured with an optical microscope after each experiment.

To check the obtained results, the fracture toughness was also calculated by the Rolfe-Novak correlation<sup>31</sup> for the upper shelf region. The relation between the measured factors ( $K_{TH}$ ,  $K_{Ic}$ ) and the yield strength of the investigated steel is shown in Fig. 6. The plot presents also the relation by eq. (9) calculated on the basis of measured values for steel with fully martensitic microstructure after quenching (points M). Considering the equation (10), a value of 5770 N mm<sup>-2</sup> was calculated for the constant β.

The straight line for  $[H]_r^{cr}/[H] = \text{const.}$  proves that linear interpolation is acceptable at yield strengths above 1200 N mm<sup>-2</sup>.

The threshold stress intensity factor  $K_{TH}$  for tempered martensitic-bainitic microstructure with only few percents of bainite after quenching (point M+B) has the same value as that for a fully martensitic tempered microstructure with the same yield strength ( $K_{TH} = 2100$  N mm<sup>-3/2</sup>).

Hydrogen has no noticeable influence, if any at all, on the fracture toughness of the investigated steel. However, at the same yield strength, the fracture toughness,

na sliki 6. V diagramu je vrisana tudi odvisnost (9), izračunana na osnovi izmerjenih vrednosti za jeklo s povsem martenzitno mikrostrukturo po kaljenju (točki M). Upoštevaje izraz (10) ima konstanta  $\beta$  vrednost  $5770 \text{ Nmm}^{-2}$ .

Premica za  $[H]^{cr}/[H] = \text{konst.}$  dokazuje, da je pri meji plastičnosti nad  $1200 \text{ Nmm}^{-2}$  dopustna linearna interpolacija.

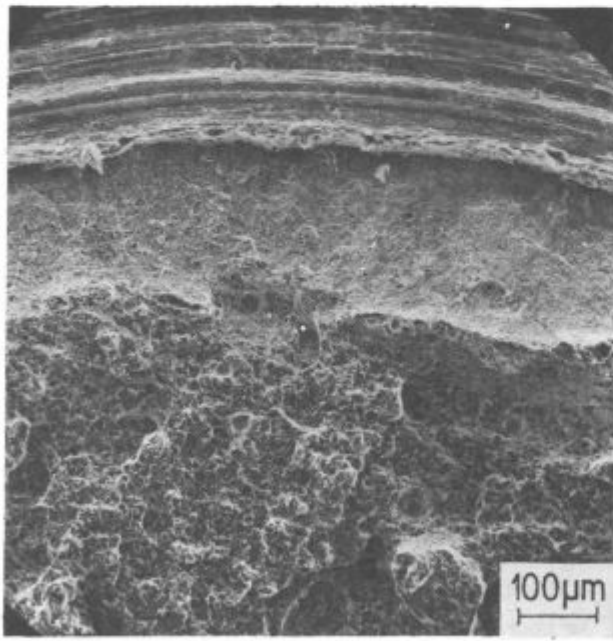
Mejni napetostni intenzitetni faktor  $K_{TH}$  za popuščeno martenzitno-bainitno mikrostrukturo z le nekaj odstotki bainita po kaljenju (točka M+B) ima enako vrednost, kot je bila določena za jeklo z mikrostrukturo popuščenega martenzita ter enako mejo plastičnosti ( $K_{TH} = 2100 \text{ Nmm}^{-3/2}$ ).

Vodik nima večjega, če ima sploh kakšen vpliv na lomno žilavost preiskovanega jekla. Pri enaki meji plastičnosti pa je lomna žilavost, v nasprotju z mejnim napetostnim intenzitetnim faktorjem, nekoliko odvisna od majhnih mikrostrukturnih variacij jekla. Tako ima jeklo s popuščeno martenzitno-bainitno mikrostrukturo ter mejo plastičnosti  $1230 \text{ Nmm}^{-2}$  lomno žilavost med 2310 in  $2360 \text{ Nmm}^{-3/2}$ , kar je nekoliko več od z linearno interpolacijo določene lomne žilavosti za popuščeno martenzitno mikrostrukturo enake meje plastičnosti ( $K_{lc} = 2250$  in  $2320 \text{ Nmm}^{-3/2}$ ).

### 3.5 Mikromorfologija prelomov

Mikrofraktografske preiskave prelomnih površin navodičenih cilindričnih nateznih preizkušancev z zarezo po obodu, so bile opravljene z vrstičnim elektronskim mikroskopom.

Slika 7 kaže del prelomne površine nateznega preizkušanca z zarezo, z mikrostrukturo popuščenega martenzita ter mejo plastičnosti  $1185 \text{ Nmm}^{-2}$ . Statična



Slika 7

Z zapoznanim lomom nastala prelomna površina preizkušanca z mikrostrukturo popuščenega martenzita ter mejo plastičnosti  $1185 \text{ N mm}^{-2}$  posneta z vrstičnim elektronskim mikroskopom.

Fig. 7

Scanning electron micrographs of the delayed fracture surfaces of specimen with the tempered martensitic microstructure and yield strength  $1185 \text{ N mm}^{-2}$ .

contrary to the threshold stress intensity factor, depends slightly on small microstructure variations of steel. For instance, steel with the martensitic-bainitic microstructure with yield strength  $1230 \text{ N mm}^{-2}$  has fracture toughness between  $2310$  and  $2360 \text{ N mm}^{-3/2}$ , which is slightly above the value of  $K_{lc}$  being between  $2250$  and  $2320 \text{ N mm}^{-3/2}$  found by linear interpolation for the tempered martensitic microstructure with the same yield strength.

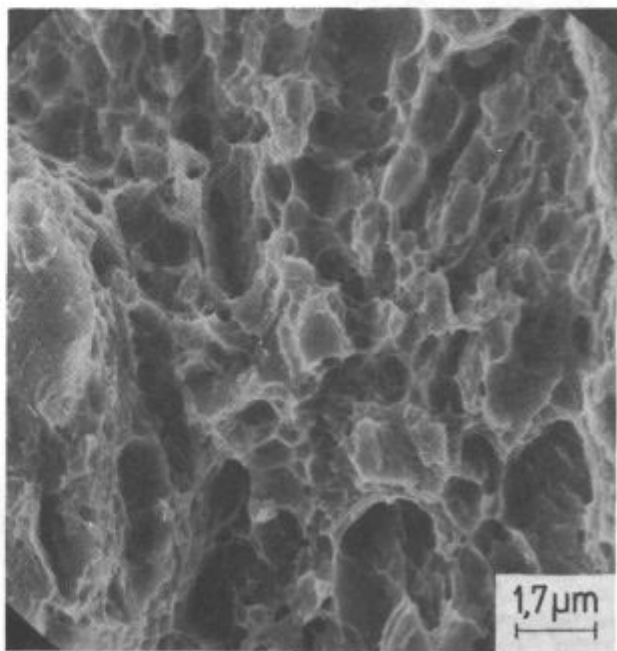
### 3.5 Micromorphology of Fractures

Microfractographic investigations of fracture surfaces of round notched tensile specimens charged with hydrogen were performed in a scanning electron microscope.

Fig. 7 shows a part of fracture surface of a round notched tensile specimen with fully martensitic tempered microstructure and with yield strength  $1185 \text{ N mm}^{-2}$ . Static load i.e. applied stress intensity factor  $2190 \text{ N mm}^{-3/2}$  was close to the limiting value ( $K_{TH} = 2180 \text{ N mm}^{-3/2}$ ) which caused the delayed fracture of the specimen after 181 hours. Right along the notch (above), an area of slow crack propagation can be seen separated by an unsharp boundary from the fracture surface formed by an instantaneous failure (below).

The area of slow crack propagation, which is completely undefined at low magnification, is shown in Fig. 8 at a higher magnification. This area is predominantly ductile and irregularly shaped dimples are found next to the well defined dimples. Irregular dimples indicate that decohesion occurred at a very low plastic deformation. It is also possible that some details are a consequence of cleavage too.

A similar micromorphology of the area of slow crack propagation is observed on samples with the tempered

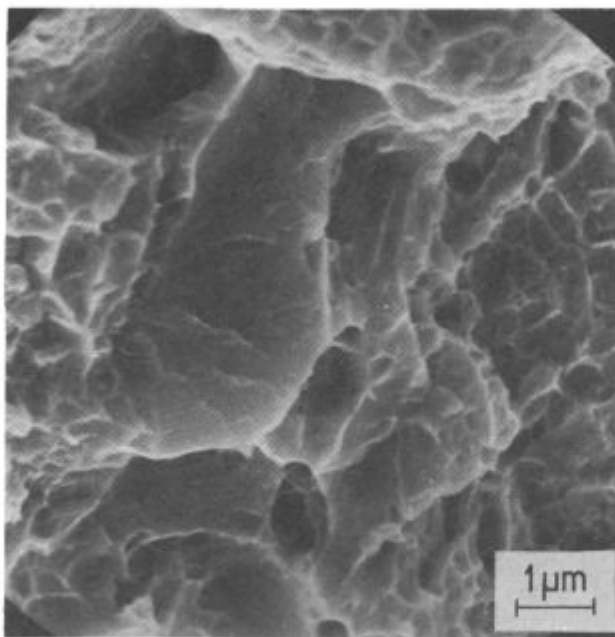


Slika 8

Področje počasne propagacije s slike 7. Pretežno duktilna oblika preloma.

Fig. 8

The area of slow crack propagation from Fig. 7. Predominantly ductile fracture.



Slika 9

Področje počasne propagacije na preizkušancu s popuščeno martenzitno mikrostrukturo ter mejo plastičnosti  $1290 \text{ N mm}^{-2}$ . Duktilna oblika preloma s posameznimi cepilnimi ploskvami.

Fig. 9

The area of slow crack propagation in specimen with the tempered martensitic microstructure and yield strength  $1290 \text{ N mm}^{-2}$ . Ductile fracture with single cleavage facets.

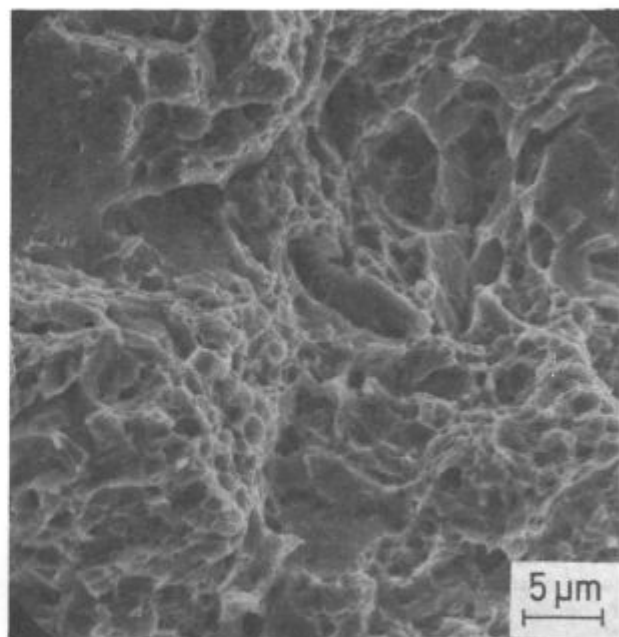
obremenitev, namreč aplicirani napetostni intenzitetni faktor  $2190 \text{ Nmm}^{-3/2}$ , je bila blizu mejni vrednosti ( $K_{TH} = 2180 \text{ Nmm}^{-3/2}$ ), kar je povzročilo zapozneli lom preizkušanca po 181 urah.

Neposredno ob zarezi (zgoraj) je moč videti cono počasnega napredovanja mikrorazpok, ne ostro ločeno od prelomne površine, nastale s hipno porušitvijo (spodaj).

Cona počasnega napredovanja mikrorazpok, ki je pri nizki povečavi povsem neopredeljiva, je pri večji povečavi prikazana na sliki 8. To področje je pretežno duktilno, poleg dobro definiranih jamic pa najdemo tudi jamicice nepravilnih oblik. Nepravilne jamicice kažejo, da se je dekohezija izvršila z zelo malo plastične deformacije in prav mogoče je, da so nekateri detaili tudi proizvod cepljenja. Podobno mikromorfologijo preloma v coni počasnega napredovanja mikrorazpok zasledimo tudi na preizkušancih s popuščeno martenzitno-bainitno mikrostrukturo, medtem ko je na preizkušancih s popuščeno martenzitno mikrostrukturo ter mejo plastičnosti  $1290 \text{ Nmm}^{-2}$  že tudi občutnejši delež cepilnih ali kvazicepilnih ploskvic (slika 9). Področje naglo zlomljenega osrednjega dela preizkušanca slike 7 je pri večji povečavi prikazano na sliki 10. Prevladujejo področja duktilnega tipa preloma, čeprav je opaziti tudi cepilne oziroma kvazicepilne ploskvice, a v manjšem obsegu.

Podobna je mikromorfologija preloma osrednjega, naglo zlomljenega dela preizkušancev s popuščeno martenzitno-bainitno mikrostrukturo, kot tudi preizkušancev s popuščeno martenzitno mikrostrukturo ter mejo plastičnosti  $1290 \text{ Nmm}^{-2}$ , čeprav je v slednjem primeru število kvazicepilnih ploskvic povečano.

Pojavljanje cepilnega oziroma kvazicepilnega tipa preloma v coni počasnega napredovanja mikrorazpok je le sporadično, v nasprotju s prevladajočo duktilno obliko preloma, zato sklepamo, da je nukleacija mikro-



Slika 10

Področje naglega loma iz slike 7. Duktilno, cepilno in kvazi-cepilno.

Fig. 10

Region of fast fracture from Fig. 7. Ductile, cleavage and quasi-cleavage.

martenitic-bainitic microstructure, while a noticeable amount of cleavage or quasi-cleavage facets appear in the samples with the martensitic microstructure and the yield strength  $1290 \text{ N mm}^{-2}$  (Fig. 9).

The area of fast fracture, already shown in Fig. 7, is shown again in Fig. 10 at a higher magnification. Here, the ductile type of fracture prevails though cleavage or quasi-cleavage facets can also be observed but in smaller extent.

A similar micromorphology of the areas of fast fracture is also observed on the samples with the tempered martensitic-bainitic microstructure as well as on the samples with the tempered martenitic microstructure and with yield strength  $1290 \text{ N mm}^{-2}$ , though in the latter case the number of quasi-cleavage facets is larger.

Cleavage or quasi-cleavage type of fracture in the area of slow crack propagation is merely sporadic in comparison to the prevailing ductile type of the fracture, thus the conclusion can be made that the crack nucleation as well as the slow crack propagation are mainly strain induced processes related to the decrease of fracture ductility i. e. decrease of the microplasticity in the area of stress induced segregation of hydrogen at the crack tip.

#### 4. CONCLUSIONS

An appropriate method was developed for the detection of the nucleation and the propagation of microcracks at the notch tip of hydrogen charged static loaded cylindrical round notched tensile specimens. The limit of the detectability of microcrack propagation was about  $0.1 \mu\text{m}$ .

Measurements of the threshold stress intensity factor  $K_{TH}$  of the hydrogen charged chromium-molybdenum C.4732 steel with the tempered martensitic microstruc-

razpok ter njih počasno napredovanje deformacijsko inducirani proces povezan s poslabšanjem lomne duktilitnosti, t. j. poslabšanjem mikroplastičnosti v področju napetostno induciranega segregiranja vodika ob konici razpoke.

#### 4. ZAKLJUČKI

V okviru opravljenega dela je bila razvita primerna metoda za preučevanje nastajanja ter napredovanja mikrorazpok iz korena zareze na obodu navodičenih ter statično obremenjenih cilindričnih nateznih preizkušancev z zarezo. Najmanjši korak propagacije mikrorazpok, ki ga je bilo moč zaslediti, je znašal okoli  $0,1 \mu\text{m}$ .

Merjenja mejnega napetostnega intenzitetnega faktorja  $K_{TH}$  navodilnega krom-molibdenskega jekla, vrste Č.4732, z mikrostrukturo popuščenega martenzitom oziroma popuščeno martenzitno-bainitno mikrostrukturo enake meje plastičnosti, kažejo, da majhne mikrostrukturne variacije preiskovanega jekla ne vplivajo na  $K_{TH}$ .

Ti rezultati se ujemajo z ugotovitvami Nakasata in Terasakija<sup>32</sup>, ki potrjujeta, da mejni napetostni intenzitetni faktor  $K_{Ic}$  pri enaki trdnosti jekla ni odvisen od mikrostrukturnih variacij visokotrdnega jekla. Če je ta ugotovitev splošna, potem je utemeljena hipoteza, po kateri je nukleacija mikrorazpok, ki povzroči zapozneli lom jekla, vedno omejena na martenzitne dele mikrostrukture (najprej dosežena  $[H]^*$ ). Le na ta način namreč lahko razložimo, da majhni deleži bainita v pretežno martenzitni mikrostrukturi popuščenega visokotrdnega jekla nimajo vpliva na mejni napetostni intenzitetni faktor. Zdi se, da se različna jekla pri enaki vsebnosti vodika ter enaki meji plastičnosti v pogledu nukleacije mikrorazpok obnašajo kot elastični kontinuum.

Merjenja kritičnega napetostnega intenzitetnega faktorja kažejo, da majhne koncentracije vodika v preiskovanem jeklu nimajo opaznejšega vpliva na lomno žilavost jekla. Pač pa je pri enaki meji plastičnosti lomna žilavost (v nasprotju z mejnim napetostnim intenzitetnim faktorjem) odvisna tudi od majhnih mikrostrukturnih variacij jekla, saj ima jeklo s popuščeno martenzitno-bainitno mikrostrukturo nekoliko višjo lomno žilavost, kot isto jeklo s popuščeno martenzitno mikrostrukturo enake meji plastičnosti.

Rezultati teh preiskav se ujemajo s podatki, ki so jih objavili Ohtani, Terasaki in Kunitake<sup>33</sup>, ki so povečano žilavost duplex mikrostrukture razlagali s koristno vlogo majhnih deležev bainita pri zmanjšanju delov posameznih avstenitnih zrn, ki se transformirajo v martenzit. Takšna mikrostruktura ima povečano odpornost proti napredovanju razpok, t. j. manjšo občutljivost k zapozneemu lomu.

Porajanje mikrorazpok v področju maksimalnih deformacij, kot tudi pretežno duktilna oblika preloma v coni počasnega napredovanja mikrorazpok navajata k sklepui, da je nukleacija mikrorazpok deformacijsko inducirani proces, povezan s poslabšanjem lomne duktilitnosti med trajanjem obremenjevanja.

ture or the tempered martensitic-bainitic microstructure and with the same yield strength showed that small microstructure variations of the investigated steel had no influence on  $K_{TH}$ .

These results confirm the Nakasato's and Terasaki's statements<sup>32</sup> according to which the threshold stress intensity factor  $K_{Ic}$  at the same tensile strength does not depend on the microstructure variations of high strength steel. If this statement is general, the hypothesis suggesting that the microcrack nucleation leading to the delayed fracture is always confined to martensitic areas of the microstructure ( $[H]^*$  is at first reached) has argument. It seems that this is the only way to explain the lack of influence of small portion of bainite in a predominantly martensitic microstructure of the tempered high strength steel on the threshold stress intensity factor. As far as the crack nucleation is concerned, it seems that various steels with the same yield strength and the same hydrogen concentration behave as an elastic continuum.

The measurements of the critical stress intensity factor show that small concentrations of hydrogen in the investigated steel has no noticeable influence on the fracture toughness of steel. However, at the same yield strength the fracture toughness (contrary to the threshold stress intensity factor) depends also on small microstructure variations of steel, since steel with the tempered martensitic-bainitic microstructure has slightly higher fracture toughness than the same steel with the tempered martensitic microstructure and with the same yield strength. The results of this investigation agree with the data published by Ohtani, Terasaki and Kunitake<sup>33</sup> who explained the higher toughness of the duplex microstructure by the beneficial effect of small quantity of bainite which reduces the size of single austenite-grain parts in which the martensitic transformation takes place. Such a microstructure has a better resistance to crack propagation i. e. it is less sensitive to the delayed fracture.

The nucleation of the crack in the region of maximal strain as well as the predominantly ductile type of fracture in that area suggest the conclusion that the nucleation of microcracks is a strain induced process related to the decrease of fracture ductility during the loading.

#### LITERATURA/REFERENCES

1. G. L. Hanna, A. R. Troiano in E. A. Steigerwald: Transactions of the ASM, 57, 1964, 658-671
2. A. R. Troiano: Transactions of the ASM, 52, 1960, 54
3. L. S. Darken in R. P. Smith: Corrosion 5, 1949, 1
4. R. A. Oriani: Acta Metall. 18, 1970, 147
5. Y. Sakamoto in J. Eguchi: Proc. Japan Congress on Materials Research 19, 1976, 91
6. A. P. Miodownik: Stress corrosion cracking and hydrogen embrittlement of iron base alloys, NACE, Huston, 1977
7. A. Zielinski, B. Lunarska in M. Smialowski: Acta Metall. 25, 1977, 551

8. A. J. Kumnick in H. H. Johnson: *Acta Metall.* 28, 1980, 33
9. A. M. Adair in R. E. Hook: *Acta Metall.* 10, 1962, 741
10. A. J. Kumnick in H. H. Johnson: *Metallurgical Transactions* 5A, 1974, 1199
11. G. M. Evans in E. C. Rollason: *Japan Iron Steel Inst.*, 1969, 1484
12. D. M. Allen-Booth in J. Hewitt: *Acta Metall.* 22, 1974, 171
13. H. Hargi, Y. Hayashi in L. L. Shreir: *Corrosion Science* 11, 1971, 25
14. G. W. Hong in J. Y. Lee: *J. Mat. Sci.* 18, 1983, 271
15. T. Asaoka, G. Lapasset in M. Aucouturier: *Corrosion* 34, 1978, 39
16. G. M. Pressouyre in I. M. Bernstein: *Metallurgical Transactions* 9A, 1978, 1571
17. A. McNabb in P. K. Foster: *Trans. Am. Inst. Min. Engrs.* 227, 1963, 618
18. W. Tyson: *Canadian Metallurgical Quarterly*, Vol. 18, 1979, 1—11
19. J. C. M. Li, L. S. Darken in R. A. Oriani: *Zeitschrift für Physikalische Chemie Neue Folge* 9, 1966, 271
20. H. L. Ewalds in R. J. H. Wanhill: *Fracture mechanics*, Edward Arnold Ltd., 1985
21. povzeto po A. G. Guy: *Essentials of Materials Science*, McGraw-Hill, 1976
22. W. W. Gerberich: Effect of hydrogen on high-strength and martensitic steels, *Hydrogen in Metals — Proceedings of an international conference*, 23.—27. September 1973, Seven Springs Conference Center, Champion, Pa. USA, Library of Congress Catalog Card Number: 73—86455
23. R. A. Oriani: *Ber. der Buns. Gesell.* 76, 1972, 848
24. C. D. Beachem: *Metallurgical Transactions* 3, 1972, 437
25. K. Farrell in A. G. Quarrell: *J. Iron Steel Inst.*, 202, 1964, 1002
26. C. D. Kim in A. W. Loginow: *Corrosion* 24, 1968, 313
27. K. Heckel: *Einführung in die technische Anwendung der Bruchmechanik*, Carl Hanser Verlag, München 1970
28. B. Moran in D. M. Noris: *Metallurgical Transactions A*, 1978, 1685
29. L. S. Darken in R. P. Smith: *Corrosion* 5, 1949, 60
30. B. Ule: *Zapozneli lom zaradi vodika v jeklu*, Magistrsko delo, Univerza E. Kardelja v Ljubljani, 1987
31. S. T. Rolfe in S. R. Novak: Slow-bend  $K_{Ic}$  testing of medium-strength high-toughness steels, *STP 463*, 1970, 124—159 kot tudi R. B. Scarlin in M. Shakeshaft: *Metals Technology*, Jan. 1981, 1—9
32. F. Nakasato in E. Terasaki: *Transactions ISIJ*, 15, 1975, 290—291
33. H. Ohtani, F. Terasaki in T. Kunitake: *Transactions ISIJ*, 12, 1972, 185

## *Doktorska in magistrska dela v letu 1986*

### *Ph. D. and M. Sc. Theses at the Department of Geology, Mining and Metallurgy, Section Metallurgy, in Year 1986*

#### **DOKTORSKO DELO**

**Mirko Dobršek:** Konstrukcija trokomponentnih sistemov Pd-Au-Zn, Pd-Cu-Zn, Au-Cu-Zn

(Mentor: I. Kosovinc, 18/12/1986)

Zgoraj omenjeni sistemi so osnova sistema Pd-Au-Ag-Cu-Zn. Paladij zaradi svoje majhne gostote, korozionske obstojnosti, katalizatorskih sposobnosti ter nizke cene vedno uspešnejše nadomešča drago zlato in platino. Avtor je izdelal neizotermne preseke teh ternarnih sistemov, določil fazna področja z rentgensko fazno analizo, ki jo je dopolnil še z metalografsko analizo. V vseh treh sistemih je ugotovil široko enofazno področje ternerne trdne raztopine, ki se širi iz obrobnih sistemov popolne topnosti v ternarni prostor. Delo ima praktično uporabno vrednost predvsem na področju dentalnih zlitin in omogoča nadaljnje raziskave večkomponentnih sistemov v ožjih, tehnično-ekonomsko zanimivih koncentracijskih območjih.

82 strani

29 cit.

#### **PH. D. THESIS**

**Mirko Dobršek:** Construction of Ternary Pd-Au-Zn, Pd-Cu-Zn, and Au-Cu-Zn Phase Diagrams

(Supervisor: I. Kosovinc, 18/12/1986)

The upper mentioned systems are the basis of the Pd-Au-Ag-Cu-Zn system. Palladium due to its low density, corrosion resistance, catalytic properties, and low price successfully substitutes more expensive gold and platinum. Nonisothermal cross sections in these ternary diagrams were constructed. The phase regions were determined by the X-ray phase analysis which was complemented also with the metallographic analysis. In all the three systems a wide one-phase region of the ternary solid solution was found which extends from the edge binary systems of complete solubility into the ternary space. The project has practical applicability mainly in the field of dental alloys, and it enables further investigations of the multi-component systems in the narrower, technically and economically interesting regions of compositions.

82 pages

29 ref.

#### **MAGISTRSKA DELA**

**Mihail Tolar:** Kohezivne cone v plavžu

(Mentor: J. Lamut, 4/3/1986)

Plavž je agregat, v katerem potekajo fizikalno-kemične reakcije v odvisnosti od razporeditve plinskih tokov ter temperaturnega polja. Lega in oblika kohezivne cone v delovnem prostoru plavža sta odločilni pri razporeditvi plinskih tokov iz spodnjega v zgornji del peči.

Avtor je v svojem delu obravnaval termostabilnost mineralnega vsipa in obnašanje koksa po višini delovnega prostora peči, prehod silicija in žvepla iz vročega koksa v grodelj, oblikovanje mehčalno-talilne cone v peči ter kohezivne cone, skupaj z ukrepi, ki vplivajo na njihovo obliko in lego. Kohezivne cone so kompaktne nataljene plasti mineralnega vsipa, ki so vrnjene med plasti koksa in jih med seboj ni možno več ločiti. Predstavljajo prehod med začetkom mehčanja in dokončno stalištvijo vsipa. Običajno imajo te cone obliko V ali W. Obnašanje vsipa pri pogrezanju je avtor zasledoval z jemanjem vzorcev na 7 ravneh v plavžu. Ugotavljal je stopnjo redukcije in metalizacije, delež FeO ter nastajanje žlindre. Hod preizkovanega jeseniškega plavža je bil periferen.

110 strani

173 cit.

#### **M. SC. THESES**

**Mihail Tolar:** Cohesive Zones in the Blast Furnace

(Supervisor: J. Lamut, 4/3/1986)

Course of physico-chemical reactions in the blast furnace depends on the distribution of gas flows and the temperature field. Position and shape of the cohesive zones in the operation area of the blast furnace are essential for the distribution of the gas flows from the lower into upper section of the furnace.

Further, thermostability of the burden, behaviour of coke along the height of the furnace region of operation, transfer of silicon and sulphur from hot coke into pig iron, formation of the softening-melting zone in the furnace and the cohesive zones are treated together with the measures which can influence the shape and the position of the cohesive zones. These zones are compact partially melted layers of the burden which intrude into the coke layers, and they cannot be separated anymore. They represent the transition between the initial softening and the final melting of the burden. Usually these zones have the shape of letter V or W. Behaviour of the burden during descending was followed by sampling on 7 levels in the furnace. Degrees of reduction and metallization, portion of FeO and formation of slag were analyzed. Running of the blast furnace in the Jesenice Iron-works was peripheral.

110 pages

173 ref.

**Miraš Djurović: Vpliv induktivnega mešanja taline na kinetiko reakcij med talino in žlindro pri izdelavi jekla za kroglične ležaje Č.4146.**

(Mentor: J. Lamut, 14/5/1986)

Moderno postopki izdelave elektrojekla vključujejo tudi obdelavo taline izven peči. Kroglični ležaji zahtevajo zelo kakovostno jeklo. V delu je bil poudarek na študiju vpliva induktivnega mešanja. Raziskave so bile v jeklarni Železarne Boris Kidrič v Nikšiću. Avtor je najprej obdelal osnovne značilnosti ležajnega jekla Č.4146, osnove reakcij med talino in žlindrom ter izvenpečno obdelavo tekočega jekla s poudarkom na intenzifikaciji reakcij. Zasledoval je gibanje žvepla v jeklu med obdelavo v napravi ASEA-SKF, vpliv sestave sintetične žlindre, pomen delovne temperature, sestavo dobljene žlindre in možnost reoksidacije. Na osnovi rezultatov raziskav je avtor predložil tehnologijo za izdelavo ležajnega jekla v obločni peči skupaj z rafinacijo v ASEA-SKF napravi in litjem ingotov.

73 strani

9 cit.

**Miraš Djurović: Influence of Inductive Stirring of Melt on the Kinetics of the Melt/Slag Reactions in Manufacturing Č.4146 Ball-Bearing Steel**

(Supervisor: J. Lamut, 14/5/1986)

Modern processes in manufacturing steel in electrical furnaces include also the treatment of melt outside the furnace. Ball bearings demand a high-grade steel. Influence of the induction stirring was analyzed. Investigations were made in the Boris Kidrič Ironworks in Nikšić. Initially, the basic characteristics of the ball-bearing Č.4146 steel are presented, together with the basic reactions between melt and slag, and the out-of-furnace treatment of molten steel with a special emphasis on the intensification of reactions. Variation of the sulphur content in steel during the treatment in the ASEA-SKF equipment was followed, together with the influence of the composition of synthetic slag, and the importance of operating temperature, composition of the obtained slag, and the possibility of the reoxidation. Based on the results of the investigation an improved technology for manufacturing ball-bearing steel in electric arc furnace together with the refining in the ASEA-SKF set-up, and casting the ingots was proposed.

73 pages

9 ref.

**Henrik Kaker: Kvantitativna energijsko disperzijska analiza Nimonic 80 A v rastrskem elektronskem mikroskopu**

(Mentor: V. Marinković, 8/7/1986)

Avtor je na nikljevi zlitini Nimonic 80 A obravnaval postopke obdelave zbranega spektra z energijskim spektrometrom, metode kvantitativne mikroanalize in računske postopke za popravke v koncentracijah analiziranih elementov vsled razlik v atomskem številu med vzorcem in standardom (etalonom), absorpcije in sekundarne fluorescence rentgenskega sevanja. Naredil je tudi primerjavo med metodo s standardi in brez njih ter dobljene rezultate primerjal z rezultati kemijske analize. Analiziral je napake, ki vplivajo na točnost kvantitativne mikroanalize z energijskim spektrometrom. Ugotovil je, da je relativna napaka pri metodi brez standardov pod 1 % pri koncentracijah nad 20 mas. %, naraste pa na okoli 16 % pri koncentracijah pod 1 mas. %. Glavna prednost metode je njena hitrost. Zelo primerna je, če nimamo na razpolago ustreznega standarda in če točnost pri nizkih koncentracijah ni odločilna. Metoda s standardi je pri majhnih koncentracijah sicer bolj natančna, a je bistveno počasnejša. Mikroanaliza faz v zlitini Nimonic 80 A je pokazala prisotnost Ti karbonitridov in Cr karbidov na kristalnih mejah ter enakomerno porazdeljeno fazo  $\gamma'$  v osnovi.

74 strani

43 cit.

**Henrik Kaker: Quantitative Energy Dispersion Analysis of Nimonic 80 A by the Scanning Electron Microscope**

(Supervisor: V. Marinković, 8/7/1986)

The author has chosen the Nimonic 80 A nickel alloy to present the methods for treating the spectrum obtained by the energy spectrometer, the methods of quantitative microanalysis, and the mathematical methods to correct the obtained concentrations of analyzed elements due to the differences in atomic numbers between the sample and the standard, in the absorption, and the secondary fluorescence of X-radiation. A comparison was made between the method where standards were applied and the method without applying standards. The both obtained results were compared to the results of chemical analysis. Further, the analysis of errors influencing the accuracy of quantitative microanalysis by the energy spectrometer was made too. It was found, that the relative error with the method where standards were not applied was below 1% for concentrations above 20 mass % of elements, but this error is increased to about 16% if concentrations are reduced below 1 mass %. The basic advantage of this method is that it is fast. It is suitable when a corresponding standard is not available and when the accuracy at lower concentrations is not essential. The method applying standards is more accurate for lower concentrations but it is essentially slower. The microanalysis of phases in the Nimonic 80 A alloy revealed the presence of Ti carbonitrides and Cr carbides on the grain boundaries, and the uniformly dispersed  $\gamma'$  phase in the matrix.

74 pages

43 ref.

# Železarski zbornik, 21, 1987, 1–4

## 1. KRONOLOŠKO KAZALO

- Todorović Gojko, J. Lamut, B. Dobovišek, J. Kramer, J. Zapušek, B. Sedlar: Naogljicanje železa med redukcijo in taljenjem plavžnega vsipa . . . . . ŽZB 21 (1987) 1, 1–5  
 Arh Jože, V. Prešeren: Dosežki Železarne Jsenice na področju sekundarne obdelave jekla . . . . . ŽZB 21 (1987) 1, 7–17  
 Vodopivec Franc, M. Gabrovšek: Meja plastičnosti konstrukcijskih jekel, fizikalno metalurške osnove . . . . . ŽZB 21 (1987) 1, 19–28  
 Vodopivec Franc, F. Marinšek, F. Grešovnik: Rekrystalizacija in rast zrn pri žarjenju hladno valjanega jekla z 0,03 % C, 1,8 % Si, 0,3 % Mn in 0,3 % Al . . . . . ŽZB 21 (1987) 1, 29–37  
 Kaker Henrik: Mikroanaliza faz v zlitini Nimonic 80 A s kombinacijo REM-EDS . . . . . ŽZB 21 (1987) 1, 39–43  
 Azman Alojz, D. Sikošek, A. Šteblaj, J. Triplat, J. Arh: Tehnična novica: Novi konstrukcijski mikrolegrirani jekli Niomol 390 in Niomol 490 . . . . . ŽZB 21 (1987) 1, 45–52  
 Brdar Božidar: Ohlajanje jeklenega valja na vozičku . . . . . ŽZB 21 (1987) 2, 85–92  
 Brdar Božidar: Strjevanje jekla v kokili . . . . . ŽZB 21 (1987) 4, 137–150  
 Čurčija Dušan: Vpliv hitrosti valjanja na proces hladnega valjanja z mazivi . . . . . ŽZB 21 (1987) 3, 131–136  
 Gnamuš Janko, G. Rihtar: Reparaturno varjenje orodnih jekel . . . . . ŽZB 21 (1987) 2, 73–76  
 Grešovnik Ferdo: Računanje temperaturnih napetosti v elastičnem področju . . . . . ŽZB 21 (1987) 2, 77–83  
 Kaker Henrik: Mikroanaliza faz v zlitini Nimonic 80 A s kombinacijo REM-EDS . . . . . ŽZB 21 (1987) 1, 39–43  
 Kmetič Dimitrij, F. Mlakar, V. Tucić, J. Žvokelj, F. Vodopivec, M. Jakupović, B. Rallc: Bele kromove litine legirane z molibdenom za valje . . . . . ŽZB 21 (1987) 4, 151–165  
 Kosec Ladislav, F. Kosek: Nastanek in rast utrujenostne razpoke v koroziskem mediju . . . . . ŽZB 21 (1987) 4, 175–182  
 Leskovšek Vojteh: Tehnična novica: Predstavitev enokomorene vakuumsko peči IPSEN VTC 324-R s homogenim plinskim hlajenjem pod visokim tlakom . . . . . ŽZB 21 (1987) 1, 53–57  
 Arh Jože: Tehnična novica: Druga evropska konferenca o električnem jeklarstvu . . . . . ŽZB 21 (1987) 1, 59–63  
 Paulin Andrej, J. Lamut, D. Dretnik: Reaktivnost koksa in njen vpliv na delo plavža . . . . . ŽZB 21 (1987) 2, 65–71  
 Gnamuš Janko, G. Rihtar: Reparaturno varjenje orodnih jekel . . . . . ŽZB 21 (1987) 2, 73–76  
 Grešovnik Ferdo: Računanje temperaturnih napetosti v elastičnem področju . . . . . ŽZB 21 (1987) 2, 77–83  
 Kaker Henrik: Mikroanaliza faz v zlitini Nimonic 80 A s kombinacijo REM-EDS . . . . . ŽZB 21 (1987) 1, 39–43  
 Kmetič Dimitrij, F. Mlakar, V. Tucić, J. Žvokelj, F. Vodopivec, M. Jakupović, B. Rallc: Bele kromove litine legirane z molibdenom za valje . . . . . ŽZB 21 (1987) 4, 151–165  
 Kosec Ladislav, F. Kosek: Nastanek in rast utrujenostne razpoke v koroziskem mediju . . . . . ŽZB 21 (1987) 4, 175–182  
 Leskovšek Vojteh: Tehnična novica: Predstavitev enokomorene vakuumsko peči IPSEN VTC 324-R s homogenim plinskim hlajenjem pod visokim tlakom . . . . . ŽZB 21 (1987) 1, 53–57  
 Paulin Andrej, J. Lamut, D. Dretnik: Reaktivnost koksa in njen vpliv na delo plavža . . . . . ŽZB 21 (1987) 2, 65–71  
 Paulin Andrej: Mehanizem zgorevanja koksa . . . . . ŽZB 21 (1987) 3, 105–112  
 Risteski B. Ico: O periodičnosti kristalizacije kovin . . . . . ŽZB 21 (1987) 3, 127–130  
 Vodopivec Franc, F. Grešovnik, F. Marinšek, M. Kmetič, O. Kürner: O tekstuji valjanja, razogljicanja in rekrystalizacije v jeklu z 0,03 C, 1,8 Si in 0,3 Al . . . . . ŽZB 21 (1987) 3, 113–118  
 Uranc Franc: Vpliv trenja, poti, drsne hitrosti in pritiska na obrabo . . . . . ŽZB 21 (1987) 3, 119–125  
 Risteski B. Ico: O periodičnosti kristalizacije kovin . . . . . ŽZB 21 (1987) 3, 127–130  
 Čurčija Dušan: Vpliv hitrosti valjanja na proces hladnega valjanja z mazivi . . . . . ŽZB 21 (1987) 3, 131–136  
 Brdar Božidar: Strjevanje jekla v kokili . . . . . ŽZB 21 (1987) 4, 137–150  
 Kmetič Dimitrij, F. Mlakar, V. Tucić, J. Žvokelj, F. Vodopivec, M. Jakupović, B. Rallc: Bele kromove litine legirane z molibdenom za valje . . . . . ŽZB 21 (1987) 4, 151–165  
 Rodič Tomaž, D. R. J. Owen: Osnovni koncept numerične simulacije radialnega kovanja . . . . . ŽZB 21 (1987) 4, 167–174  
 Todorović Gojko, J. Lamut, B. Dobovišek, J. Kramer, J. Zapušek, B. Sedlar: Naogljicanje železa med redukcijo in taljenjem plavžnega vsipa . . . . . ŽZB 21 (1987) 4, 1–5  
 Ule Boris, F. Vodopivec, J. Žvokelj, M. Grašič, L. Kosec: Zapozneli lomjeklazvisoko trdnostjo . . . . . ŽZB 21 (1987) 4, 183–192  
 Uranc Franc: Vpliv trenja, poti, drsne hitrosti in pritiska na obrabo . . . . . ŽZB 21 (1987) 3, 119–125  
 Vodopivec Franc, M. Gabrovšek: Meja plastičnosti konstrukcijskih jekel, fizikalno metalurške osnove . . . . . ŽZB 21 (1987) 1, 19–28  
 Vodopivec Franc, F. Marinšek, F. Grešovnik: Rekrystalizacija in rast zrn pri žarjenju hladno valjanega jekla z 0,03 % C, 1,8 % Si, 0,3 % Mn in 0,3 % Al . . . . . ŽZB 21 (1987) 1, 29–37  
 Vodopivec Franc, O. Kürner, A. Lagoja, F. Grešovnik, A. Rodič, S. Senčič, F. Vizjak: Tehnična novica: Orazvojnih možnostih jekelin nekaterih posebnih zlitin ter postopkov za njihovo izdelavo, predelavo, ulivanje in plemenitenje . . . . . ŽZB 21 (1987) 2, 93–98  
 Vodopivec Franc, F. Grešovnik, F. Marinšek, M. Kmetič, O. Kürner: O tekstuji valjanja, razogljicanja in rekrystalizacije v jeklu z 0,03 C, 1,8 Si in 0,3 Al . . . . . ŽZB 21 (1987) 3, 113–118

## 2. AVTORSKO KAZALO

- Arh Jože, V. Prešeren: Dosežki Železarne Jsenice na področju sekundarne obdelave jekla . . . . . ŽZB 21 (1987) 1, 7–17  
 Arh Jože: Tehnična novica: Druga evropska konferenca o električnem jeklarstvu . . . . . ŽZB 21 (1987) 1, 59–63  
 Azman Alojz, D. Sikošek, A. Šteblaj, J. Triplat, J. Arh: Tehnična novica: Novi konstrukcijski mikrolegrirani jekli Niomol 390 in Niomol 490 . . . . . ŽZB 21 (1987) 1, 45–52  
 Brdar Božidar: Ohlajanje jeklenega valja na vozičku . . . . . ŽZB 21 (1987) 2, 85–92  
 Brdar Božidar: Strjevanje jekla v kokili . . . . . ŽZB 21 (1987) 4, 137–150  
 Čurčija Dušan: Vpliv hitrosti valjanja na proces hladnega valjanja z mazivi . . . . . ŽZB 21 (1987) 3, 131–136  
 Gnamuš Janko, G. Rihtar: Reparaturno varjenje orodnih jekel . . . . . ŽZB 21 (1987) 2, 73–76  
 Grešovnik Ferdo: Računanje temperaturnih napetosti v elastičnem področju . . . . . ŽZB 21 (1987) 2, 77–83  
 Kaker Henrik: Mikroanaliza faz v zlitini Nimonic 80 A s kombinacijo REM-EDS . . . . . ŽZB 21 (1987) 1, 39–43  
 Kmetič Dimitrij, F. Mlakar, V. Tucić, J. Žvokelj, F. Vodopivec, M. Jakupović, B. Rallc: Bele kromove litine legirane z molibdenom za valje . . . . . ŽZB 21 (1987) 4, 151–165  
 Kosec Ladislav, F. Kosek: Nastanek in rast utrujenostne razpoke v koroziskem mediju . . . . . ŽZB 21 (1987) 4, 175–182  
 Leskovšek Vojteh: Tehnična novica: Predstavitev enokomorene vakuumsko peči IPSEN VTC 324-R s homogenim plinskim hlajenjem pod visokim tlakom . . . . . ŽZB 21 (1987) 1, 53–57  
 Paulin Andrej, J. Lamut, D. Dretnik: Reaktivnost koksa in njen vpliv na delo plavža . . . . . ŽZB 21 (1987) 2, 65–71  
 Paulin Andrej: Mehanizem zgorevanja koksa . . . . . ŽZB 21 (1987) 3, 105–112  
 Risteski B. Ico: O periodičnosti kristalizacije kovin . . . . . ŽZB 21 (1987) 3, 127–130  
 Rodič Tomaž, D. R. J. Owen: Osnovni koncept numerične simulacije radialnega kovanja . . . . . ŽZB 21 (1987) 4, 167–174  
 Todorović Gojko, J. Lamut, B. Dobovišek, J. Kramer, J. Zapušek, B. Sedlar: Naogljicanje železa med redukcijo in taljenjem plavžnega vsipa . . . . . ŽZB 21 (1987) 4, 1–5  
 Ule Boris, F. Vodopivec, J. Žvokelj, M. Grašič, L. Kosec: Zapozneli lomjeklazvisoko trdnostjo . . . . . ŽZB 21 (1987) 4, 183–192  
 Uranc Franc: Vpliv trenja, poti, drsne hitrosti in pritiska na obrabo . . . . . ŽZB 21 (1987) 3, 119–125  
 Vodopivec Franc, M. Gabrovšek: Meja plastičnosti konstrukcijskih jekel, fizikalno metalurške osnove . . . . . ŽZB 21 (1987) 1, 19–28  
 Vodopivec Franc, F. Marinšek, F. Grešovnik: Rekrystalizacija in rast zrn pri žarjenju hladno valjanega jekla z 0,03 % C, 1,8 % Si, 0,3 % Mn in 0,3 % Al . . . . . ŽZB 21 (1987) 1, 29–37  
 Vodopivec Franc, O. Kürner, A. Lagoja, F. Grešovnik, A. Rodič, S. Senčič, F. Vizjak: Tehnična novica: Orazvojnih možnostih jekelin nekaterih posebnih zlitin ter postopkov za njihovo izdelavo, predelavo, ulivanje in plemenitenje . . . . . ŽZB 21 (1987) 2, 93–98  
 Vodopivec Franc, F. Grešovnik, F. Marinšek, M. Kmetič, O. Kürner: O tekstuji valjanja, razogljicanja in rekrystalizacije v jeklu z 0,03 C, 1,8 Si in 0,3 Al . . . . . ŽZB 21 (1987) 3, 113–118

**3. KAZALO PO STROKAH — UDK****53 FIZIKA**

531 Splošna mehanika

Grešovnik Ferdo: Računanje temperaturnih napetosti v elastičnem področju . . . . . ŽZB 21 (1987) 2, 77—83

536 Nauk o topotri. Termodynamika

Brutar Božidar: Ohlajenje jeklenega valja na vozičku . . . . . ŽZB 21 (1987) 2, 85—92

**62 — INŽENIRSTVO, TEHNIKA****620.17 Preskušanje mehanskih lastnosti**

Uranc Franc: Vpliv trenja, poti, drsne hitrosti in pritiska na obrabo . . . . . ŽZB 21 (1987) 3, 119—125

**620.18 Metalografija**

Kaker Henrik: Mikroanaliza faz v zlitini Nimonic 80 A s kombinacijo REM-EDS . . . . . ŽZB 21 (1987) 1, 39—43

**620.19 Napake v materialu**

Kosec Ladislav, F. Kosel: Nastanek in rast utrujenostne razpoke v koroziskem mediju . . . . . ŽZB 21 (1987) 4, 175—182

**621.73 Kovanje**

Rodič Tomaž, D.R.J. Owen: Osnovni koncept numerične simulacije radialnega kovanja . . . . . ŽZB 21 (1987) 4, 167—174

**621.74.047 Kontinuirno litje**

Risteski B. Ico: O periodičnosti kristalizacije kovin . . . . . ŽZB 21 (1987) 3, 127—130

**621.77 Valjanje, stiskanje, vlečenje**

Čurčija Dušan: Vpliv hitrosti valjanja na proces hladnega valjanja z mazivi . . . . . ŽZB 21 (1987) 3, 131—136

Vodopivec Franc, F. Grešovnik, F. Marinšek, M. Kmetič, O. Kürner: O teksturi valjanja, razogljičenja in rekristalizacije v jeklu z 0,03 C, 1,8 Si in 0,3 Al . . . . . ŽZB 21 (1987) 3, 113—118

**621.78 Toplotna obdelava kovin**

Leskovšek Vojteh: Tehnična novica: Predstavitev enokomorne vakuumsko peči IPSEN VTC 324-R s homogenim plinskim hlajenjem pod visokim tlakom . . . . . ŽZB 21 (1987) 1, 53—57

**621.791 Varjenje in podobni postopki**

Gnamuš Janko, G. Rihtar: Reperaturno varjenje orodnih jekel . . . . . ŽZB 21 (1987) 2, 73—76

**66 KEMIJSKA TEHNIKA, KEMIČNE IN SORODNE INDUSTRIJE****669 — Metalurgija**

Vodopivec Franc, O. Kürner, A. Lagoja, F. Grešovnik, A. Rodič, S. Senčič, F. Vizjak: Tehnična novica: O razvojnih možnostih jekel in nekaterih posebnih zlitin ter postopkov za njihovo izdelavo, predelavo, ulivanje in plemenitenje . . . . . ŽZB 21 (1987) 2, 93—98

**669.01 Splošna in teoretična metalurgija**

Paulin Andrej: Mehanizem zgorevanja koksa . . . . . ŽZB 21 (1987) 3, 105—112

Vodopivec Franc, F. Marinšek, F. Grešovnik: Rekristalizacija in rast zrn pri žarjenju hladno valjanega jekla z 0,03 % C, 1,8 % Si, 0,3 % Mn in 0,3 % Al . . . . . ŽZB 21 (1987) 1, 29—37

**669.14 Zlitine železa z ogljikom. Jeklo nasprotno**

Ule Boris, F. Vodopivec, J. Žvokelj, M. Grašič: Zapoznelli lom jekla z visoko trdnostjo . . . . . ŽZB 21 (1987) 4, 183—193

Vodopivec Franc, M. Gabrovšek: Meja plastičnosti konstrukcijskih jekel, fizikalno-metalurške osnove . . . . . ŽZB 21 (1987) 1, 19—25

Ažman Alojz, D. Sikošek, A. Šteblaj, J. Triplat, J. Arh: Tehnična novica: Novi konstrukcijski mikrolegirani jekli Niomol 390 in Niomol 490 . . . . . ŽZB 21 (1987) 1, 45—52

**669.15 Zlitine železa z drugimi elementi, razen ogljikom. Legiranje jekla. Ferozlitine**

Kmetič Dimitrij, F. Mlakar, V. Tucić, J. Žvokelj, F. Vodopivec, M. Jakupović, B. Ralić: Bele kromove litine legirane z molibdenom za valje . . . . . ŽZB 21 (1987) 4, 151—165

**669.16 Proizvodnja grodija**

Todorovič Gojko, J. Lamut, B. Dobovišek, J. Kramer, J. Zapušek, B. Sedlar: Naogljicanje železa med redukcijo in taljenjem plavžnega vsipa . . . . . ŽZB 21 (1987) 1, 1—5

**669.18 Proizvodnja jekla**

Brutar Božidar: Strjevanje jekla v kokili . . . . . ŽZB 21 (1987) 4, 137—150

Arh Jože, V. Prešeren: Dosežki Železarne Jesenice na področju sekundarne obdelave jekla . . . . . ŽZB 21 (1987) 1, 7—17

Arh Jože: Tehnična novica: Druga svetovna konferenca o elektro jeklarstvu . . . . . ŽZB 21 (1987) 1, 59—63

**669.4 Svinec. Svinčeve zlitine**

Paulin Andrej, J. Lamut, D. Dretnik: Reaktivnost koksa in njen vpliv na delo plavža . . . . . ŽZB 21 (1987) 2, 65—71

# VSEBINA

UDK: 669.18:669.112.223:620.192.43  
ASM/SLA: N21, M28h, E25n, D9p, 9-69

Metalurgija — jeklarstvo — strjevanje jekla — izceje — sekundarni lunker

B. Brdar

## Strjevanje jekla v kokili

Železarski zbornik 21 (1987) 4 s 137—150

Na osnovi simulacij ohlajanja bloka v kokili po poenostavljenem modelu smo prišli do nekaterih novih ugotovitev glede poteka strjevanja. Predvsem smo žeeli povezati potek izračunanih izoterm s potekom izceje. Da bi se prepričali o pravilnosti svojih predpostavk, smo rekonstruirali kokilo OK 650.

Vlili smo 4 poskusne bloke avtomatnega jekla Č 3990, jih prerezali po dolgem, naredili Baumannov odčis in fotografirali jedkano ploskev. Iz primerjave med posameznimi slikami sklepamo, da je mogoče s primerno stanjano steno kokile vplivati tudi na porazdelitev izceje V v glavi bloka. Pričakujemo, da bi na ta način lahko odpravili probleme, ki nastopajo pri valjanju nekaterih kvalitet, kadar je za to vzrok nehomogenost v sredi bloka.

Avtorski izvleček

UDK: 669.15'26-194:669.14.018.255  
ASM/SLA: M28, N8b, TSK, 5, Cr, W23k

Metalurgija — bele kromove litine — mikrostruktura — TTT in CTT diagrami

D. Kmetič, F. Mlakar, V. Tucić, J. Žvokelj, F. Vodopivec, M. Jakupović, B. Ralić

## Bele kromove litine legirane z molibdenom za valje

Železarski zbornik 21 (1987) 4 s 151—165

Delo obravnava mikrostrukturne značilnosti belih kromovih litin legiranih z molibdenom vitem in toplotno obdelanem stanju.

Na izoblikovanje eutektičnih karbidov, delež karbidne faze in mikrostrukturo matice vitem stanju vplivajo poleg pogojev strjevanja in ohlajanja, razmerje Cr/C in vsebnost ogljika in molibdena v litini.

Podani so izotermini transformacijski diagrami za destabilizacijo austenita in za destabiliziran austenit in kontinuirni transformacijski diagram za destabiliziran austenit.

Avtorski izvleček

UDK: 621.73.045:519.6  
ASM/SLA: F22, Q24, 1-66, U4g, U4k  
Metalurgija, kovanje, matematični model

T. Rodić, D. R. J. Owen:

## Osnovni koncept numerične simulacije radialnega kovanja

Železarski zbornik 21 (1987) 4 s 167—174

MKE je pogosto uporabljena metoda za analizo preoblikovalnih procesov. V primerjavi s klasičnimi metodami ima naslednje prednosti: z MKE lahko rešujemo primere z zahtevno geometrijo preoblikovanca; problem lahko rešujemo z različnimi materialnimi modeli; možno je obravnavanje nestacionarnih napetostno-deformacijskih in temperaturnih polj. V prihodnje pričakujemo vgrajevanje novih spoznanj s področja fizikalne metalurgije v numerične modele. Prvi koraki v tej smeri so bili že storjeni.<sup>17, 18</sup>

Avtorski izvleček

UDK: 620.193.01  
ASM/SLA: R1h, R1e, R2j, Q26p

Metalurgija — Temperaturna utrujenost — Korozija  
L. Kosec, F. Kosel

## Nastanek in rast utrujenostne razpoke v koroziskem mediju

Železarski zbornik 21 (1987) 4 s 175—182

V koroziskih medijih se površine kovin prekrijejo s koroziskimi produkti. To je posebej izrazito pri oksidaciji kovin na površinah ali visokih temperaturah. Mehanska nestabilnost teh plasti je vzrok, da skozi nastale razpoke prihaja koroziski medij v stik s kovino, zaradi česar rastejo koroziski produkti v obliki klinov. Menjajoče ali stalne natezne napetosti povzročajo trajno nestabilnost koroziskih produktov in pospešeno napredovanje klinov v globino kovine. V sistemih s koroziskimi klini nastanejo značilna napetostno-deformacijska stanja, ki vplivajo na oblikovanje sistema. Motnje, ki preprečujejo hiter dotok koroziskskega medija do kovine na vrhu klinov, zavirajo njihovo rast. Posebej uspešne v tem so kompozitne plasti (kovina-oksid), ki so mehansko zelo stabilne. Skupine oksidnih klinov rastejo v enakih pogojih počasnejše kot če je v sistemu en sam klin enake velikosti. V kemično nehomogenih materialih (s kristalnimi izcejami) so praviloma negativne izceje mesto, v katerem nastanejo in rastejo oksidni klini.

Avtorski izvleček

UDK: 669.14.018.2:539.56:620.192.3  
ASM/SLA: Q26s, SGBa, ST, 2-60, EGn, 3-66

Metalurgija — fizika kovin

B. Ule, F. Vodopivec, J. Žvokelj, M. Grašič in L. Kosec

## Zapozneli lom jekla z visoko trdnostjo

Železarski zbornik 21 (1987) 4 s 183—192

Prispevek obravnava teoretično analizo napetostno inducirane segregacije vodika, ki pri jeklu z visoko trdnostjo povzroči zapozneli lom.

Na osnovi merjenja kritičnega in mejnega napetostnega intenzitetnega faktorja ter ob pomoči mikrofaktografskih preiskav je bilo ugotovljeno, da ima popuščena martenzitna mikrostruktura enak  $K_{IIc}$  kot popuščena martenzitno-bainitna mikrostruktura, enake meje plastičnosti, da pa ima slednja boljšo lomno žilavost.

Avtorski izvleček

UDK: 621.73.045:519.6  
ASM/SLA: F22, Q24, 1-66, U4g, U4k  
Metalurgija, kovanje, matematični model

T. Rodić, D. R. J. Owen:

## Osnovni koncept numerične simulacije radialnega kovanja

Železarski zbornik 21 (1987) 4 s 167—174

MKE je pogosto uporabljena metoda za analizo preoblikovalnih procesov. V primerjavi s klasičnimi metodami ima naslednje prednosti: z MKE lahko rešujemo primere z zahtevno geometrijo preoblikovanca; problem lahko rešujemo z različnimi materialnimi modeli; možno je obravnavanje nestacionarnih napetostno-deformacijskih in temperaturnih polj. V prihodnje pričakujemo vgrajevanje novih spoznanj s področja fizikalne metalurgije v numerične modele. Prvi koraki v tej smeri so bili že storjeni.<sup>17, 18</sup>

Avtorski izvleček

# CONTENTS

UDK: 620.193.01  
ASM/SLA: R1h, R1e, R2j, Q26p

Metallurgy — Thermal Fatigue — Corrosion

L. Kosec, F. Kosec

**Occurrence and Growth of Fatigue Cracks in Corrosion Environment**

Železarski zbornik 21 (1987) 4 P 175—182

In corrosion environment metal surfaces become covered by corrosion products. This is a typical feature of metal oxidation at temperature rise and high temperatures. The mechanical instability of these layers is the reason for the occurrence of cracks through which the oxidant gets in contact with the metal, making the corrosion products grow in the form of wedges. Changing or constant tensile stresses cause a permanent instability of corrosion products and intensify the growth of wedges deep into the metal. In corrosion wedge systems typical stress-strain states occur, affecting their morphology. Barriers preventing a rapid access of the oxidant to the metal at the wedge tip, retard the growth. Especially successful barriers are composite metal/oxide layers which are mechanically very stable. In equal conditions groups of oxide wedges grow more slowly than if there is only one wedge of the same size. In chemically nonhomogeneous materials with crystal segregations oxide wedges would as a rule start growing in the areas of negative segregations.

Author's Abstract

UDK: 669.14.018.2-539.56/620.192.3  
ASM/SLA: Q26s, SGBa, ST, 2-60, EGn, 3-66

Metallurgy — materials Science

B. Ule, F. Vodopivec, J. Žvokelj, M. Grašič in L. Kosec

**Delayed Fracture of High-strength steel**

Železarski zbornik 21 (1987) 4 P 183—192

The paper presents theoretical analysis of stress induced hydrogen segregation, which produces delayed fracture of high-strength steels. On the basis of measurements of the critical and the threshold stress intensity factor and by means of microfractographic examinations, it was established that the tempered martensitic microstructure has the same  $K_{TH}$  as the tempered martensitic-bainitic microstructure with the same yield strength, the latter having a better fracture toughness.

Author's Abstract

UDK: 669.18/669.112.223/620.192.43  
ASM/SLA: N21, M28h, E25n, D9p, 9-69

Metallurgy — steelmaking — solidification of steel — segregations — secondary pipe

B. Brdar

**Solidification of Steel in a Mould**

Železarski zbornik 21 (1987) 4 P 137—150

On the basis of simulations of solidification of an ingot in the mould using the simplified model new facts about the process of solidification were obtained. We wished to correlate the calculated isotherms with the course of segregations. In order to check the validity of our assumptions we reconstructed the mould OK 650. There were 4 test ingots of the free cutting steel Č 3990 cast. They were cut longitudinally and the sulphur prints and the photos of the etched cross-sections were made. From the comparison among different figures it could be concluded that it was possible to influence the distribution of segregates by a proper thinning of the mould wall. This holds especially for the V-segregates in the upper part of the ingot. We expect that in this way some problems occurring with the rolling of some qualities could be suppressed when it is supposed that the unhomogeneities in the middle of the ingot are the reason for them.

Author's Abstract

UDK: 669.15/26-194/669.14.018.255  
ASM/SLA: M28, N8h, Tsk, S, Cr, W23k

Metallurgy — White Chromium Cast Irons — Microstructure — TTT and CTT Diagrams

D. Kmetič, F. Mlakar, V. Tucić, J. Žvokelj, F. Vodopivec, M. Jakupović, B. Ralić

**White Chromium Cast Irons for Rolls, Alloyed with Molybdenum**

Železarski zbornik 21 (1987) 4 P 151—165

The paper treats the microstructural characteristics of the white chromium cast irons alloyed with molybdenum, as cast and as heat treated.

Formation of eutectic carbides, portion of carbide phase, and microstructure of matrix in the cast state are influenced by the Cr/C ratio, and carbon and molybdenum contents in the alloy beside the conditions of solidification and cooling.

Isothermal transformation diagrams for destabilization of austenite, and for destabilized austenite, next to the continuous transformation diagram for destabilized austenite are presented.

Author's Abstract

UDK: 621.73.045.519.6  
ASM/SLA: F22, Q24, I-66, U4g, U4k

Metallurgy, forging, mathematical model

T. Rodić, D. R. J. Owen:

**Basic Concepts of Numerical Simulation of a Radial Forging Process**

Železarski zbornik 21 (1987) 4 P 167—174

The FEM is now widely used for the analysis of metal forming processes. In comparison with classical methods the FEM has certain advantages: various complex shapes can be considered, it enables implementation of different material models and treatment of transient stress-strain and temperature fields. In the future the inclusion of the metallurgical development in the numerical modelling of hot working processes is expected. The first steps toward this goal have already been made<sup>17,18</sup>.

Author's Abstract